An investigation into the effects on leaching select low-grade gold ores in the Witwatersrand Basin

By

Samira N. Alex

2399093

A dissertation submitted to the Faculty of Science, University of the Witwatersrand in fulfilment of the requirements for the degree of Master of Science

Supervisor(s): Prof. Glen Nwaila

Co-supervisor: Dr. Julie E. Bourdeau

January, 2023

Declaration

I declare that this dissertation is my own, unaided work. It is being submitted for the Degree of Master of Science at the University of the Witwatersrand, Johannesburg. It has not been submitted before for any degree or examination in any other University.

_____Samira_____ Samira N. Alex

11th day of June 2023, at The University of the Witwatersrand, Johannesburg.

Abstract

The mining industry currently faces challenges including, but not limited to: gold price volatility, declining ore grade, complex ores, escalating production costs and increasing pressure to be environmentally responsible. As green mining becomes a strong focus of the 21st Century mining industry, an opportunity exists to explore non-cyanide green leaching alternatives. In the past, several non-cyanide reagents such as thiosulfate, chloride, bromide, ammonia, thiourea have been proposed to replace cyanide, however all present unique shortcomings. Glycine is a promising green alternative due to its ease in handling, affordability and recyclability. This research project aims to determine how complex and low-grade Middelvlei Reef from the Witwatersrand Basin in South Africa can be successfully leached using the glycine system.

The selected Witwatersrand ore was characterised by using optical microscopy, scanning electron microscope-energy dispersive X-ray spectroscopy (SEM-EDS), quantitative X-ray diffraction (QXRD), Tescan integrated mineral analyser (TIMA) and micro-X-ray computed tomography (Micro-XCT). Experimental results shows that gold is semi-refractory due to it being physically associated with gangue minerals (e.g., pyrite, carbonaceous matter) and the presence of electrum has been detected which is known to influence leaching kinetics. The occurrence of minerals such as quartz, pyrite and carbonaceous matter in the ore impedes leaching by displaying preg-robbing behaviour, reagent consumption or lowering gold recoveries. A multi-elemental analysis, conducted prior to glycine leaching, highlighted the presence of deleterious base metals such as of Cu = 67.57 ppm and Co = 97.80 ppm. These results highlight that the traditional method of processing needs to be reconsidered.

Leaching experiments were aimed at optimizing gold recoveries while remaining sustainable. Results demonstrate that the optimum parameters that yielded high gold recoveries are: 1) glycine to permanganate ratio of 1:1, 20% solids (ore) and 80% liquids, pH 10. 5 and a temperature of 25 °C. Experiments demonstrate that glycine as a reagent yields average recoveries of 66.7% from all the different experiments conducted. The lowest recovery was 56% and the highest recovery was 92%. The implications of the results are that the Middelvlei Reef shows great potential for glycine leaching, however vital pre-treatment steps should follow prior to leaching. An ore pre-treatment will ensure that the correct measures are put in place to counteract the refractory and complex nature of the ore and obtain higher recoveries.

Acknowledgements

"Our deepest fear is not that we are inadequate. Our deepest fear is that we are powerful beyond measure. It is our light, not our darkness, that most frightens us." – Marianne Williamson. I extend great thanks to Prof. Glen Nwaila, Dr. Julie Bourdeau and the Geometallurgy and Machine Learning study cohort, for your exceptional knowledge and expertise on geometallurgy. I thank you for seeing a vision within me and for pushing me to my limits. I would humbly like to say thank you for affording me the chance to further my studies and in essence for contributing to my growth as an individual. Thank you for seeing a great vision within me. This journey has provided me with invaluable skills I can apply to many facets of my career.

Furthermore, I would also like to extend great appreciation to the University of Witwatersrand, which offered me the chance to do my masters and access to world-class facilities and technology. The community at the university will always stay close to me, they have all played an immense role in helping me put this thesis together. Special thanks to everyone who assisted me in the school of geosciences and chemical engineering, this was only possible with access to the necessary facilities. Lastly, I extend great thanks to my study cohort for motivating me and for the lifelong friendships we have formed, my parents for their constant motivation, and Standard Bank Namibia for funding my studies and cultivating leaders in Africa.

Table of Contents

Chapter 1: Introduction 12
1.1 Introduction to gold mining 12
1.2 Gold production in the Witwatersrand Basin 13
1.3 The Middelvlei Reef 15
1.4 The history of cyanidation 16
1.5 Non-cyanide gold leaching 17
1.6 Problem statement 17
1.7 Aim 18
1.8 Hypotheses 18
1.9 Research key questions 18
1.10 Research approach 19
1.11 Thesis organisation 19
Chapter 2: Regional Geology 21
2.1 Geological background of the Kaapvaal Craton 21
2.2 The Witwatersrand-type gold deposits 23
2.3 Geological background of the Witwatersrand Basin 23
2.4 Ore paragenesis of gold deposits in the Witwatersrand Basin 25
2.5 Petrography and mineralogy of the gold ores in the Witwatersrand Basin 27
2.6 The Middelvlei Reef 31
Chapter 3: Literature review 35
3.1 Overview of gold processing 35
3.4 Non-cyanide reagents 41
3.5 The glycine leaching system 42
3.5.2 Glycine leaching of gold 44
3.5.3 Parameters that influence glycine leaching 45
Chapter 4: Methodology 47
4.1 Sampling and sample preparation 47
4.2.1 Reflected light microscopy 48
4.2.2 Scanning electron microscope – energy dispersive spectroscopy (SEM-EDS) 48
4.2.4 Quantitative X-ray diffraction (XRD) 48
4.2.5 Inductively coupled plasma mass spectrometry (ICP-MS) 49

4.2.7 TESCAN TIMA....50
4.2.8 Micro X-Ray computed tomography (Micro-XCT)....51
Image reconstruction and phase segmentation....52
4.3 Metallurgical test work – bottle roll leaching....56
Chapter 5: Results....59
5.1 Mineralogical assemblage of the Middelvlei Reef as determined by optical microscopy and SEM-EDS 59
5.2 Modal mineralogy of the Middelvlei Reef as determined by TIMA....62
5.4 Gold deportment of the Middelvlei Reef using automated mineralogy....63
5.4.1 The association of gold with gangue mineralogy and the liberation status of gold....63
5.4.2 Grain size classification of gold and gangue mineralogy....68
5.5 Micro-XCT....69
5.5.1 Texture characterisation....69
5.5.2 Gold and sulphide mineral grain characteristics....72
5.6 Data validation between Micro-XCT and TIMA....75
Chapter 6: Multi-element analysis....77
6.1 Comprehensive multi-element geochemical analysis of the Middelvlei Reef....77
7.1 Metallurgical test work....79
Chapter 8: Discussion....86
8.1 Mineralogical characterisation....86
8.2 Gold deportment study using TIMA....87
8.3 The implications of ore mineralogy on leaching....88
8.4 Limitations of automated mineralogy....89
8.5 Ore characterisation using Micro-XCT....90
8.6 Limitations of Micro-XCT....92
8.7 Insights from the multi-elemental analysis of the Middelvlei Reef....93
8.8 Effects of various parameters on glycine leaching; the way forward....95
8.8.1 Optimum leaching conditions (glycine-permanganate vs cyanide)....96
8.8.2 Ore characterisation....97
Chapter 9: Conclusion and Recommendations....99
9.1 Ore characteristics and glycine leaching potential....99
9.3 Concluding remarks....101
9.4 Future recommendations....101

Figure 1.1: *South Africa's gold production (mostly from the Witwatersrand Basin) in comparison to the rest of the world. Figure modified from Frimmel and Nwaila (2021). The red arrow refers to the peak in gold production in South Africa in the 1970s……15*
Figure 1.2: *Production of Witwatersrand conglomerate-hosted gold deposits (per 1,000 metric tons) and the variation of gold grade as a function of age (Ga). The richest deposits lie between the ages of 2.86 Ga and 2.90 Ga. Diagram modified from Frimmel (2018)……16*

Figure 1.3: *Simplified map of the Driefontein mining operations in the Carletonville goldfield, South Africa……18*
Figure 1.4: *Methodology approach used for this research project. QXRD = quantitative X-ray diffraction, SEM-EDS = scanning electron microscope-energy dispersive X-ray spectroscopy, OM = optical microscope, TIMA = Tescan integrated mineral analyser, Micro-XCT = micro-X-ray computed tomography, ICP-MS = inductively coupled mass spectrometry, FA = fire assays, XRF = X-ray fluorescence……21*

Figure 1.5: *Schematic diagram of this thesis with relevant chapter descriptions……22*
Figure 2.1: *Simplified geological maps of the Kaapvaal Craton, the Witwatersrand Basin and Supergroup, and the Carletonville gold field. Figure modified from McCarthy (2006), Frimmel (2005) and Nwaila et al. (2020). A) Location of the Witwatersrand Basin on the Kaapvaal Craton in southern Africa. B) Map of the Witwatersrand Basin and generalised stratigraphic sequence. Younger cover rocks have been removed from the illustration. C) Map of the Carletonville goldfield. Included in the subfigure is the stratigraphic succession of the area……24*
Figure 2.2: *Photomicrographs under reflected light illustrating the mineralogy of the Witwatersrand Basin ores. A) Concentrically laminated inclusion-bearing pyrite (py-2). B) Gold (Au) associated with carbon in quartz (Qz) matrix. C) Aggregates of euhedral hydrothermal pyrite (Py-3). D) Detrital pyrite (py-1) associated with carbonaceous matter……30*
Figure 3.1: *Simplified flow chart for gold processing. Modified after Cairncross and Anhaeusser (1992)……37*
Figure 3.2: *schematic diagram of gold dissolution modified after Kudryk and Kellogg (1954)……38*
Figure 3.3: *Schematic diagram of the different associations of gold with ore minerals. Illustration modified from Khalesi et al., (2009)……39*

Figure 3.4: *Basic structure of an amino acid……43*

Figure 3.5: *The zwitterion state of glycine……44*

Figure 3.6: *Positively charged glycine ion……44*

Figure 3.7: *Negatively charged glycine ion……44*

Figure 4.1: *Major and minor elements validation using XRF assays against calculated TIMA assays……50*

Figure 4.2: *A) Raw CT data before conversion into slices. B) A screenshot of the image reconstruction process from the CT Pro 3D software……53*

Figure 4.3: *Linear attenuation coefficients of different minerals encountered in the Middelvlei Reef as a function of X-ray energy, using the XCOM database. Modified after Kyle and ketcham (2015)……55*

Figure 4.4: *Phase segmentation of minerals in the scanned ore blocks, with false colours (left). To the right the phases are identified on a histogram. Red is gold, purple is rutile, yellow are the sulphides and green are the silicates……57*

Figure 4.5: *Laboratory set-up of bottle-roll leaching experiments A) Preparation of chemicals for leaching. B) Conditioning of the bottle rolls. C) Bottle rolls placed on rollers at an rpm of 150, at room temperature conditions. D) Filtering of residue and liquids using a filter press. E) Packaging of dried residue to be sent for fire assays……59*

Figure 5.1: *Reflected light photomicrographs of the Middelvlei Reef ore. (A) Detrital pyrite (Py-1) with micro-inclusions of chalcopyrite (Cp). (B) Sub-rounded aggregate pyrite surrounded by quartz and carbonaceous material (Py-5). (C) Concentrically laminated pyrite (Py-4). (D) Aggregates of sulphides, pyrite-pyrrhotite and rutile (Py-3)……62*

Figure 5.2: *2D SEM images illustrating pyrite and gold morphologies as well as the distribution of gold in the Middelvlei Reef. A) An anhedral grain of gold locked in quartz (Qtz) in the conglomerate matrix. B) Anhedral gold is hosted in quartz (Qz) and rutile (Rt). C) A subhedral grain of gold present at the grain boundary of rutile. D) Gold present as a minor inclusion in rutile. E) Euhedral to subhedral grains of gold locked in quartz from the conglomerate matrix. F) Gold present at the grain boundary of pyrite (Py)……63*

Figure 5.3: *Pie chart of the modal mineralogy (weight percent) of the Middelvlei Reef……64*

Figure 5.4: *Quantitative modal mineralogy as determined by QXRD……65*

Figure 5.5: *Scanned ore block of the Middelvlei Reef using TIMA……66*
Figure 5.6: *Mineralogical association of gold with gangue mineralogy on the samples S2-P1 using TIMA……67*
Figure 5.7: *TIMA high-resolution phase maps that show the relationships between gold (Au) and the gangue mineralogy. A) Gold is locked at the grain boundary between chlorite and quartz. B) Gold is enclosed and locked in quartz. C) Gold is present as in-fillings in microfractures in pyrite……67*
Figure 5.8: *Liberation status of gold in the Middelvlei Reef as determined using TIMA……68*
Figure 5.9: *Schematic diagram of relationship between free-surface area and liberation modified after Spencer and Sutherland (2000)……69*
Figure 5.10: *Free-surface area analysis of gold using TIMA……69*
Figure 5.11: *Grain size distribution of gold measured by TIMA……70*
Figure 5.12: *The grain size distribution of pyrite as determined by TIMA……71*
Figure 5.13*: Mineral phases in the Middelvlei Reef grouped according to volume colour scale (mm). Gold is reflected as a bright white due to the density of the mineral. Blue corresponds to low-volume minerals phases and red corresponds to high-volume mineral phases……72*
Figure 5.14: *An ore block scanned in 3D using Micro-XCT with separation of the different mineral phases. False colours were applied to classify individual minerals and mineral phases. Green corresponds to the silicate phases (mostly quartz), yellow represents the sulphide phases (mostly pyrite), purple represents rutile and red represents gold……73*
Figure 5.15: *Histogram of the gold grain size distribution as calculated by using the defect analysis tool in VG Studio Max……73*
Figure 5.16: *Grain sphericity of gold determined by the defect analysis tool in VG Studio Max……74*
Figure 5.17: *Grain size distribution of sulphide phases as determined using the defect analysis tool in VG Studio Max……74*
Figure 5.18: *Sphericity of sulphide minerals as determined using the defect analysis tool in VG Studio Max……75*
Figure 5.19: *Modal mineralogy comparison between Micro-XCT and TIMA. The TIMA modal mineralogy was grouped according to Micro-XCT mineral grouping…… 76*
Figure 7.1: *Direct glycine leaching results for experiments A – E. Parameters are detailed in Table 7.1…… 81*

Figure 7.2: *Recovery of gold vs concentration of potassium permanganate. Parameters are further detailed in Table 7.1……82*
Figure 7.3: *Recovery of gold vs leaching time (hours). Parameters are further detailed in Tables 7.1 and 7.3……83*
Figure 7.4: *Recovery of gold vs pH. Parameters are further detailed in Table 7.1……84*
Figure 7.5: *Recovery of gold vs slurry density. Parameters are further detailed in Tables 7.1 and 7.4……85*
Figure 8.1: *Limitations of using automated mineralogy A) BSE-image of suspected inclusions of gold present in porous pyrite. B) Phase-maps generated from the BSE image where gold is over-quantified after incorrect identification……90*
Figure 8.2: *Schematic diagram of elements that cause refractory behaviour during leaching. Modified after Larrabure et al. (2021)……94*

List of Tables

Table 2.1: *Main evidence and interpretations supporting the hydrothermal, modified, and palaeo-placer models……22*

Table 2.2: *Detailed classification scheme of the different types of pyrite grains present in the Witwatersrand Basin modified after da Costa et al., (2020)……25*

Table 2.3: *Middelvlei Reef facies at the Driefontein operations……29*

Table 3.1: *Classification of gold-bearing ores (Zhou and Cabri, 2004)……31*

Table 3.2: *Summary of major innovations in the gold mining industry from 1973 to – the present date……34*

Table 3.3: *Grain size classification modified after Hausen (2000)……39*

Table 3.4: *Criteria that should be considered for gold lixiviants (Hilson and Monhemius, 2006)……43*

Table 3.5: *A summary of some of the non-cyanide lixiviants that have been developed (Senanayake, 2004)……43*

Table 3.6: *A summary of typical metallurgical tests for gold ores (modified after Angove, 2005)……49*

Table 4.1: *Scanning parameters used to acquire data……57*

Table 4.2: *Leaching parameters used in bottle-roll leaching……58*

Table 5.1: *The simplified modal mineralogy of the MVR determined by TIMA phase maps, mineral density and attenuation coefficient provided by Bam et al., 2020. The density information of each mineral was obtained from (www.webmineral.co)……63*

Table 6.1: *Comparison between calculated TIMA mineralogy and QXRD bulk mineralogy……79*

Table 6.2: *Multi-elemental analysis, flags indicate that the element could have a negative impact on mineral processing or be detrimental to the surrounding environment……87*

Table 6.3: *Parameters used in glycine leaching experiments……89*

Table 6.4: *Head grade determined by fire-assays for each experiment Au (g/t)……89*

Table 6.5: *Leaching parameters……91*

Table 6.6: *Leaching parameters……93*

List of abbreviations

ICP-MS - inductively coupled-mass spectrometry

SEM-EDS - scanning electron microscope-energy dispersive

Micro-XCT - micro-X-ray computed tomography

TIMA - Tescan integrated mineral analyser

QXRD - quantitative X-ray diffraction

XRF - X-ray fluorescence.

Chapter 1: Introduction

1.1 Introduction to gold mining

The global mining industry currently faces numerous challenges that encompass social, techno-economic and environmental issues (Sánchez and Hartlieb, 2020). The ore grade has steadily been declining and the exploitation of complex ores, which are often polymetallic, and refractory tend to complicate the mineral extraction processes. In the long term, this may result in a supply shortfall for certain raw materials. Geological orebodies are variable and this variability is multi-dimensional, differing both laterally and vertically in terms of ore grade, mineralogy and texture (Dominy *et al.*, 2018). Ore variability is ubiquitous in all different geological orebodies and is a result of geological processes such as hydrothermal fluid action altering the orebody as well as variations in rock competencies. The incorrect metallurgical characterisation of orebodies can lead to the misspecification of the magnitude and scale of mining projects, and could subsequently result in significant economic losses (Dunham and Vann, 2007).

Geometallurgy is a science that integrates geological and mineral processing data to create a spatial model that facilitates the production planning of a mine (Lehmann, 2010). The discipline serves as a hybrid team-based, multi-disciplinary field that extends to mine plant operations including: comminution, blending, leaching and metal recovery (Zhou and Gu, 2016; Lishchuk and Pettersson, 2021). Geometallurgy serves the purpose of identifying, understanding, and characterising ore variability to improve the metallurgical recovery of complex orebodies (Lishchuk and Pettersson, 2021). Typically, an entire orebody is explored with the intention to identify and quantify spatial domains which may result in variable responses during mineral processing (Alruiz *et al.*, 2009; Mwanga *et al.*, 2015). However, changing the existing design plan of process plants is expensive and mines are increasingly tasked with adapting their processing methods to accommodate ore variability. This is a challenge, as process plants are historically designed to process ores based on ore-type definitions and are unequipped to cater to ore variability (Dominy *et al.*, 2018).

The gold mining industry in South Africa is the background of this study, with a focus on selected gold-endowed layers, locally described as ‘reefs’ in the Witwatersrand Basin. The Witwatersrand Basin is world renowned as the greatest gold anomaly in the world (Frimmel, 2019) and is, by far, the largest gold producer in South Africa. However, there has been a decrease in gold production since the 1970s and production is expected to continue declining soon (Fig. 1.1). Additionally, current exploration for high-grade gold ores is limited due to deposits being too deep (≥4 km) for safe extraction (Neingo and Tholana, 2016). Gold grades across the Witwatersrand Basin declined from 12 g/t in the 1970s to 5 g/t

in 2016, and is expected to drop to 0.9 g/t in 2050 (Neingo and Tholana, 2016), meaning that low grade ores have increasingly been selected for processing. Low-grade ores (1 g/t) from the Witwatersrand Basin are in principle challenging to process due to their complex behaviour during mineral processing (Nwaila *et al.*, 2020). Furthermore, low-grade gold ores currently mined in the basin require more energy, reagents, and water per unit of gold production (Mudd, 2007).

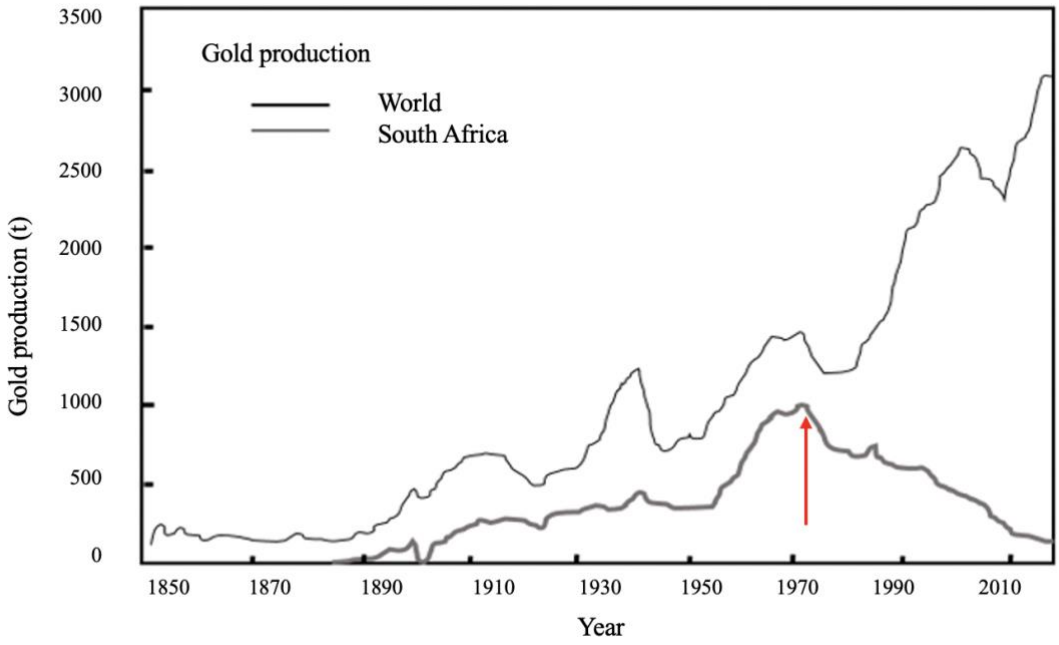

Figure 1.1: South Africa's gold production (mostly from the Witwatersrand Basin) in comparison to the rest of the world. Figure modified from Frimmel and Nwaila (2021). The red arrow refers to the peak in gold production in South Africa in the 1970s.

1.2 Gold production in the Witwatersrand Basin

Majority of South Africa's gold deposits are geographically located in the Witwatersrand Basin. Gold and uranium-bearing minerals are localised in conglomerate beds (hereon referred to as reefs) that contain carbon seams. At the base of the basin lies the 3086 ± 3 to 3074 ± 6 Ma Dominion Group rocks (Armstrong *et al.*, 1990; Robb *et al.*, 1992). The Witwatersrand Supergroup (2.96 to 2.78 Ga) superimposes the Dominion group and is divided into the West Rand and Central Rand groups (Kositcin and Krapež, 2004). The reefs in the Central Rand Group are of great economic significance and have contributed towards more than 55 % of gold production in the Witwatersrand Basin as seen in Fig. 1.2

(Main, Carbon Leader, Nigel reefs) (Frimmel, 2018). The richest gold deposits were endowed between 2.8 - 2.9 Ga (Fig. 1.2). Currently, the South African gold mining production needs to maximise gold recovery by embracing and/or implementing technological advancements since resources are gradually nearing exhaustion (Fig. 1.1).

Innovations in the industry are important because they can be used as means of enhancing processes efficiency whilst simultaneously reducing operating costs to meet environmental and social demands. In recent years, the South African mining industry has seen green technological advancements that have been beneficial to not only the environment but to communities as well. The "Green Mining Initiative" includes water management, sustainable practices in mining, environmental management, energy-efficient mining, and beneficiation (Huang *et al.*, 2021). As an example, hydrometallurgical technology advances promoted by the green mining initiative have been used to process low-grade ores, which has allowed for better control of co-products, whilst lowering environmental impacts (Chagnes, 2019). Advancements in hydrometallurgical technology have indeed facilitated the upgrade of sub-economic ores into economical ones (West, 2011).

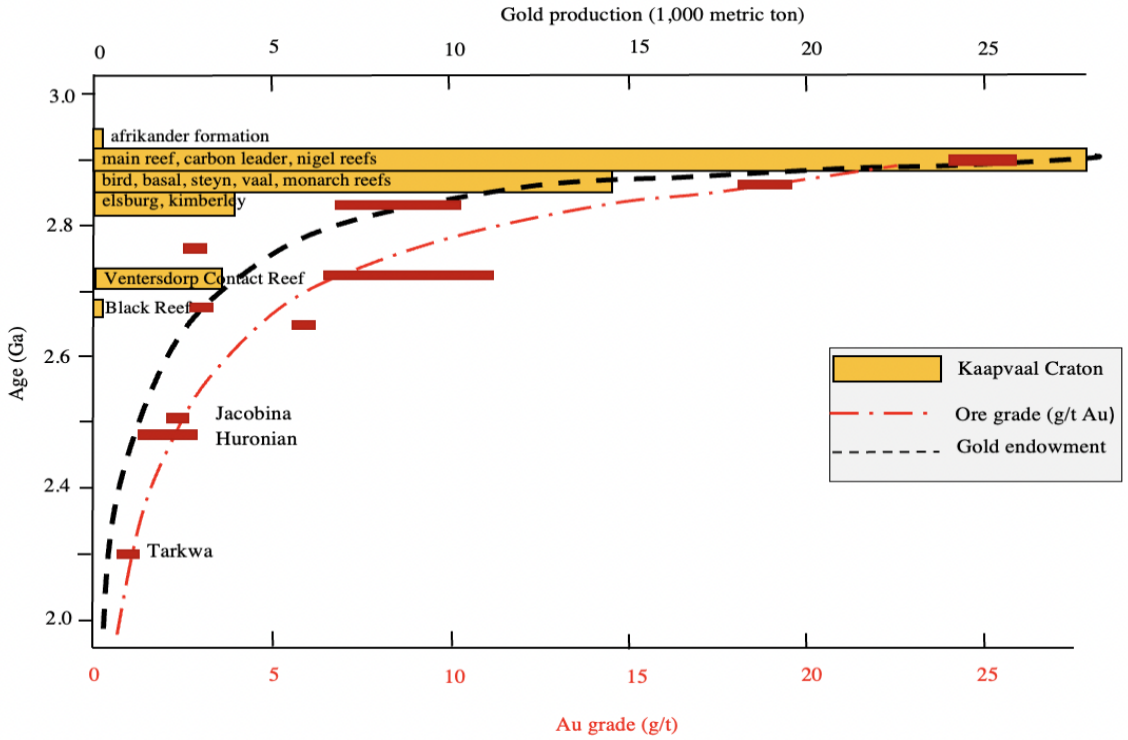

Figure 1.2: Production of Witwatersrand conglomerate-hosted gold deposits (per 1,000 metric tons) and the variation of gold grade as a function of age (Ga). The richest deposits lie between the ages of 2.86 Ga and 2.90 Ga. Diagram modified from Frimmel (2018).

1.3 The Middelvlei Reef

The Middelvlei Reef, located in the Johannesburg subgroup in the Central Rand Group, Witwatersrand Supergroup, is studied in this research project (see Chapter 2 for its geological description). The reef is situated near the base of the Central Rand Group and was deposited in a braided fluvial plain environment (Els, 1983). The reef attains a maximum thickness of seven meters and is characterised by an oligomictic quartz-pebble auriferous conglomerate, coarse-grained arenite, and mudstone laminae (Els, 1991). The reef is underlain and overlain by quartz wackes and quartz-arenites showing trough-crossbedding (Jolly, 1984a). The Middelvlei Reef has an average gold grade (26.1 g/t) than the Carbon Leader Reef (40 g/t) and exhibits an erratic lateral distribution of gold (Els, 1991). The area of the Middelvlei Reef extends across various mining operations, and in our study (Driefontein and Kloof operations), is under the ownership of Sibanye-Stillwaters (Fig. 1.3). The Middelvlei Reef is mined to depths greater than three km and covers an area of more than 500 km^2 (Myers *et al.*, 1993). The Middelvlei Reef only accounts for 9 % of gold ore mined at the Kloof and 7 % at the Driefontein operations (Sibanye-Stillwater Limited, 2021).

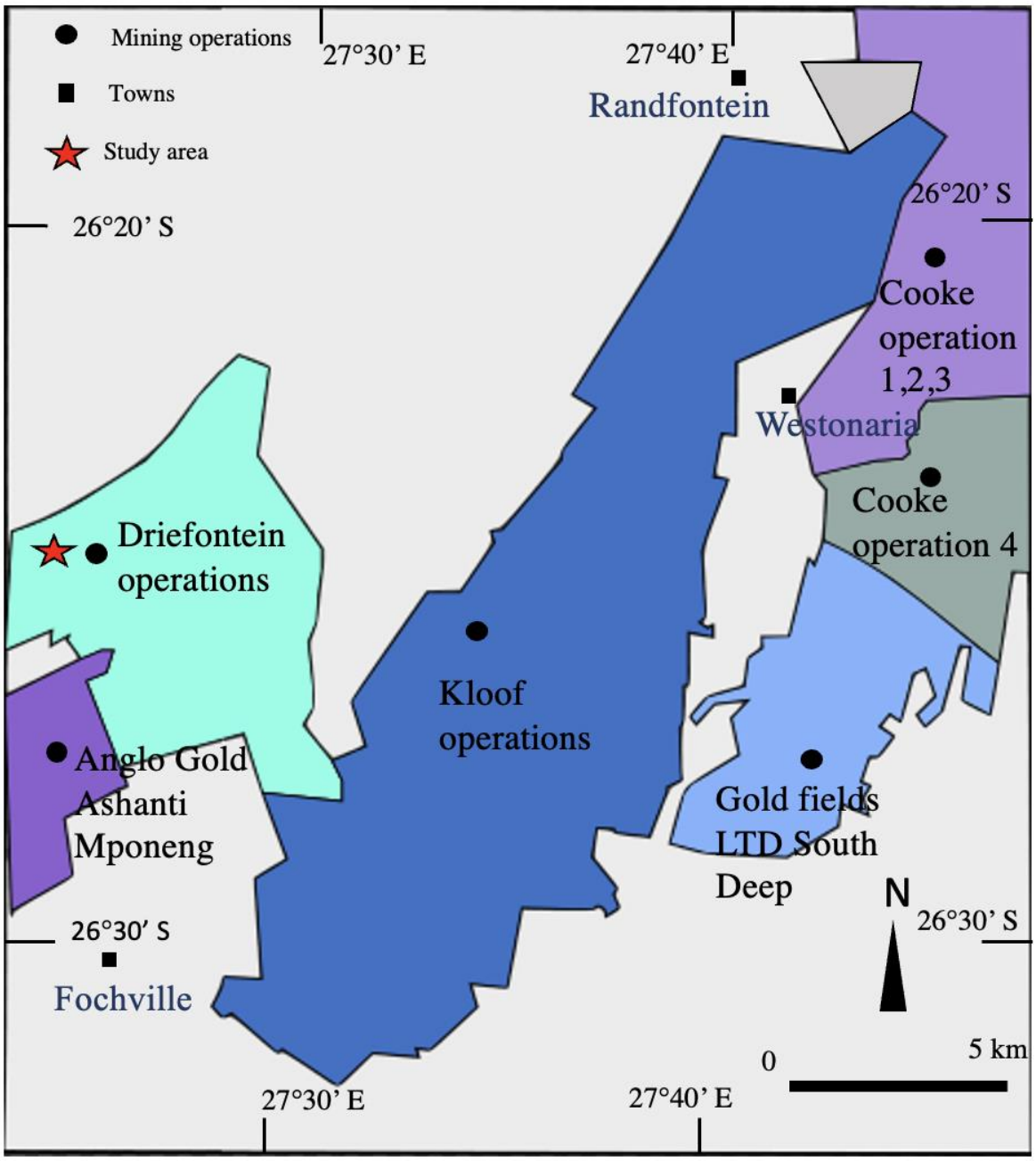

Figure 1.3: Simplified map of the Driefontein mining operations in the Carletonville goldfield, South Africa.

1.4 The history of cyanidation

Witwatersrand gold is recovered after communition by cyanidation technology. Cyanidation has been proven to be very efficient in the recovery of gold, with recoveries exceeding 90 % (Fraser *et al.,* 1991). Due to such high recoveries, the gold mining industry has utilized cyanide for more than a century. The reagent itself is inexpensive, efficient and has a high degree of selectivity towards gold and silver during

leaching (Hilson and Monhemius, 2006). Furthermore, the lixiviant is simple to handle and only requires oxygen as an oxidant, reducing processing costs (Altinkaya *et al.*, 2020). Cyanide is also a popular choice for recovering gold from low-grade ores, as the reagent is economically advantageous (Azizi and Ghaedrahmati, 2015). However, the cyanidation process raises several environmental, societal and economic (i.e., yields low recoveries when processing complex ores) concerns (La Brooy *et al.*, 1994; Sparrow and Woodcock, 1995; Senanayake, 2004).

Direct cyanide leaching is most efficient when applied to free-milling gold ores (Udupa *et al.*, 1990). Conversely, the past decade has seen the recovery of free-milling gold has become increasingly difficult due to increasing complexity in ore mineralogy, chemistry, and texture. For example, the presence of carbonaceous material absorbs the gold-cyanide complex (preg-robbing). Additionally, silica encapsulation of gold and the association of gold with sulphide minerals makes the ore impervious to cyanidation following the ore undergoing fine-grinding (Senanayake, 2004; Vaughan, 2004). The slow leaching kinetics and high cyanide consumption in the presence of refractory minerals (e.g., silica) and carbonaceous material results in increased production costs (Hilson and Monhemius, 2006; Adams, 2016; Altinkaya *et al.*, 2020).

1.5 Non-cyanide gold leaching

The mining industry has explored various non-cyanide reagents over the years (e.g., iodine, thiosulfate, thiourea, chloride and bromide) and the reagent of choice for this research investigation is glycine. Glycine is a promising environmentally benign reagent that shows great potential for gold extraction. Multiple studies using the reagent have been conducted by authors such as Liedberg *et al.,* (1985), Eksteen and Oraby (2015) and Altinkaya *et al.,* (2020), these studies all ascertain the potential of glycine in gold leaching under the correct parameters. The alkaline glycine leaching procedure was initially developed and patented for extracting copper from highly oxidized ores (Eksteen and Oraby, 2014). The procedure was then extended into gold and silver leaching in the mid-2010s (Eksteen and Oraby, 2015). The lixiviant has a high affinity for gold and presents many attractive advantages, namely: the reagent is recyclable, non-toxic, affordable, and non-volatile reagent (Tanda *et al.*, 2017; Oraby *et al.*, 2020).

1.6 Problem statement

Majority of the remaining gold ores mined in the Witwatersrand Basin are classified as low-grade ores, which are variable (or complex) in mineralogy, chemistry and texture (Frimmel, 2014). The complex mineralogy, chemistry and texture impact the effectiveness of gold extraction processes using cyanidation. Cyanide has known shortcomings, the most prominent being that it is hazardous to the

environment, as evidenced by a succession of environmental calamities at numerous gold mines around the world which have subsequently raised concerns over its use (Senanyako, 2004; Marsden and House, 2014; Chao *et al.*, 2021). The mining industry, therefore, needs to find solutions to overcome the phenomena of ore complexity coupled with the need to move towards more sustainable, eco-friendly processing solutions. Thus, there is a knowledge gap regarding the implications of leaching low-grade, complex ores with an environmentally benign reagent. This geometallurgical study will investigate the gold recovery performance of glycine in comparison to cyanide.

1.7 Aim

The all-encompassing aim of this research project is to investigate the effect(s) of using an environmentally friendly lixiviant, glycine, to recover gold from selected Witwatersrand Basin low-grade and complex ores. The study will focus on low-grade ores found in the Middelvlei Reef of the Driefontein operations within the Witwatersrand Supergroup. A major component of this research project will involve a detailed characterisation of low-grade and complex ores' mineralogy, chemistry, and texture. Samples from the Middelvlei Reef will be used as representative Witwatersrand ores. A second component of the project involves performing leaching experiments using bottle-roller reactors. The metallurgical recovery of gold will then be modelled using a spatial model that will provide a quantitative forecast of the metallurgical performance of gold in a cyanide-free leaching system. Findings from this study can serve as a proxy to determine whether leaching gold with an environmentally friendly reagent, such as glycine, is appropriate for treating low-grade and complex gold ores in the future.

1.8 Hypotheses

The mineralogy, chemistry, and texture of the Middelvlei Reef influence the metallurgical recovery of gold by glycine. By primarily characterising the low-grade and complex gold ores from the Middelvlei Reef, the metallurgical response of gold will be understood, and thus, it will be possible to predict gold behaviour during glycine bottle roll leaching.
Alternatively, the mineralogy, chemistry and texture of the Middelvlei Reef do not influence the metallurgical performance of gold recovery by glycine leaching, and further investigation would be needed to find a suitable alternative reagent.

1.9 Research key questions

To accomplish the purpose of this research project, the following key questions will be addressed:

- Are there mineralogical assemblages that may affect the recovery of gold using glycine?

- Is it possible to use mineralogical, chemical and textural information to predict gold's processing behaviour and recovery in glycine?
- What are the optimal parameters using glycine as a reagent that will yield maximum gold recoveries while being economically and environmentally responsible?
- What factors influence the leaching kinetics of glycine?

1.10 Research approach

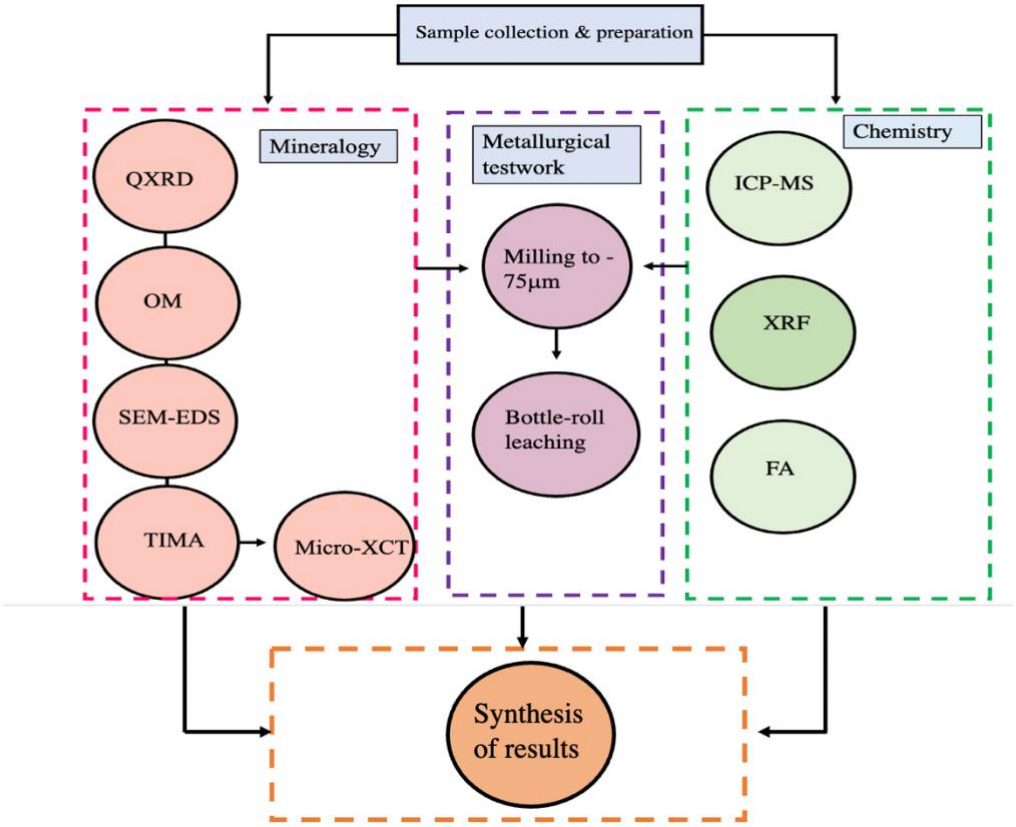

Figure 1.4: Methodology approach used for this research project. QXRD = quantitative X-ray diffraction, SEM-EDS = scanning electron microscope-energy dispersive X-ray spectroscopy, OM = optical microscope, TIMA = Tescan integrated mineral analyser, Micro-XCT = micro-X-ray computed tomography, ICP-MS = inductively coupled mass spectrometry, FA = fire assays, XRF = X-ray fluorescence.

1.11 Thesis organisation

This thesis is organised into nine chapters (Fig. 1.5). Chapter 1 (this current chapter) provides details on the background of the study, the problem statement, aims, hypotheses and key questions conveyed

to address the intended goals of this research project. Chapter 2 reviews the geological background of the Kaapvaal Craton, Witwatersrand Basin and Middelvlei Reef. Chapter 3 reviews the relevant literature and highlights gaps present in eco-friendly leaching. Chapter 4 presents a systematic description of the methods and analytical equipment used for this research project. Chapter 5 details the results produced from the experimental procedure employed in this thesis followed by chapter 6 which consists of a multi-elemental geochemistry analysis of the Middelvlei Reef. Chapter 7 details the bottle-roll leaching experiments, chapter 8 provides the discussion and chapter 9 lastly, provides a conclusion of the study and provides future recommendations for industry.

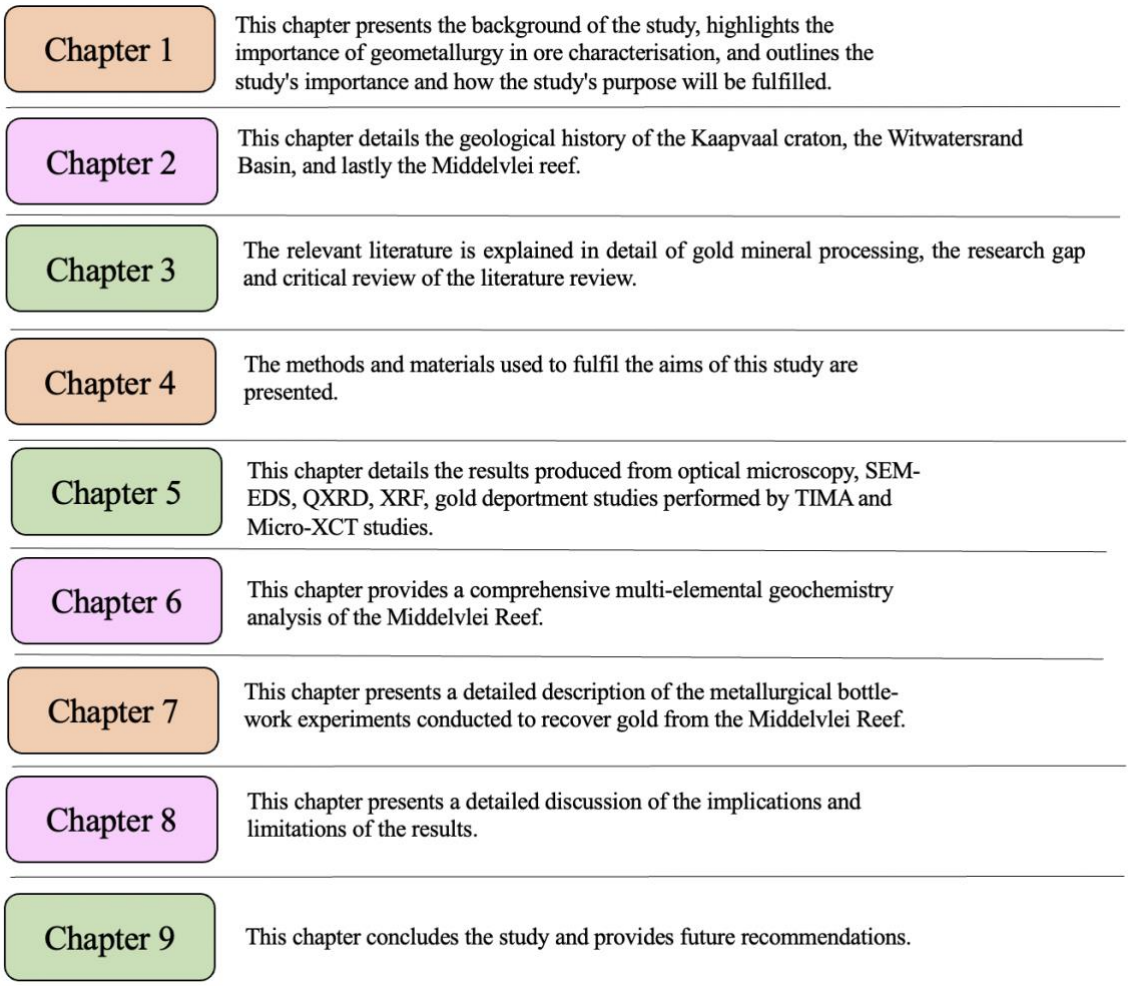

Figure 1.5: Schematic diagram of this thesis with relevant chapter descriptions.

Chapter 2: Regional Geology

The chapter entails a synopsis of the Archaean geology of southern Africa. This chapter will detail the formation of the Kaapvaal Craton and the sub-basins that formed on the craton, with specific emphasis on the Witwatersrand Basin. The chapter will then delve into the processes that formed the Witwatersrand Basin and describe the different ore paragenesis models liable for the formation of the basin's gold deposits. The chapter closes off by describing the representative Witwatersrand Basin orebody, namely, the Middelvlei Reef.

2.1 Geological background of the Kaapvaal Craton

The Kaapvaal Craton (Fig. 2.1A) is among the most ancient well-preserved Archaean continental fragments on Earth, providing insights into the development of the early Earth (Poujol *et al.*, 2003; Anhaeusser, 2019). The Kaapvaal and Pilbara cratons are the only ones that provide pristine evidence of pre-3100 Ma rocks (Brandl *et al.*, 2006). The Craton amassed during the Archaean Eon through a series of complex tectonic processes similar to the modern-day plate tectonics (Hofmann *et al.*, 2019). The formation of the Kaapvaal Craton took place episodically throughout a billion years (between 3.7 – 2.5 Ga), and involved numerous processes such as magmatic arc formation, accretion, and tectonic amalgamation (De wit *et al.*, 1992; Lowe, 1994; Poujol and Robb, 1999). The Kaapvaal Craton's development can be divided into two main periods: 1) the first stage of separation of the continental lithosphere from the mantle and stabilisation of the basement (3.7 – 3.1 Ga), and 2), continental growth through continental accretion and subduction processes (3.1 – 2.6 Ga) (De wit *et al.*, 1992). The Kaapvaal Craton is geographically separated into four domains, namely the: 1) eastern, 2) central, 3) northern, and 4) western domains (De wit *et al.*, 1992; Poujol *et al.*, 2003). The domain situated in the east consists of the Barberton Greenstone Belt and granitoids extending into Eswatini (Swaziland), including the notable Pongola Supergroup. The domain situated in the centre includes the Johannesburg and Vredefort domes, the latter of which is an important geological impact structure. The domain located in the north is characterised by the Murchison, Giyani and Pietersburg greenstone belts. Finally, the western domain – encompasses the Kraaipan, Amalia and Madibe greenstone belts (Anhaeusser, 2019).

The Kaapvaal Craton basement stabilised between 3.7 – 2.7 Ga and was covered by Archaean- to Paleoproterozoic-aged basins (Tinker, 2002). The point of convergence between the Zimbabwe and Kaapvaal cratons between 2.7 – 2.5 Ga (Fig. 2.1A), led to the NE-SW transpression, characterised by basement uplift and, subsequently, basin creation (Coward *et al.*, 1995; Robb and Meyer, 1995;

Catuneanu, 2001). As a result, the Witwatersrand, Pongola, Dominion and Transvaal basins were created (Tinker, 2002). Of specific interest to this study, the Witwatersrand Basin is positioned close to the centre of the Kaapvaal Craton (Fig. 2.1B).

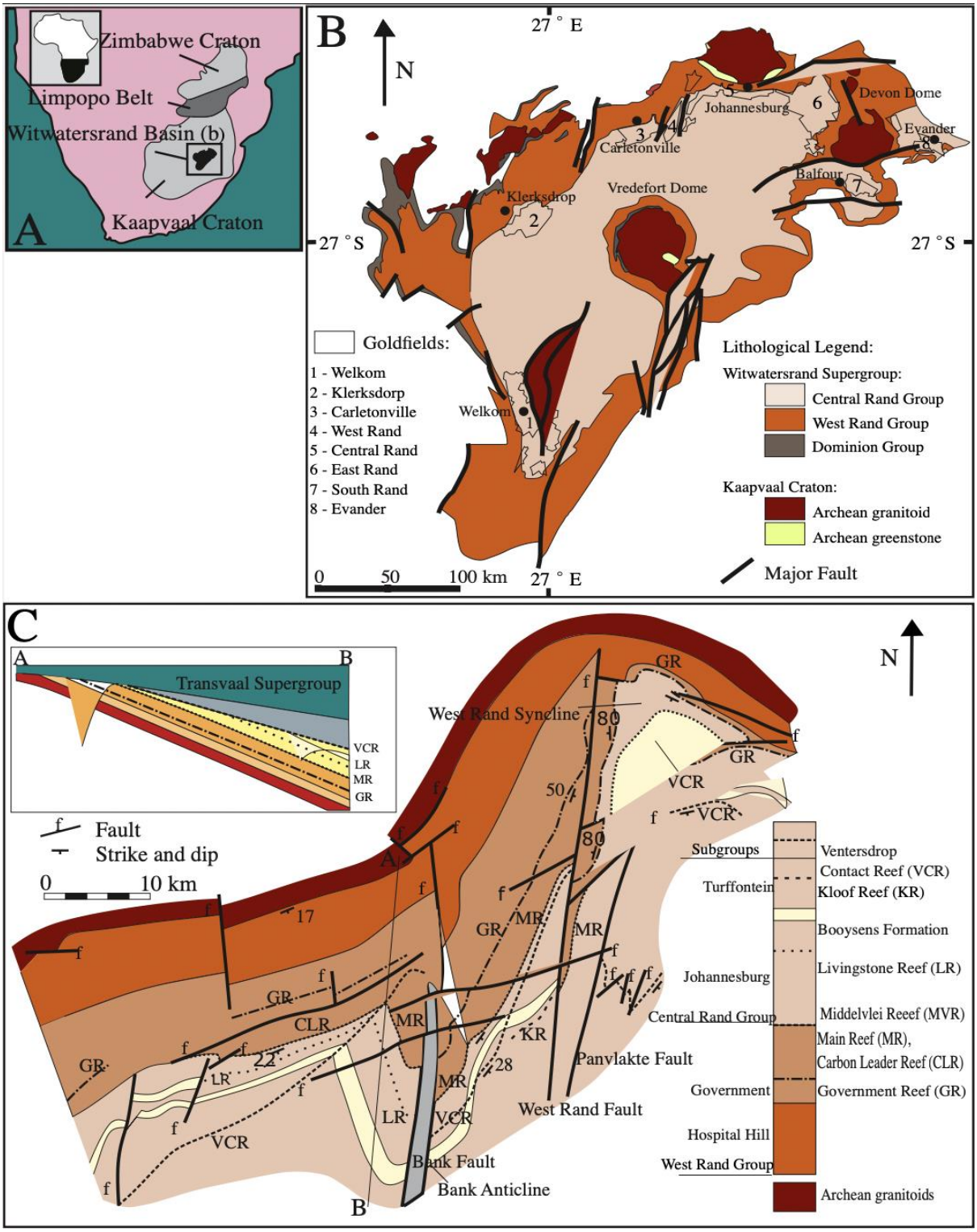

Figure 2.1: Simplified geological maps of the Kaapvaal Craton, the Witwatersrand Basin and Supergroup, and the Carletonville gold field. Figure modified from McCarthy (2006), Frimmel (2005) and Nwaila et al. (2020). A) The position of the Witwatersrand Basin on the Kaapvaal Craton in southern Africa. B) Map of the Witwatersrand Basin and generalised stratigraphic sequence. Younger cover rocks have been removed from the illustration. C) Map of the Carletonville goldfield. Included in the subfigure is the stratigraphic succession of the area.

2.2 The Witwatersrand-type gold deposits

Witwatersrand-type gold deposits are a group of palaeo-placer deposits which are found in Archaean- and Palaeoproterozoic-aged cratons (Frimmel, 2014). These deposits are found on every single continent except Antarctica and formed in a range of tectonic settings, including 1) continental rifts, 2) passive margins, and 3) synorogenic foreland basins (Frimmel, 2014). Notable lithologies that exhibit Witwatersrand-style gold mineralisation include the: Witwatersrand, Transvaal (i.e., Black Reef Formation, South Africa) and Huronian (Canada) supergroups (Mossman and Harron, 1983). Overall, Witwatersrand-type gold deposits are variably textured, high mineralisation, and are associated with high concentrations of Os (Minter *et al.*, 1993). The Mesoacrchaean-aged Witwatersrand Basin, situated near the interior of the Kaapvaal Craton, is arguably the greatest gold field on earth (Gartz and Frimmel, 1999; Frimmel, 2019). Around 53,000 t of gold have been extracted from the basin since its discovery in 1884 (Frimmel and Nwaila, 2020; Sillitoe et al., 2020). Mining has reached a mature stage in the Witwatersrand Basin, but the basin itself remains the most significant gold anomaly in the world (Frimmel and Nwaila, 2021).

2.3 Geological background of the Witwatersrand Basin

The Mesoarchaean-aged Basin is a long-lived sedimentary basin. Approximately 7,000 m thick sequences of arenaceous and argillaceous sediments coupled with minor rudaceous lithologies which were deposited in a fluvial-deltaic environment define the basin (Fig. 2.1B) (Robb and Meyer, 1995). The basin is to have formed in an Andean-style collisional setting (Jolley *et al.*, 2004), extending 200 km in the north-western direction and 350 km in the north-eastern direction (Nwaila *et al.*, 2021). The palaeo-basin is defined by multiple cratonic successor basins, that overlie the Archaean-aged Kaapvaal Craton basement, itself characterised by granitic rocks, greenstone belts, and continental flood basalts (Eriksson *et al.*, 1981; Frimmel *et al.*, 2005; Frimmel, 2018). The basin is most appropriately depicted as a successor basin that comprises of remnants of superimposed sediments which were deposited in two separate sub-basins referred to as the West and Central Rand groups (Frimmel, 2005; Koglin *et al.*,

2010). Unfortunately, most lithologies belong to the Witwatersrand Supergroup are buried, preventing detailed observation from the surface. Minor exposures were fortunately exposed, permitting the discovery of gold, due to the 2023 ± Ma Vredefort impact up-doming event (Kamo *et al.*, 1996).

The Witwatersrand Basin gold deposits have been subjected to a series of alteration and metamorphic events. This includes regional metamorphism to lower greenschist facies, regional heating due to the emplacement of the Bushveld Igneous Complex (2.06 Ga) and shock metamorphism from the Vredefort asteroid (2023 ± 2 Ma), all of which remobilised gold and ore components (Phillips and Law, 1994; Frimmel, 2019). The widespread percolation of fluids (whether they be considered hydrothermal or metamorphic) led to the formation of textures and geochemical features which caused a prolonged and vivacious debate about the provenance of the gold (Frimmel, 2019).

Stratigraphically, the base of the basin is defined by the 3086 ± 3 to 3074 ± 6 Ma Dominion group rocks (Armstrong *et al.*, 1990; Robb *et al.*, 1992). The Witwatersrand Supergroup (2.96 to 2.78 Ga) superimposes the Dominion Group, and is divided into the West Rand and Central Rand groups (Fig.2.1C; Kositcin and Krapež, 2004). The West Rand and Central Rand groups are described in more detail below.

The West Rand Group

The West Rand Group (2985 ± 14 Ma) reaches its greatest thickness at 5,150 m (Frimmel, 2019). Sequences belonging to the West Rand Group were deposited in a shallow to deep marine environments along a passive continental margin (Frimmel, 2005). The group is dominated proportions of shale and qua that are equal to each other, with trivial iron formations and conglomerates (Eriksson *et al.*, 1981; Law *et al.*, 1990). Most conglomerates are confined to the upper parts of the group and are distal (Frimmel, 2019). Both sandstones and conglomerates were deposited in a shallow marine environment, whereas shales and minor iron formations were deposited in a deep marine environment (Eriksson *et al.*, 1981; de la Winter and Brink, 1991; Smith *et al*, 2013). Three parallel iron formation markers are present in the West Rand Group, namely the Water Tower and Contorted Bed iron formations in the Parktown Formation of the Hospital Hill Subgroup, and the Silverfield iron formation bed in the Coronation Formation of the Government Subgroup (Smith *et al.*, 2013). Conglomerate sequences are of economic interest as they are often gold-bearing and are thus currently being mined. The West Rand Group is further subdivided into three subgroups, namely the: 1) Hospital, 2) Government, and 3) Jeppestown subgroups (Fig. 2.1C; Frimmel, 2005; Simanovich, 2009).

The Central Rand Group

The Central Rand Group (2780 ± 3 Ma) reaches its greatest thickness at 2,880 m (Gumsley *et al.*, 2018). The Central Rand Group was deposited into a retro-arc foreland basin after the Witwatersrand

Basin underwent a 10 m.y. sedimentation hiatus at around 2900 Ma, which resulted in an unconformable contact that is traceable across the basin (Minter, 2006). The retro-arc foreland basin experienced regression in reaction to crustal accretion, which was followed by significant accumulations of gold formation in the basin (Catuneanu, 2001). The Central Rand Group is dominated by fluvial to fluvio-deltaic sandstones and conglomerates, with minor shales (Simanovich, 2009). The gold-rich Central Rand Group accounts for the majority of mining activities in the Witwatersrand Basin (Frimmel, 2019). Gold is existent in at least 30 reefs, which correspond to planar orebodies (Goldfarb, 2021). Conglomerate beds rich in gold and uranium are spatially positioned proximally in the basin, where palaeo-river entry points are visible (Nwaila *et al.*, 2021). The Group is further subdivided into the Johannesburg and the Turffontein subgroups (Fig. 2.1C).

2.4 Ore paragenesis of gold deposits in the Witwatersrand Basin

Various genetic models have been put forward to explain the formation of the gold deposits in the Witwatersrand Basin and the debate is far from resolved. The most favoured genetic models include the: 1) palaeo-placer, 2) hydrothermal, and 3) modified placer models (Minter, 1978; Barnicoat *et al.*, 1997; Phillips and Law, 2000; Frimmel, 2005). Specifically, the palaeo-placer model suggests that gold, heavy minerals (e.g., uranite, pyrite) and clastic materials were brought into the basin as clastic sediments by erosional processes from a gold-laden hinterland (or source) (Minter, 1978). The hydrothermal model suggests that gold precipitated from metamorphic hydrothermal fluids during basin alteration which occurred after sedimentation (Barnicoat *et al.*, 1997; Phillips and Law, 2000; Phillips and Powell, 2011; Fuchs *et al.*, 2017). Gold and heavy minerals deposited into the basin are of detrital origin, according to the modified placer model. Both gold and heavy minerals then underwent remobilisation after burial, resulting in texture and compositional changes (Minter *et al.*, 1993; Frimmel, 2005). Table 2.1 presents the evidence and interpretations used to support the abovementioned genetic models.

Table 2.1. Main evidence and interpretations supporting the palaeo-placer, hydrothermal and modified placer models.

Component	Palaeo-placer model (syngenetic)	Hydrothermal model	Modified placer model

Gold and U-bearing minerals	Intensive chemical weathering of the source area (hinterland) resulted in metal-rich solutions which migrated to shallow-water environments. There, microbial activity facilitated the chemical and biological precipitation of gold and uranium (Mossman *et al.*, 2008).	Hydrothermal fluids from underneath or outer to the basin transported gold and uranium into the basin following sediment deposition (Barnicoat *et al.*, 1997; Phillips and Law, 2000; Phillips and Powel, 2011).	Gold and uranium were first deposited into the basin by fluvial processes and were subsequently remobilised by hydrothermal fluids (Frimmel, 2014; Burron *et al.*, 2018).
Oxidation conditions:	The Archaean atmosphere was reducing. Anoxic conditions prevailed (Frimmel *et al.*, 2005; Burron *et al.*, 2018)	The Archaean atmosphere had oxidizing conditions (Ohmoto *et al.*, 1999).	The Archaean atmosphere was reducing and this is supported by the existence of redox-sensitive detrital uraninite (Burron *et al.*, 2018).
Controls on gold deposition	Gold grade distribution was determined by sedimentological controls (Frimmel *et al.*, 2005).	Conglomerate beds were the favoured transport pathways for gold-bearing hydrothermal fluids (Barnicoat *et al.*, 1997).	Gold distribution was controlled by basin sedimentological controls (Frimmel *et al.*, 2005). There is no relationship between hydrothermal minerals and gold ore bodies (Kositcin *et al.*, 2003).

Pyrite	Majority of the pyrite in the basin is classified as 'buckshot pyrite' which is a type of pyrite derivative of a sedimentary provenance and is evidenced by a positive correlation of $\boldsymbol{\delta^{34}S}$ and $\boldsymbol{\Delta^{33}S}$ (Guy *et al.*, 2014).	Rounded pyrite grains in the basin were formed from the sulphidation of black sands (Phillips and Myers, 1989).	Rounded pyrite grains are detrital and support evidence of a reducing atmosphere (Hofmann *et al.*, 2009).
Gold provenance	Gold was leached from granite-greenstone terranes under an acidic atmosphere and remobilised to shallow water environments. The occurrence of bacteria facilitated the precipitation of gold and the materialisation of carbon in the reefs (Horscroft *et al.*, 2012).	There is no probable source for the Witwatersrand Basin gold. An Archaean palaeo-placer source larger than 50,000 t, 10-20 km away from the goldfields has not been located (Phillips and Powell, 2011).	Archaean gold was leached from a granite-greenstone terrane by acidic rain waters concentrated in H_2S, SO_4 and volcanic-related products originating from degassing events (Heinrich, 2015).

2.5 Petrography and mineralogy of the gold ores in the Witwatersrand Basin

Gold-bearing horizons in the Witwatersrand Basin, correspond to conglomeratic beds with varying lithological characteristics and are referred to as 'reefs' (Jolley *et al.*, 2004) The conglomerate beds vary in thickness and are bounded by erosional surfaces (Frimmel, 2005). The pebbles in the auriferous conglomerates in the basin are characterised by quartz veins (>80 %), chert veins (>10 %), quartz porphyries (2 %), and metamorphic rock fragments (1 %) (Frimmel, 2005; Simanovich, 2009). Interestingly, the greater the packing density of the pebbles (compaction), the greater the concentration of gold mineralisation in the conglomerate bed (Francisca, 2012). Ore-bearing conglomerates are characterised by well-sorted and rounded pebbles, whereas, poorly mineralised conglomerates are

comprised of poorly-sorted pebbles of variable shape and size (Law *et al.*, 1990; Simanovich, 2009; Francisca, 2012).

Texturally, the Witwatersrand gold-bearing conglomerate beds array from well-sorted and clast supported, to poorly-sorted and matrix-supported (Simanovich, 2009). Quartz (white and smokey) is the main mineral found in the conglomerate beds (Fig. 2.2A-D). Other minerals include chlorite, sericite, and calcite, all of which were formed during regional metamorphism (Law *et al.*,1990). The heavy mineral fractions present in the ore include zircon, garnet, spinel, ilmenite, monazite, pyrite and rutile (Mngoma, 2012). The economic components of the ore correspond to gold (Fig. 2.3B), pyrite and uranium-bearing minerals i.e., uranite, pitchblende, and thucholite (Simanovich, 2009). Uraninite is the most abundant uranium-bearing mineral in the basin, usually occurring as semi-rounded detrital grains with a chemical composition characteristic of a granitic/pegmatitic provenance (Frimmel, 2014). The sulphide minerals in the auriferous conglomerates include arsenopyrite, galena, sphalerite, pyrite, pyrrhotite, and chalcopyrite, among others

Gold and pyrite tend to show a strong mineral association (Koglin *et al.*, 2010). Gold is present in a variety of shapes and sizes in the ore. Grains are either mechanically rounded-, spheroid-, discoid-, or toroidal-shaped in the conglomerate matrix (Fig. 2.2B) (Law *et al*., 1990). Mechanically rounded, spheroidal to toroidal-shaped grains advocate a detrital interpretation (Frimmel, 2019 and references therein). The size of different gold grains is on average between 5 µm – 0.15 mm, with sizes varying between different reefs in the basin (Hallbauer and Joughin, 1973; Barton and Hallbauer, 1996). Grains with diameters vary in size from 0.1 – 1.5 mm are regarded as 'micro nuggets', however, despite a significant good gold endowment, the presence of visible gold is rare in the basin (Frimmel, 2019). Gold thought to be of hydrothermal in origin is found in the ore as crack infillings, euhedral overgrowths and dendritic aggregates (Phillips and Powell, 2011). Classification schemes for pyrite in the Witwatersrand Basin have been developed and refined over the years with the latest one by Da costa *et al.*, (2020), which classifies pyrite into three different types. Table 2.2 (also see Fig. 2.2) provides the detailed classification scheme used for the various types of pyrite grains present in the Witwatersrand Basin.

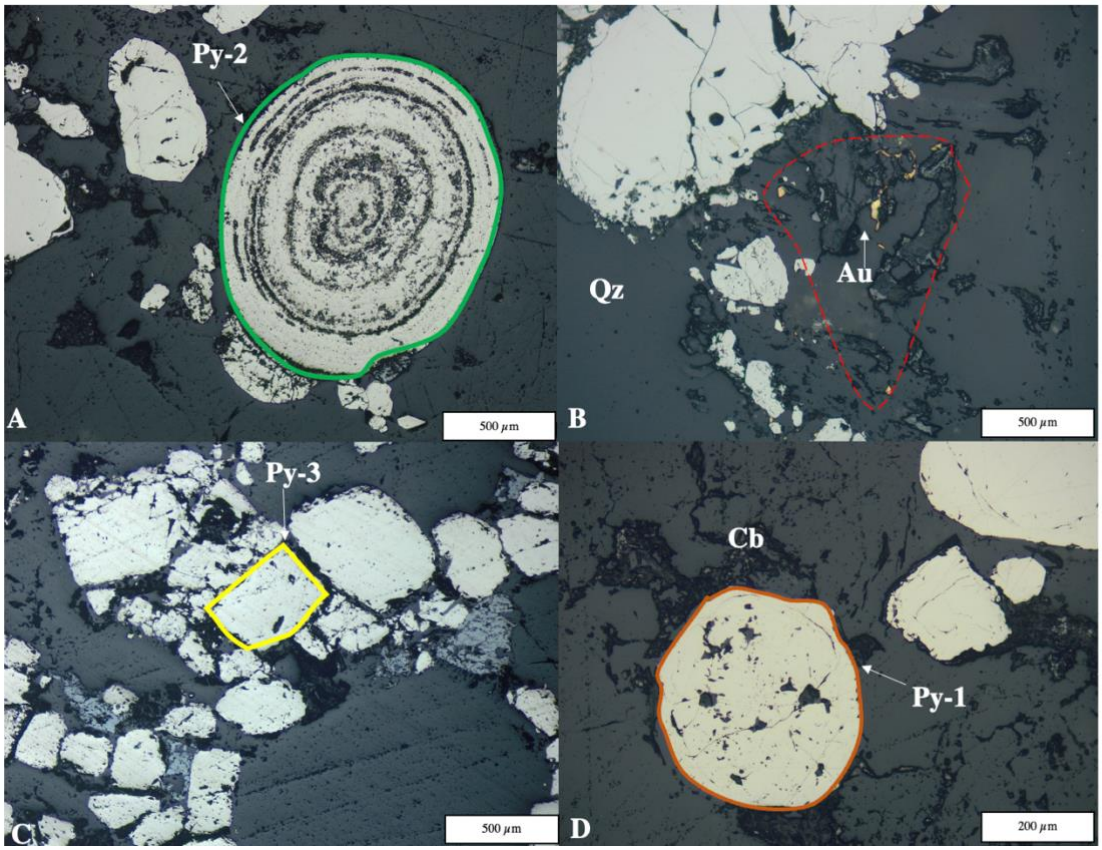

Figure 2.2: Photomicrographs under reflected light illustrating the mineralogy of the Witwatersrand Basin ores. A) Concentrically laminated inclusion-bearing pyrite (py-2). B) Gold (Au) associated with carbon in quartz (Qz) matrix. C) Aggregates of euhedral hydrothermal pyrite (Py-3). D) Detrital pyrite (py-1) associated with carbonaceous matter.

Table 2.2 Detailed classification scheme of the different types of pyrite grains present in the Witwatersrand Basin. Classification summarised after da Costa et al., (2020).

Detrital (allogenic) pyrite (py-1)	
Massive detrital pyrite (py-1) 	Massive pyrite is also known as 'compact' pyrite due to the absence of inclusions and the tightly arranged nature of individual pyrite. This form of pyrite has been witnessed in all Witwatersrand Basin reefs (Mahfouz, 2019).
Inclusion-bearing pyrite (py-2): a) Random Inclusions b) Concentrically laminated c) Micro-spherical 	Inclusion-bearing pyrite is a term used to describe a group of pyrites which contain numerous mineral inclusions (>10 vol %), organised in diverse textures (i.e., random inclusions, concentrically laminated, and micro-spherical) (England *et al.*, 2002). Due to the preservation of texture, this form of pyrite is hypothesised to preserve environmental conditions near or at the deposition site (da Costa *et al.*, 2020).
Coarsely crystalline pyrite 	Pyrite grains have a radial, elongate skeletal texture. They are thought to have formed in-situ and have undergone limited transport and reworking (da Costa *et al.*, 2020).
Hydrothermal (authigenic) pyrite	
Euhedral/subhedral pyrite (py-3) 	Authigenic pyrite is characteristically defined by a euhedral/subhedral shape and in some cases, it can bear inclusions. This form of pyrite is thought to have formed in diagenetic, hydrothermal and/or metamorphic events (England *et al.*, 2002; da Costa *et al.*, 2020).

Pseudomorphic pyrite 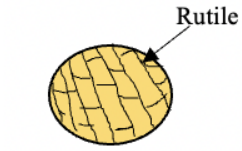	This form of pyrite occurs as pseudomorphs of non-sulphide grains that have been substituted by pyrite, they comprise of relict structures and compositions (England *et al.*, 2002; da Costa *et al.*, 2020).
Overgrowth pyrite 	Overgrowth of pyrite is found on detrital pyrite grains, giving rise to a core-rim structure (Guy *et al.*, 2014).
Infill pyrite 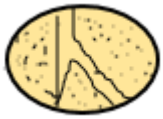	Pyrite infills fractures and primary pores of veinlets. Infill pyrite is low in trace element concentrations but is often linked with sphalerite, galena and electrum (Agangi *et al.*, 2013).

2.6 The Middelvlei Reef

Auriferous conglomerate reefs in the Basin have been delineated across seven goldfields that are situated alongside the eastern, western and northern edges of the basin (Fig. 2.1) (Tucker *et al.*, 2016). Generally, in each goldfield, usually between one or two major reefs present are interbedded with secondary reef units (Sibanye-Stillwater Limited, 2020). Within the Carletonville goldfield (Fig. 2.1), three principal orebodies are mined, the Carbon Leader Reef, Ventersdorp Contact Reef, and the Middelvlei Reef (Nwaila *et al.*, 2020). The Middelvlei Reef is found at the base of the Central Rand Group (50 – 75 m above the base), within the Carletonville goldfield (Fig. 2.3). The average dip of these reefs is approximately 35 to 35 degrees south/southeast. Reefs are laterally continuous and have clear patterns of mineralisation controlled by sedimentary characteristics (Sibanye-Stillwater Limited, 2021). In the Carletonville goldfield, the Middelvlei Reef is considered a secondary reef mined because it does not contribute a significant amount of ore within mining operations (Sibanye-Stillwater Limited, 2020).

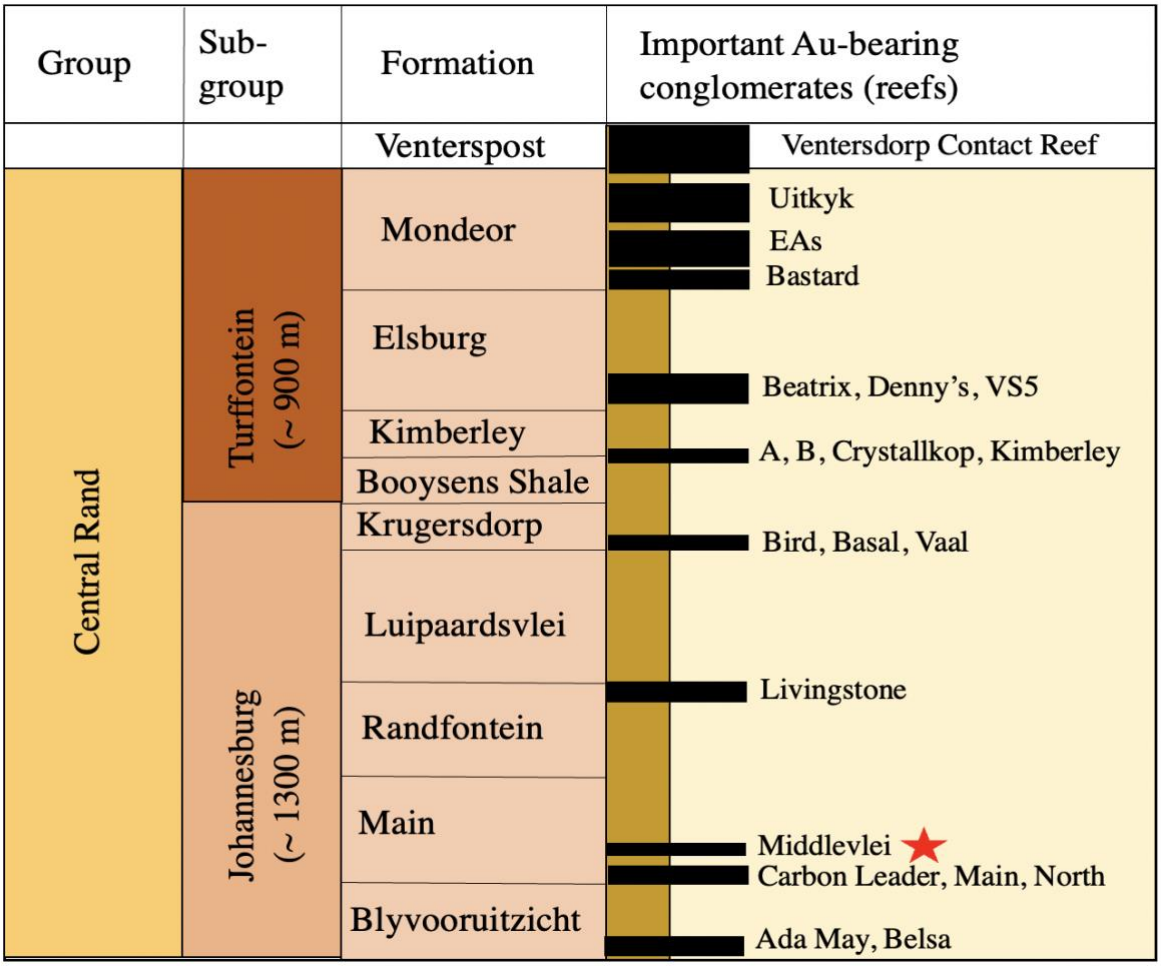

Figure 2.3: Simplified stratigraphic column of the Central Rand Group modified after (Jolley, 2006).

The Middelvlei Reef is a reef package that achieves a maximum thickness of 7m, multicyclic, and is characterised by auriferous quartz-pebble conglomerates, arenites, and mudstone laminae interbeds. Overall the reef is highly channelised in structure (Jolly, 1984b; Sibanye-Stillwater Limited, 2020). The reef is thought to correspond to a sedimentary alluvial fan as evidenced by cyclic fining-upwards sequences. The presence of gravel reflects high energy currents, and finer silt fractions reflect low-energy to still-standing water-flow conditions (Els, 1983; Sibanye-Stillwater Limited, 2020). The proposed palaeo-environmental model for the Middelvlei Reef is a prograding alluvial floodplain environment, where the tidal energy increased from west to east. The eastern side of the alluvial floodplain was characterised by a high-energy, braided fluvial plain dominated by coarse gravel (Sibanye-Stillwater Limited, 2014). The basal conglomerate units present in the reef are laterally continuous and display a decline in pebble size from east to west (Jolly, 1984a).

The Middelvlei Reef is comprised of: quartz, muscovite, and chlorite (Els, 1983; Myers *et al.*, 1993). The sulphide assemblage in the reef includes pyrite, minor chalcopyrite and pyrrhotite (Els, 1983). The reef has undergone extensive textural alteration in the form of sulphidation (Myers *et al.*, 1993), where iron sulphides have replaced sand /pebble-sized clasts in conglomerates as well as matrix material (Phillips *et al.*, 1990). The highest concentrations of gold are associated with large quartzite pebbles found in the basal unit of the Middelvlei Reef (Gm). The grade of gold decreases from east to west as the palaeo-environment changes (Jolly, 1984b). The following facies model (Table 2.3) has been developed at Driefontein operations owned by Sibanye-Stillwaters Limited. The lithofacies table describes sediments that preferably occur as fining upward sequences, with conglomerates commencing at the base, overlain by quartzite and terminating with siltstone lamina at the top layer (Els, 1983).

Table 2.3 Middelvlei Reef facies at the Driefontein operations. Details are summarised from Els (1983) and Jolly (1984b).

Middelvlei Reef facies table		
Facies code	Lithology	Lithological description and interpretation
Gm	Clast supported conglomerate	Conglomerates without any internal structures, less than 15 cm thick.
Gp	Planar cross-bedded conglomerate	Occurs rarely and only in solitary sets. These facies are deposited in migrating transverse bars.
Gt	Trough cross-bedded conglomerate	These facies represent minor channel fills which are like scour hollows.
St	Trough cross-bedded quartzite	Invariably pebbly and its origins are from migrating dune fields.
Sp	Planar cross-bedded pebbly quartzite	This facies occurs in solitary sets and contains pebbles. The facies formedin migrating waves and sand bars.

Fm	Massive siltstone	These facies occur as beds/laminae rarely thicker than 10 cm and are normally lenticular.

Recent studies done on the Middelvlei Reef at Driefontein operations simplified the litho-facies assemblages in Table 2.3 into two main litho-facies assemblages (below). The assemblages can be defined using the ratio of conglomerate to quartzite (as a percentage) as the main criteria. A second criterion is based on the thickness and type of basal Middelvlei Reef unit (Sibanye-Stillwater Limited, 2014). The two end members are:

- Facies type A: has a composite basal unit and multiple conglomerate beds, quartzite is sometimes present, and the thickness is > 80 cm.
- Facies type B: has a non-composite basal unit, attains < 25 cm in thickness, and is dominated by pebble lags.

Chapter 3: Literature review

The gold mining industry is constantly evolving, and as a result, the challenges associated with gold mining are becoming more prevalent and need to be investigated appropriately. Some of the key challenges include the: 1) mining of low-grade and complex ores; 2) high capital and operating costs; 3) complex environmental issues; and 4) tailings management, among others. The following chapter presents an overview of mineral processing and highlights the recent major advancements that have taken place in the gold mining industry to help mitigate the problem surrounding processing low-grade ores in the Witwatersrand Basin.

3.1 Overview of gold processing

Gold is an important commodity that has been mined throughout human history (Kongolo and Mwema, 1998). Gold mining started by gold panning from stream beds which involves manual or gravity-based separation methods (Burt, 1999). Beyond handpicking methods, modern advancements in gold mining began in the 1700s with the first underground mines in Russia (Bath *et al.*, 1973; Burt, 1999). Crushing, gravity concentration and amalgamation technologies were developed to help facilitate gold hydrometallurgy processes (Bath *et al.*, 1973; Kongolo and Mwema, 1998; Youlton *et al.*, 2021). In the 1800s a process to extract gold by chlorination was industrialised but needed to be more efficient in recovering gold from low-grade ores (Laplante and Gray, 2005). As a result, cyanidation technology was developed and patented in the late 1800s due to its success (Marsden and House, 2006; Marsden and Sass, 2014). Implementation of cyanidation technology to Witwatersrand gold ores facilitated the recovery of the mining industry in the 1890s, which was then experiencing a decline in production in 1890 due to the gold ore type transitioning from oxidised to sulphidic ores that contain copper, lead and zinc (Fivaz, 1988). Figure 3.1 presents a generalised flow sheet of a traditional gold mine operation plant which traditionally uses cyanidation. The flow diagram shows the different types of processing typically available to different processing scenarios that may take place when refractory ore, surface slime dams, ROM (run of mine) and surface rock dumps are being processed. A detailed schematic diagram of a mineral processing plant is attached in Appendix A.

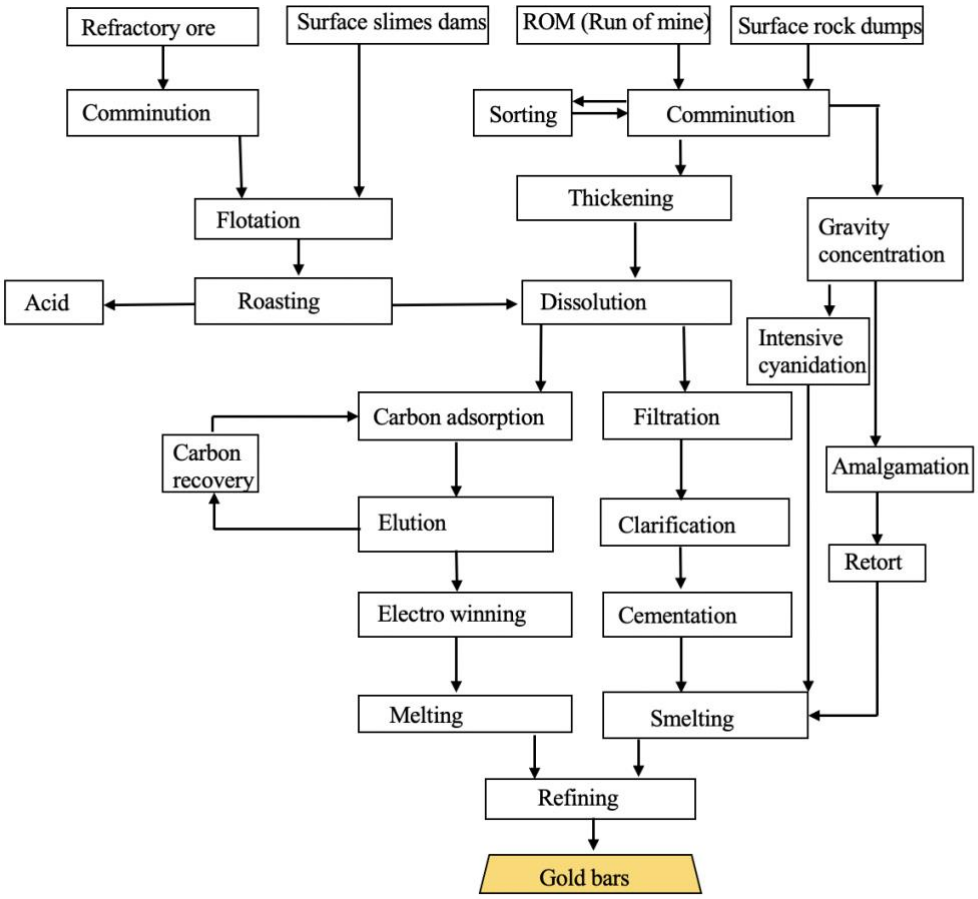

Figure 3.1: Simplified flow chart for gold processing. Modified after Cairncross and Anhaeusser (1992).

3.2 Cyanide as a reagent for gold leaching

Globally, cyanidation a common procedure applied in gold hydrometallurgy; a process used to extract gold in solution. Cyanide ($(\mathbf{CN})^-$) remains an inexpensive and highly efficient at liberating gold (Fivaz, 1988). Cyanide is commonly used in gold and silver extraction processes in the form of sodium cyanide (NaCN), with potassium cyanide (KCN) and calcium cyanide ($\mathbf{Ca(CN_2)}$) used in lesser extents (often to replace sodium cyanide). The chosen cyanide compound readily dissolves and ionises in water to form metal cations (e.g., $\mathbf{Na^+}$) and free cyanide ions ($\mathbf{CN^-}$) in solution (Nicol et al., 1992). Cyanide leaching is strongly dependent on pH of solution, being most effective at alkaline pH ranges between 9.5 - 11 (Stange, 1999; Marsden and House, 2006). Reagents such as lime and oxidants such as oxygen are added to the leaching system to enable gold leaching (Sparrow and Woodcock, 1995).

The overall leaching of gold can be denoted by the Elsner equation (Stange, 1999):

$$\mathbf{4Au + 8NaCN + O_2 + 2H_2O \rightarrow 4NaAuCN_2 + 4NaOH}$$

(Eq. 3.1)

During the reaction hydrogen peroxide (H_2O) is produced as an intermediate product and oxygen is reduced. Without cyanide present as a complexing agent, the oxidation of gold will result in the development of passivation layers in the form of oxide films on the surface of gold (Nicol, 1980; Tran, 1992). The liberation of gold is ordered by the movement of oxygen and cyanide ionic species via a diffusion membrane (Kudryk and Kellogg, 1954), as demonstrated in Fig. 3.2. The host minerals that may encapsulate the gold depends on the type of ore gold is present in.

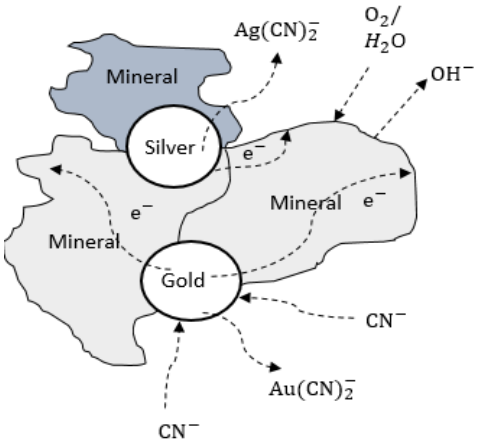

Figure 3.2: schematic diagram of gold dissolution modified after Kudryk and Kellogg (1954).

3.3 Mineralogical properties that influence leaching

Ore texture

Gold liberation is strongly influenced by ore texture. Ore texture refers to the mineral shape, size and the relationship (association) of the mineral of importance with ore minerals (Craig, 2001). A clear description of the ore texture is the first step in developing an ore treatment plan prior to gold extraction (Rees, 2000). The size of gold particles is of upmost importance for the efficiency of the recovery process. Specifically, coarse material (200 – 500 µm) will not be effectively leached and may become trapped upstream of the cyanidation circuit, and/or not carried by bubbles during froth flotation. The importance of the relationship with other ore minerals is best exemplified when ultra-fine gold (< 10 µm) is locked in sulphides and quartz (Fig. 3.3). In this case, the ore needs to undergo additional crushing and grinding to ensure that the surface area of the metal is exposed or liberated (i.e., accessible Fig. 3.3), ensuring a successful recovery during hydrometallurgical recovery (Sparrow and Woodcock,

1995). Native gold present in placer deposits is typically already liberated before processing (Zhou *et al.*, 2004).

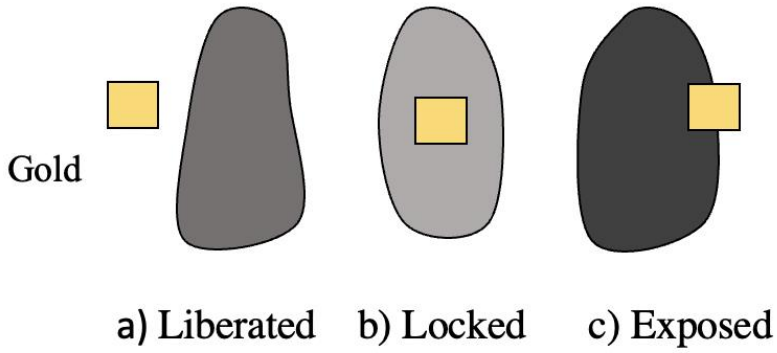

Figure 3.3: Schematic diagram of the different associations of gold with ore minerals Gold is represented as the yellow square. Illustration modified from Khalesi et al., (2009).

Chemically or refractory gold

Chemically locked gold or refractory gold is typically incorporated into the lattice structure of sulphide minerals that are rich in arsenic such as arsenopyrite and arsenian pyrite (Chen *et al.*, 2002). Chemically locked gold is often referred as 'invisible gold' because the gold cannot be detected by optical microscopy or via the scanning electron microscope (Chen *et al.*, 2002). The substitution of gold into the lattice of sulphide minerals such as pyrite, arsenian pyrite and arsenopyrite is facilitated by the presence of arsenic (Cook and Chryssoulf, 1990). Refractory gold is difficult to recover by conventional cyanidation and therefore needs to undergo pre-treatment by pressure-oxidation or roasting to destroy the host phase encapsulating the gold (Zhou *et al.*, 2004; Goodall and Scales, 2007). Gold tellurides, aurostibnite and maldonite are also considered refractory due to their slow dissolution during cyanidation (Zhou *et al.*, 2004).

Reactive gangue mineralogy

Gold leaching by a lixiviant is also accompanied by the simultaneous leaching and recovery of gangue minerals. These side reactions have the unfortunate result of oxygen and cyanide depletion in the system (Asamoah and Amankwah, 2014). Species in the system that diverge cyanide to form non-valuable complexes (gangue) and consume the oxygen in the system are known as 'cyanicides', and include

mineral species such as sulphides, sulph-arsenides and species enriched in Cu, S, Zn, Fe (Fraser *et al.*, 1991; Hausen, 2000; Petre *et al.*, 2008; Asamoah and Amankwah, 2014). Oxygen may also be consumed in the system as a result of minerals that tend to oxidize such as pyrrhotite (Fraser *et al.*, 1991). Additionally, the elements Cu, Zn, Pb, As and Sb can undergo reaction with cyanide to create metal cyanide complexes, subsequently resulting in cyanide consumption in the leaching system and leads to environmental issues (Goodall and Scales, 2007).

Preg-robbing by carbonaceous material

Preg-robbing is a phenomenon that happens when the gold cyanide complex, $\mathbf{Au(CN)_2^-}$, is robbed from the solution by components present in the ore, hence reducing the gold recovery level (Rees, 2000). The carbonaceous material causes two types of difficulties during ore processing, namely: a) the carbonic material can exhibit refractory behaviour by locking a proportion of gold and thus hinder leaching; and/or b) active carbon present in the ore acts as an adsorbent in the leach solution by adsorbing gold from the pregnant leach solution (Adam *et al.*, 2014).

Preg-robbing by other minerals/materials

Apart from carbon, other preg-robbing minerals/materials in Witwatersrand ores include pyrophyllite and shale (Zhou *et al.*, 2004). The first studies done on preg-robbing materials were performed on heavy minerals (U-bearing minerals) contained by the Witwatersrand reefs which showed preg-robbing characteristics (Urban *et al.*, 1973). Materials identified as refractory include: pyrophyllite, pyrite, khaki shale and thucholite, with the heavy minerals showing the greatest adsorption of gold in comparison to clay minerals (Urban *et al.*, 1973). Gold adsorption from materials is revocable and is a function of cyanide concentration, pH and temperature (Rees, 2000). Clay minerals such as illite, kaolinite, and montmorillonite are also preg-robbing but to a lower degree in comparison to carbonaceous material (Zhou *et al.*, 2004).

Galvanic interactions

Gold recovery can also be reduced and/or retarded during leaching by the development of insoluble coatings on the surface layer of gold particles (Marsden and House, 2006). The presence of a passivating layer or coatings arises due to an increase in a cathodic current (Lorenzen and Van Deventer, 1992). Coatings can occur in the form of sulphides, oxides or metal-cyanide complexes on the surface layer of the mineral (Lorenzen and Van Deventer, 1992; Azizi *et al.*, 2011). This is a particular issue because gold is often associated with several conductive minerals in an ore, such as pyrite, chalcopyrite, galena, pyrrhotite, arsenopyrite and sphalerite, among others (Rees, 2000). Galvanic interactions arise because

of the difference in electrochemical reactivity between gold and the conductive minerals, thus causing the development of coatings (Marsden and House, 2006). Gold surface passivation increases in the system as pH becomes more alkaline (Bagotsky, 2005).

The occurrence of sphalerite, chalcopyrite, stibnite, and chalcocite in the ore results in poor recoveries of gold (Azizi *et al.*, 2011; Asamoah and Amankwah, 2014). Chalcocite and chalcopyrite consume cyanide during leaching leading to the formation of hydrosulphide resulting in the creation of a passivating film around gold, leading to the poor dissolution of the mineral during leaching (Azizi *et al.*, 2011). Stibnite forms a passivating film of antimony oxide around gold that also results in poor dissolution (Deschenes *et al.*, 2000). Chalcopyrite, pyrite, and pyrrhotite are responsible for causing the largest decrease of gold being leached (Lorenzen and Van Deventer, 1992). Studies have established the presence of lead minerals (i.e., lead oxide, lead sulphide, and lead sulphite), improves the recovery of gold during leaching (Deschenes *et al.*, 2000).

i) Pyrite

The consequence of pyrite on leaching is highly dependent on the ore mineral's morphology, concentration, and distribution. Specifically, when ore contains a concentration of fewer than 10 % of pyrite, leaching is not impacted. However, when the ore contains a concentration of more than 20 %, the rate of gold extraction is reduced (Liu and Yen, 1995; Guo *et al.*, 2004).

ii) Pyrrhotite

Pyrrhotite being problematic during leaching is dependent on the concentration and the form (magnetic or non-magnetic) in which the mineral is present. Both forms of pyrrhotite are problematic for leaching when present. However, the magnetic form of pyrrhotite is acknowledged to be an oxygen-consumer (Becker *et al.*, 2010).

iii) Chalcopyrite

The dissolution of copper present in chalcopyrite during gold cyanidation is undesirable because it results in the consumption of oxygen and cyanide (Dai and Jeffrey, 2006).

iv) Galena

Galena is oxidised to thiocyanate, which produces lead ions. These ions then precipitate to form lead-hydroxide, reducing cyanide's efficacy and restricting extraction rates (Guo *et al.*, 2004). When chalcocite is present, the addition of galena as a source of lead helps improve the recovery of gold (Dai and Jeffrey, 2006).

3.4 Non-cyanide reagents

Cyanide has been used for more than a century to extract gold from ores (Adams, 2016). Cyanidation is the preferential leaching method because it is easy to handle, low production cost, and low consumption of reagents. However, cyanidation presents shortcomings due to the chemical being notably hazardous to the environment (Chao *et al.*, 2021). A string of environmental catastrophes at several gold mines around the world have raised apprehensions over the use of cyanide. Cyanide is not a persistent toxin but is lethal in high concentrations as the CN^- ion tends to react with chemical agents and molecules to form hundreds of compounds which may be fatal to fauna and flora (Moran, 2001). Attempts have been made to address the issues surrounding the toxicity of cyanidation by proposing various alternatives. The industry is now tasked with the challenge of developing environmentally friendly lixiviants for the gold extraction (Hilson and Monhemius, 2006). Developing an alternative lixiviant is difficult as it needs to meet a large number of criteria, including: 1) low toxicity, 2) low capital costs, 3) low emissions, 4) low extraction costs, 5) safe handling, 6) low environmental toxicity, and 7) low detoxification costs (Hilson and Monhemius, 2006). Numerous alternatives have been proposed, and these include, but are not limited to the lixiviants presented in Table 3.1.

Table 3.1: A summary of some of non-cyanide lixiviants that have been developed to replace cyanide for gold extraction (Senanayake, 2004). A total of 25 have been proposed. The most popular ones are listed below.

Ligand	Complex
Chloride	$AuCl_2^-$
Bromide	$AuBr_2^-$
Iodide	AuI_2^-
Ammonia	$Au(NH_3)_2^+$
Thiourea	$Au(SC(NH_2)_2)^+$
Glycinate	$Au(NH_2CH_2COO)_2^-$
Thiosulphate	$Au(S_2O_3)_2^{3-}$

Thiosulfate has been deemed the most viable, environmentally friendly lixiviant that has been extensively researched over the past few decades due to its high efficiency in recovering gold (Oraby *et al.*, 2020; Wang *et al.*, 2020). Thiosulfate is commonly used in the gold mining industry as a substitute to cyanide leaching due to the low toxicity and high efficiency (Altinkaya *et al.*, 2020). The lixiviant is non-toxic, and affordable and displays great efficiency in leaching carbonaceous- and copper- bearing gold ores (Sitando *et al.*, 2015; Wang *et al.*, 2020). Conversely, thiosulfate has limitations such as restricted recyclability, pH sensitivity and complexity in its use (Muir and Aylmore, 2004).

The environmentally friendly reagent of choice for this research project is glycine. The lixiviant glycine has a high attraction for gold and presents many attractive advantages, including that it is; 1) the reagent is reusable, 2) recyclable, 3) non-toxic, 4) affordable, and 5) non-volatile (Eksteen and Oraby, 2015; Tanda *et al.*, 2017; Oraby *et al.*, 2020). The curiosity in the solubilisation of gold by organic acids has been experimented in studies conducted by Brown *et al.*, (1982) and Zhang *et al.*, (1996). Glycine presents numerous benefits in comparison to cyanide and its substitutes such as thiosulfate, thiocyanate, thiourea, and halides; namely, glycine is stable over various Eh-pH values and is easier to handle in comparison to thiosulfate (Altinkaya *et al.*, 2020). The lixiviant also has a high affinity for gold and the dissolution of Al, Si, Fe, and Mn in glycine- concentrated solutions is negligible. This serves as an important advantage because Fe is a common impurity present in cyanide-free leaching and is known to be problematic for downstream processing (Altinkaya *et al.*, 2020).

3.5 The glycine leaching system

Glycine is an amino acid with a carboxylic group and an amine group, the molecular formula of the acid is NH_2CH_2COOH. Glycine is an α-amino acid (Fig. 3.4) and is categorised by a carboxyl group (COOH), an amino group (NH_2) and a side group (R) that is site-specific to a particular amino acid. The solubility of gold has been studied in different amino acids, and gold dissolution in thiosulfate solutions is significantly enhanced by the presence of amino acids (Feng and Van Deventer, 2011).

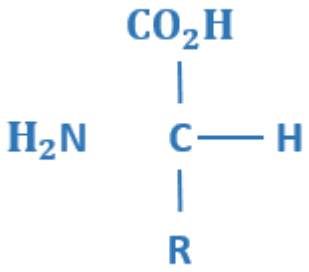

Figure 3.4: Basic structure of an amino acid.

An amino group and carbo carboxyl group renders glycine amphoteric, meaning that the amino acid can occur as either an acid (proton donor) or a base (proton acceptor) when suspended in water (Tauetsile, 2019). Glycine exists in three different forms in aqueous solutions, these forms are namely the: 1) cationic, 2) zwitterion, and 3) anionic forms (Aksu and Doyle, 2002). The zwitterion form (Fig. 3.5) is the most stable in solution, and in this state, glycine consists of both a positive and negative charge in a balanced ratio, resulting in the net electric charge of the molecule being zero (Hoyau *et al.*, 2001). The zwitterion state predominantly exists in a pH range between 2.35 to 9.78 (Tauetsile, 2019).

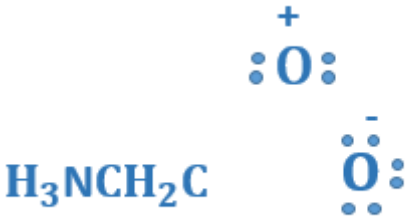

Figure 3.5: The zwitterion state of glycine.

At a pH below 6, the amino acid glycine, is in a protonated form, with a surplus of $\mathbf{H}^+$ ions in solution, that are easily attracted to the negatively charged carboxylate, imparting a positive charge on the amine group (+1) (Fig. 3.6) (Tauetsile, 2019).

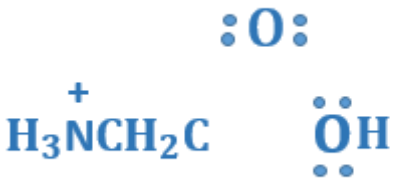

Figure 3.6: Positively charged glycine ion.

However, at a pH above 6, excess $\mathbf{OH^-}$ ions in the solution are attracted to and become attached to the amine group and subsequently resulting in the loss of $\mathbf{H^+}$. Resulting in an amino group carrying neutral charges and the total charge of the molecule being negative (Fig. 3.7) (Tauetsile, 2019).

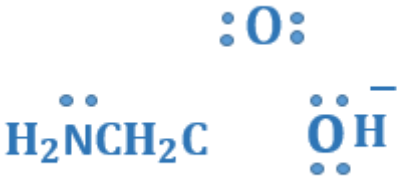

Figure 3.7: Negatively charged glycine ion.

Glycine is a chemical that is widely used in different productions. Due to its zwitterionic nature, the amino acid displays aqueous solubility in water at room temperatures and is attracted to dipolar water molecules (Yang *et al.,* 2008). Elevated temperatures result in the decomposition of glycine in oxidising environments. However, decomposition of glycine has also been noted to take place at temperatures lower than its reported melting point 200-300℃ (Yablokov *et al.*, 2009).

3.5.2 Glycine leaching of gold

Glycine as a lixiviant in gold hydrometallurgy has been investigated in studies such as Liedberg *et al.,* (1984) and Oraby *et al.,* (2014). The recovery rate of gold using glycine is slow in comparison to cyanide, but shows potential for use in heap, dump and in-situ operations (Oraby *et al.*, 2020). Improvements in the glycine leaching system include a blend of high temperature and high pH, but the rate is still slow without cyanide in the system (Eksteen and Oraby, 2015; Tanda *et al.*, 2017). Studies on gold leaching with glycine and thiosulphate-EDTA found that using glycine as a reagent was faster than thiosulphate (Tauetsile, 2019). Adding silver to glycine leaching solutions enhanced the gold leach rate by six times, and strong bonds between the amino acid and gold were formed (Pakiari and Jamshidi, 2007). The reaction of gold and glycine is described by the equation:

$$4Au + 8NH_2CH_2COOH + 4NaOH + O_2 \rightarrow 4N[Au(NH_2CH_2COO)_2] + 6H_2O$$

(Eq. 3.2)

As shown in Equation (3.2), oxygen plays an important part during the formation of the gold glycinate complex. Thus, oxidants are necessary during gold leaching (Oraby *et al.*, 2020). The use of an alkaline glycine leaching system with an elevated temperature of 60° C, oxygen used as an oxidant, 1.25 M glycine, pH of 12, and a high stirring rate (900 rpm), produced a gold recovery of more than 90% (Altinkaya *et al.*, 2020). However, using an aerated alkaline glycine leaching via the bottle-roller method with a hole to allow oxygen to reach the solution with 15 M glycine, a pH of 12.5 and a temperature between 23 - 65°C resulted in a gold recovery of 85% gold after 336 hours (Oraby *et al.*, 2019).

3.5.3 Parameters that influence glycine leaching

Glycine concentration

Experiments were done by Altinkaya *et al*., (2020) and Oraby *et al.*, (2020) reported that the highest concentrations of gold were recovered with higher concentrations of glycine were used during leaching (Altinkaya *et al.*, 2020). Concentrations from as high as 1.5M (molarity) start producing results that are feasible for gold extraction.

Effect of an oxidant

Potassium permanganate has been suggested to be the most effective oxidant for glycine leaching systems in comparison to hydrogen peroxide, sodium chlorate, and potassium iodide (Oraby *et al.*, 2020). Gold recovery levels significantly decreased when too much permanganate is used as a catalyst, caused by the oxidation of glycine, however, the loss of glycine can be accounted for by adding more glycine to the system (Oraby *et al.*, 2020). Potassium permanganate is oxidant of choice in this optimisation study. Permanganate oxidation of amines and amino acids has received special attention due to the autocatalytic nature of these reactions (Perez-Benito *et al.*, 1986). For this reason, it was selected in combination with glycine in this study. The reaction of gold in a glycine-permanganate system, expressed by the equation below:

$$Au + 2MnO_4^- + 4(NH_2CH_2COO)^- + O_2 \rightarrow 2Au(NH_2CH_2COO)_2 2MnO_2 + 2C_2O_4^{2-} + 2NH_3 + 2OH^-$$

(Eq. 3.3)

Effect of pH

Hydrometallurgical processes are performed in solutions that contain $\mathbf{H^+}$ and $\mathbf{OH^-}$, and are subsequently dependent on pH. Gold dissolution intensifies by increasing the pH to a higher alkalinity as alkaline pH solutions are most favourable for gold dissolution in glycine. This effect is a result of hydroxide radicals accelerate the rate of gold dissolution (Nowicka *et al.*, 2010).

Effect of temperature

Temperature is a important consideration in gold dissolution kinetics, where gold dissolution increases dramatically with an increase in temperature (Eksteen and Oraby, 2015). This is attributed by the rate-determining step for gold dissolution, is reaction rate constant K, and it is related to temperature (T) (McLaughlin and Agar, 1991). This can be explained by the Arrhenius equation, whereby the rate constant (K) is strongly dependent on temperature (T), whereby:

$$\mathbf{K = Ae}\ \frac{\mathbf{-E_a}}{\mathbf{RT}}$$

(Eq. 3.4)

Where A corresponds to an experimental constant, $\mathbf{E_a}$ is the activation energy (dissolution) and the universal gas constant R (McLaughlin and Agar, 1991).

Chapter 4: Methodology

The following chapter is sectioned into three main divisions that detail the analytical procedures used in this study. Section 4.1 explains the methodology used to obtain and prepare representative underground ore samples. Section 4.2 details the analytical equipment used to conduct the mineralogical and chemical analyses. Lastly Section 4.3 details the metallurgical test work conducted in this study.

4.1 Sampling and sample preparation

Representative samples were acquired from the Middelvlei Reef, which is in the Carletonville goldfield, ca. 70 km west of Johannesburg (South Africa; Fig. 2.1). Underground samples were amassed from the Driefontein mine, owned and operated by Sibanye-Stillwater Limited. While sampling, the differences between the various facies of the Middelvlei Reef were also investigated (i.e., lithologies, ore textures and mineralogical assemblages). The selected samples for this project have no spatial constraints. Large samples (20 kg) were provided from the mine.

Polished sections (ore blocks) of coherent whole rock material were cut to size using a diamond saw for the examination, identification and textural interpretation of ore minerals using reflected light microscopy, scanning electron microscope (SEM-EDS), Tescan integrated mineral analyser (TIMA) and Micro X-ray computed tomography (Micro-XCT). Ten samples were used (S1 - S10) and an extra subset were also used (P1- P4) because they showed interesting features, for TIMA. The same samples were used for SEM, TIMA and Micro-XCT. Samples were then crushed, milled and sub-sampled for subsequent laboratory analyses. The samples were crushed by means of a jaw crusher at the University of the Witwatersrand. Between samples, both the crusher, the mill, work bench and collection basket were wiped and cleaned to minimise any contamination between samples. The jaw crusher was also vacuumed to remove any impurities that could not be removed by wiping. A portion (10 kg) of the crushed sample was split using the coning and quartering method. The split samples were pulverised using the TS-250 mill, manufactured by Dickie & Stockler and hosted at the University of the Witwatersrand. Samples were milled to ≤ 75 µm in size to provide adequate exposure of gold for bottle roll leaching experiments (Marsden and House, 2006; Coetzee *et al.,* 2011). Crushed and milled split samples were collected for and sent for X-ray fluorescence (XRF), X-ray diffraction (XRD), inductively coupled plasma-mass spectrometry (ICP-MS), and fire assay analyses.

4.2 Analytical equipment used for mineralogical and chemical investigations

4.2.1 Reflected light microscopy

A total of ten polished ore blocks were made for mineral and textural identification. The mineral assemblages, gold particles, and mineral textures were identified using an Olympus BX53M/DP74 microscope in the University of Witwatersrand School of Geosciences.

4.2.2 Scanning electron microscope – energy dispersive spectroscopy (SEM-EDS)

Ten samples that showed strong mineralisation (e.g., abundant pyrite and visible gold) using reflected light microscopy were selected for imaging using a Zeiss EVO® MA15 Scanning Electron Microscope, located at the School of Chemical and Metallurgical Engineering, University of the Witwatersrand. Selected samples were glazed with a carbon film before any analytical work was done. Samples were imaged to identify mineral morphologies (especially pyrite), gold species (electrum), and phases that were too complex to be identified using reflected light microscopy. The operating conditions that were used to conduct these analyses were an operating voltage = 20 Kv, working distance = 8.5 mm, acquisition time = 30 seconds and a magnification that ranged between 100 – 800 X. Back-scatter electron (BSE) images coupled with X-rays were collected using electron dispersive energy.

4.2.3 X-ray fluorescence spectrometry (XRF)

XRF major elements

Major and minor element oxides were determined via XRF at the School of Geosciences, University of the Witwatersrand. A 0.35 g ration of the sample was fused with 2.0 g of Johnson Matthey Spectro flux at 1000 °C. The fused samples were then evaluated using the Panalytical Axios X-ray spectrometer at the operating conditions of 50kV and 50 mA. Primary data (raw) was rectified using in-house software. Standard calibrations using 12 reference materials, include synthetic oxide mixtures and international standard rocks, as well as in-house controls. Precision is 1 % for elements in abundance of greater than 5 wt.%.

4.2.4 Quantitative X-ray diffraction (QXRD)

Approximately 5 g of milled samples were couriered to XRD Analysis and Consulting in Pretoria. The XRD analyses were used to determine the bulk modal mineralogy of the Middelvlei Reef by identifying

the crystalline phases in the sample. The sample powders were evaluated with a Panalytical Aeries diffractometer that has a PIXcel detector and fixed slits with Fe-filtered Co-Kα radiation. Phase identification of the different phases in the reef was performed using the Bruker Eva V4.1 software. This was followed by quantifying the phases identified using the Bruker Topas V4.1 software, based on the Rietveld method. The lower detection limit of this method ranges between 0.5-2 wt. %, dependent on the minerals and their respective crystal structure.

Quantitative X-ray diffraction (QXRD) is a technique also used to validate and support the mineralogical data generated by TIMA. The modal abundances of the minerals identified by TIMA were compared to the modal mineral abundances quantified by QXRD, and the results show a strong correlation. QXRD determines the bulk modal mineralogy of the entire ore and uses a detection limit, the detection limit varies according to the mineral's crystallinity and how the XRD instrument was set up for analyses. Samples selected for TIMA analyses were selected from areas of interest, whereas results generated from QXRD are representative of the entire ore. TIMA modal mineralogy results produced a higher modal abundance for pyrite due to sampling selection, samples with areas of pyrite mineralisation were selected for analyses.

4.2.5 Inductively coupled plasma mass spectrometry (ICP-MS)

Trace elements were analysed at the University of the Witwatersrand using a Thermo Scientific iCAP RQ ICP-MS instrument. Samples were first digested using the open beaker/hotplate method. First, 50 mg of the sample was placed into a 15 ml savilex beaker with 3 ml of ultra-high purity 2:1, HF: HNO_3 acid. The beaker was then placed on a hotplate for 70˚C and left to evaporate. Once dry, 3 ml of HF: HNO_3 was added. The beaker was then capped and placed on the hotplate at 70˚C for 72 hours. The sample was then dried down at 70˚C and 3 ml HNO_3 was added. The solution was then allowed to evaporate. The solutions were then diluted to 50 ml (dilution factor 1:1000) with 5 % HNO_3, 100 ppb Re and Rh. Both Re and Rh were added to monitor the accuracy and precision of the data. Fluorides were minimised by preventing contact between the sample and HF while still accomplishing the total digestion. Samples are visually inspected for fluorides which occur as a precipitate once samples are diluted.

Calibration Standards were made at 5 different concentrations (10, 30, 50, 75 and 100 ppb) with all the elements to be analysed present (40 elements). The standards were purchased from the International Certified Reference Materials. Three total procedure blank (TPB) samples, corresponding to a sample that has undergone digestion but has no sample material present, were analysed to quantify contamination. All data is TPB subtracted.

4.2.6 Gold fire assays

Head samples (10 sample bags) were leached were sent to SGS laboratories in Randfontein to determine gold ore grade via lead collection gold fire assay. The samples were first weighed and mixed in a fluxing agent and smelted, wherein 15-20 drops of lead were injected as a collector. The sample with the added collector was then heated in a furnace at 1000 °C. The blend produced was poured into an iron mould wherein the silicate slag floats to the surface, and the lead which alloyed with the precious metals, descends to the base, and forms a 'button'. This button contains precious metals which have formed and is then extracted by a process called cupellation.

4.2.7 TESCAN TIMA

Ore blocks that showed high concentrations of mineralisation (e.g., abundant pyrite and visible gold) were also selected for TIMA analysis. These ore blocks underwent carbon coating prior to conducting any analyses. The samples were measured by energy-dispersive X-ray spectroscopy (EDS) using the VEGA3 X64 TESCAN SEM instrument and the VEGA3 X64 TESCAN TIMA 2.4.0. software, housed at the University of the Witwatersrand. The beam operating settings during quantitative analyses on the VEGA3 X64 TESCAN SEM were 25 kV accelerating voltage, 43 µA emission current, a working distance of 15 mm, a specimen beam current of 17.68nA and a spot size of 590.00 nm with an absorption current of < 1 pA. TIMA high-resolution mapping method (THRM) was used to perform automated mineralogical analysis of the Middelvlei Reef samples. The BSE images were initially taken at a high resolution to identify the margins between mineral phases. The selected mineral phases were thereafter digitised with a low-resolution X-ray point mesh for EDS measurements. Areas with analogous BSE and EDS values were immediately segmented, and mineral phases were routinely defined based on these signatures.

Data cross-validation

Data cross-validation was performed by comparing TIMA against XRF results in excel. The XRF methodology employed in this study follows immediately below. The XRF analysis provides the geochemistry (major and minor element oxides) of the ore, whereas TIMA uses the element-to-mineral conversions (EMC) calculations to determine the ore mineralogy. Due to sampling bias, iron and silicon have been removed from the graph to avoid outliers (Fig. 4.1).The graph was formulated in excel by plotting the points against each other and ensuring that the y and x axis showed uniform units to ensure accuracy. Specifically, samples selected for TIMA analysis solely focused on areas with sulphide

mineralisation. Acceptable correlations were drawn between the major and minor elements of TIMA and XRF results, providing confidence that the data produced by TIMA have a high confidence level of accuracy.

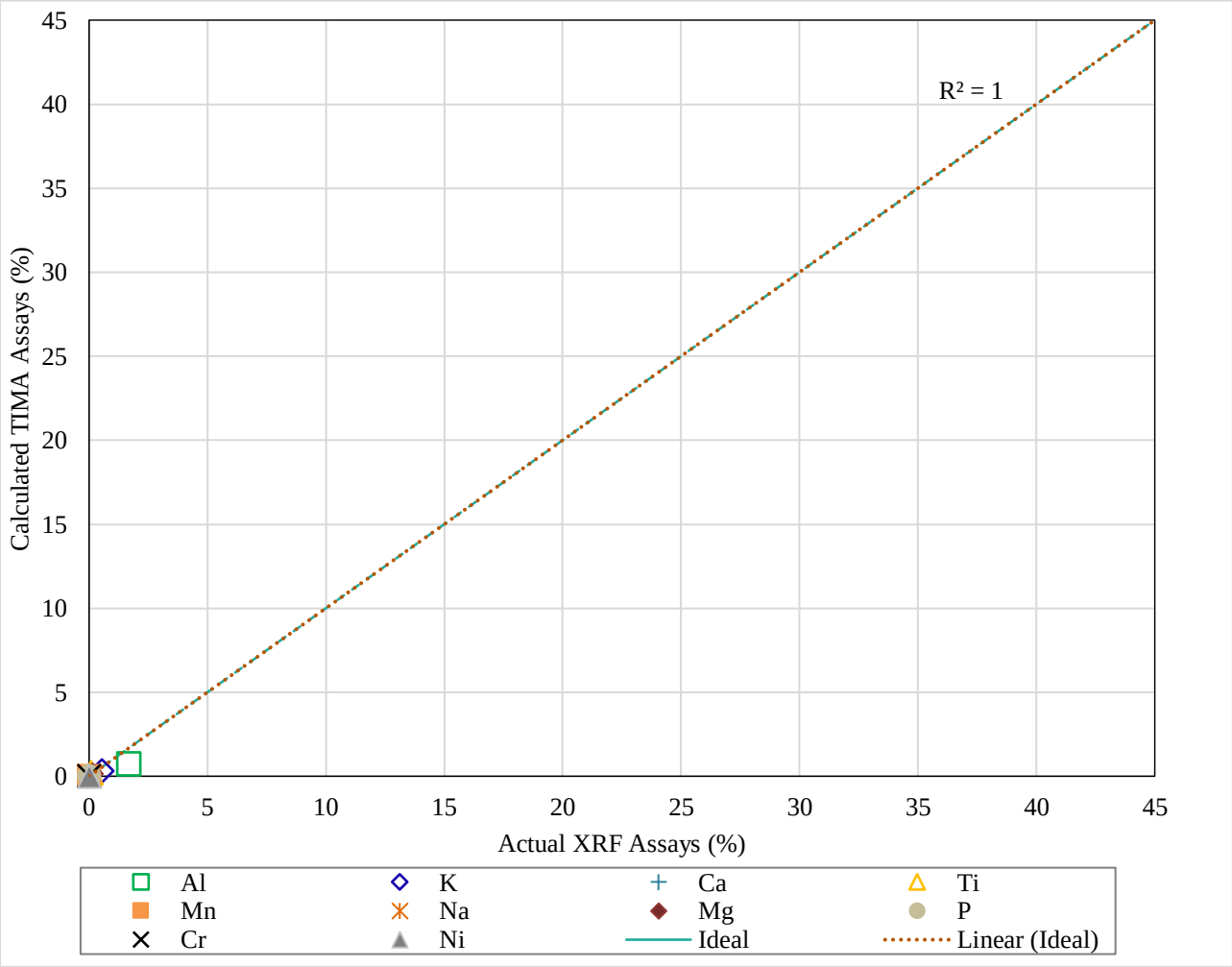

Figure 4.1: Major and minor elements validation using XRF assays against calculated TIMA assays.

4.2.8 Micro X-Ray computed tomography (Micro-XCT)

The NIKON Micro X-ray computed tomography MIXRAD system at the South African Nuclear Energy Corporation (Necsa) was utilised to conduct the analyses. Micro-XCT was used to characterise ore texture and identify the mineralogy present in the Middelvlei Reef in nine selected ore blocks. The scanning parameters used in the study are presented in Table 4.1.

Table 4.1: Micro-XCT scanning parameters used to acquire data

Voxel size (resolution)	16.13 um
Number of projections	2000
X-ray energy	180 kV
Beam current	56 uA
Scan duration	45 min

The Micro-XCT scanned data was reconstructed using the VG Studio Max software (version 3.2) at Necsa. Image reconstruction and phase segmentation process was conducted on mineral phases to extract the region of interest (ROI) using histogram rendering. A defect analysis (Appendix B) was conducted on the ROI of selected phases to provide a report on the grain characteristics and other scanning parameters.

Image reconstruction and phase segmentation

Image reconstruction is a mathematical process used to convert the raw Micro-XCT data into images called 'slices' (Fig. 4.2A) (Kyle and Ketcham, 2015). The reconstruction software allows for a reconstruction transformation of raw Micro-XCT data. Image reconstruction was performed using software called CT Pro 3D. The software allows for both the optimisation of contrast and minimisation of noise (Bam *et al.*, 2020). Image reconstruction needs to be done before any analysis can take place using VG Studio Max. The image reconstruction process is simple, to perform an image reconstruction, the specimen needs to be in a 360° view. An .xtctet file (raw data) with all the information about the sample is opened in the CT Pro 3D software wherein the slices are created by following three simple steps in the software, namely (Fig. 4.2B): 1) centre of rotation – where the image accuracy is calibrated to a high-quality; 2) setup – an option called beam hardening is selected and configured, beam hardening is the most important artefact in XCT images which prevents qualitative measurements due to poor contrasts between minerals; 3) calibration – this step was skipped, as no further calibration needs to be done; and 4) volume rendering – a 16 bit tiff image is created that is in full range of view.

Figure 4.2: A) Raw CT data before conversion into slices. B) A screenshot of the image reconstruction process from the CT Pro 3D software.

Several databases are available to calculate the X-ray attenuation of numerous minerals. Examples include the XCOM database developed by Kyle and Ketcham (2015), as well as the database developed by Bam *et al.* (2020). The ore blocks from the Middelvlei Reef scanned with Micro-XCT technology were also scanned with TIMA to discriminate the ore mineralogy accurately. Multiple studies have proved that Micro-XCT does not discriminate ore mineralogy in detail in comparison to TIMA, especially for minerals with attenuation co-efficient values that are too small. The excel database created by Bam *et al.* (2020) was used to calculate the X-ray attenuation of minerals detected by TIMA in the Middelvlei Reef.

Mineral identification

The minerals present in the Middelvlei Reef were determined by X-ray attenuation coefficient values, which produced a specific grey-scale value for each mineral. The incidence of X-rays with minerals is dependent on the mineral density, thickness, and atomic number (Bam *et al.*, 2020). Therefore, when the density variation amongst minerals in the sample is considerable, the X-rays beams will produce distinctive grey scale values to discriminate minerals from each other. However, due to low-grade ores showing an increased complexity in mineralogy due to alteration and weathering, the best way to identify minerals would be to use a database that contains different mineral attenuation coefficients. The attenuation coefficient values of the minerals as a function of X-ray energy, identified in the Middelvlei Reef are presented in Figure 4.3.

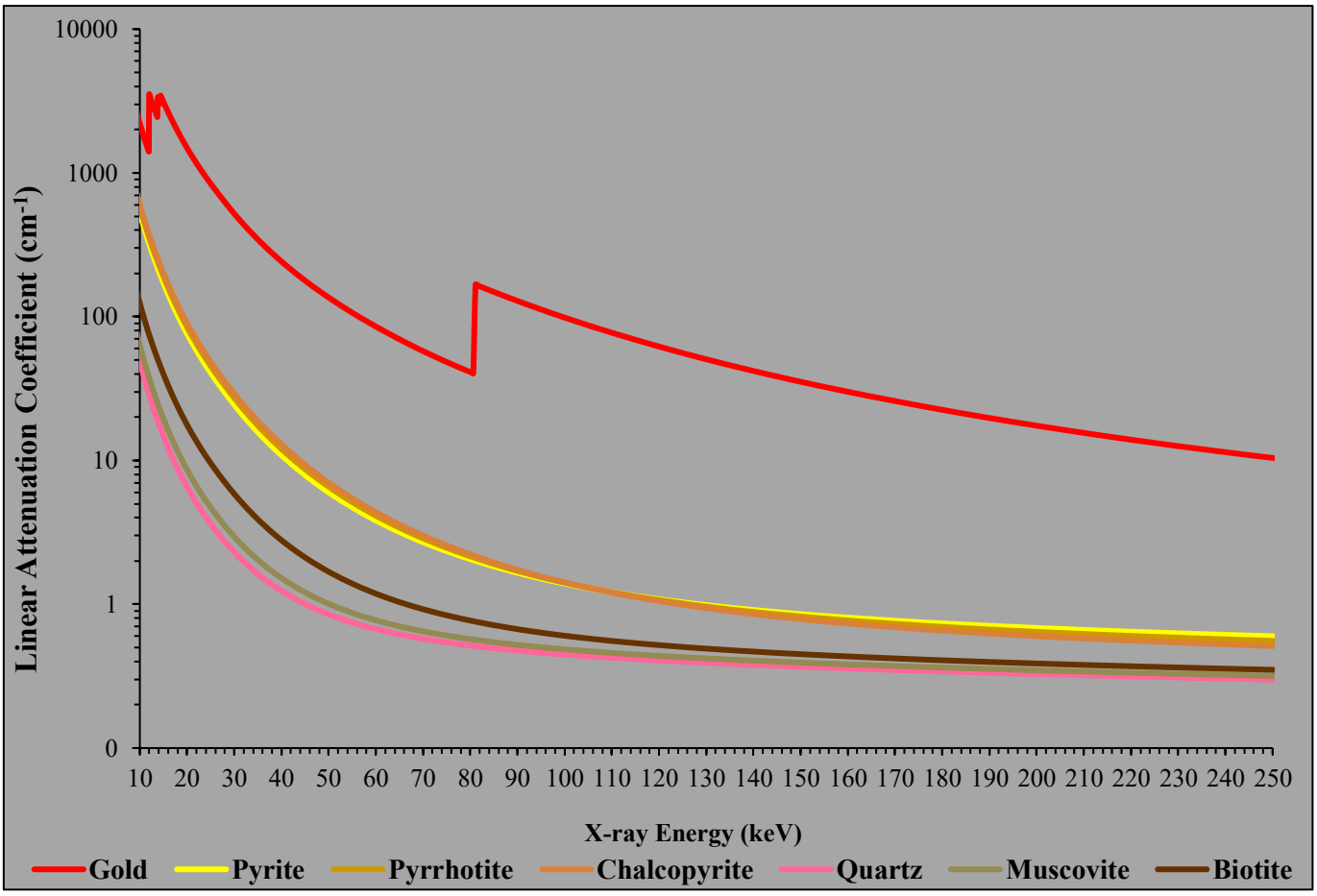

Figure 4.3: Linear attenuation coefficients of different minerals encountered in the Middelvlei Reef as a function of X-ray energy, using the XCOM database. Modified after Kyle and Ketcham (2015).

Table 4.2: The modal mineralogy of the Middelvlei Reef determined by TIMA phase maps. Mineral density and attenuation coefficients are those from Bam et al., (2020) and the density information of certain minerals were obtained from http://www.webmineral.com/.

Mineral name	Modal wt. %	Density (g/cm^3)	Attenuation coefficient (cm^{-1})
Quartz	84.60	2.65	0.64
Pyrite	6.12	5.01	3.48
Muscovite	3.16	2.82	0.94
Chlorite	0.42	2.95	0.73

Rutile	0.29	4.23	
Biotite	0.25	3.09	
Zircon	0.05	4.71	8.26
Chromite	0.03	4.79	3.42
Pyrrhotite	0.02	4.61	3.56
Kaolinite	0.02	2.65	0.85
Chalcopyrite		4.19	3.78
Gold		19.30	

Mineral phases with different grey values and attenuation coefficients from each ore block were segmented using VG Studio Max 3.5.1. This software allows for phase segmentation by using histograms to select regions of interest (ROI). The segmentation method applied for each ore block was similar due to the mineralogy being consistent throughout each ore block of the Middelvlei Reef. High-density minerals tend to be favoured over lower-density ones, creating an issue when discriminating between minerals. To overcome this, careful segmentation with grey values was used. Phase segmentation is an intricate process and needs to be done with great detail to avoid the overestimation of gold and gangue mineralogy as this will have a negative impact on the predictive model for mineral processing. The background in the image stack or 'slices' that are imported into VG studio Max needs to be defined first before grey values are selected.

A range of grey values are selected to define each mineral phase present. The highest grey value present is 65,535.0. The range of grey values used to select gold was an upper limit of 65,535.0 and a lower limit of 3029.0. Once the range of grey values was selected for gold, the rutile phase was identified and had grey values between an upper limit of 30,285.0 and a lower limit of 13,000.0. The following phase was identified as pyrite, the upper limit of 12,897.0 and lower limit of 11,017.0. The last phase identified are the silicates, which have an upper limit of 11,000.0 and a lower limit of 0. As mentioned earlier, minerals with similar attenuation coefficients are difficult to identify due to the minerals having similar grey values. To simplify this problem, sulphide (pyrite, pyrrhotite and chalcopyrite) minerals were grouped and classified as one mineral group during phase segmentation. The same strategy was used to classify the remaining minerals in the Middelvlei Reef. Quartz, mica, chlorite and biotite have attenuation values with small differences, and were therefore grouped as silicates. False colours were then applied to each phase identified in the ore to distinguish the phases from each other, red represents

gold, purple was allocated as rutile, yellow represents the sulphides and lastly green was allocated to the silicates (Fig. 4.4).

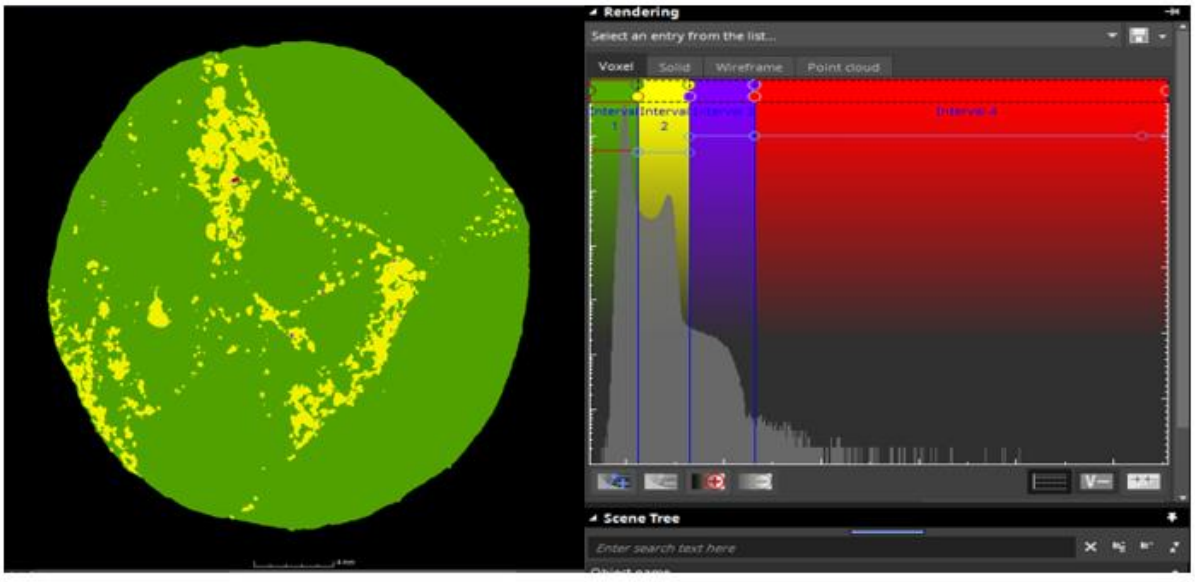

Figure 4.4: Phase segmentation of minerals in the scanned ore blocks, with false colours (left). To the right the phases are identified on a histogram. Red is gold, purple is rutile, yellow are the sulphides and green are the silicates.

4.3 Metallurgical test work – bottle roll leaching

Bottle-roll leaching experiments were performed at the University of the Witwatersrand at the school of chemical engineering (Fig. 4.5). The experiments were aimed at investigating the amenability of Witwatersrand gold ores to glycine leaching. Bottle-roll leaching was conducted on solids milled to 100 % passing -75 µm size fractions to ensure that gold is sufficiently in contact with the leaching agent. Deionised water was used specifically to guarantee no unwanted ions into the system. A desired pulp density of 30 % solids (500 g): 70 % solution (1167.67 ml) and 20 % solids (300g): 80 % solution (1200 ml) were used. The pH of each slurry was modified using sodium hydroxide (NaOH) and conditioned for 1 hour (Fig. 4.5B). Thereafter, the bottles were instantly positioned on the bottle roller. During bottle-roll leaching the finely milled ore material was agitated with the environmentally friendly lixiviant glycine and the oxidant potassium permanganate, in a 2.5L Winchester bottle. All experiments were conducted at room temperature 22° C. The mixture was agitated by rolling the bottle roll at 150 rotations per minute and each bottle roll was ventilated with oxygen through a 5 mm hole in the cap,

enabling oxygen transfer (Fig. 4.5C). Ventilation is important to ensure an ensure an oxygen shortage does not constrain the reaction rate (Oraby and Eksteen, 2014).

The slurry was monitored during leaching to ensure that no leakages occurred. A crison alkaline pH meter measured pH and temperature. The slurry obtained from bottle-rollers was then washed, dried in an oven, and then fire assayed for residual gold content (Fig. 4.5E). These experiments are optimisation experiments and were developed to identify how the parameters influenced the success rate of glycine leaching. The constraints used in this optimisation test work are detailed in Table 4.2, with more details provided in Chapter 6.

Table 4.2: Overview of leaching parameters used in bottle-roll leaching

Reagent	Glycine
Oxidant	Potassium permanganate
Temperature	Room temperature (22 ° C)
Optimum pH	10.5
Grind size	-75 µm
Rotations per minute (rpm)	150 rpm
pH modifier	NaOH
Slurry density (mg/l)	0.25 – 0.43
Leaching time (hours)	24 – 48

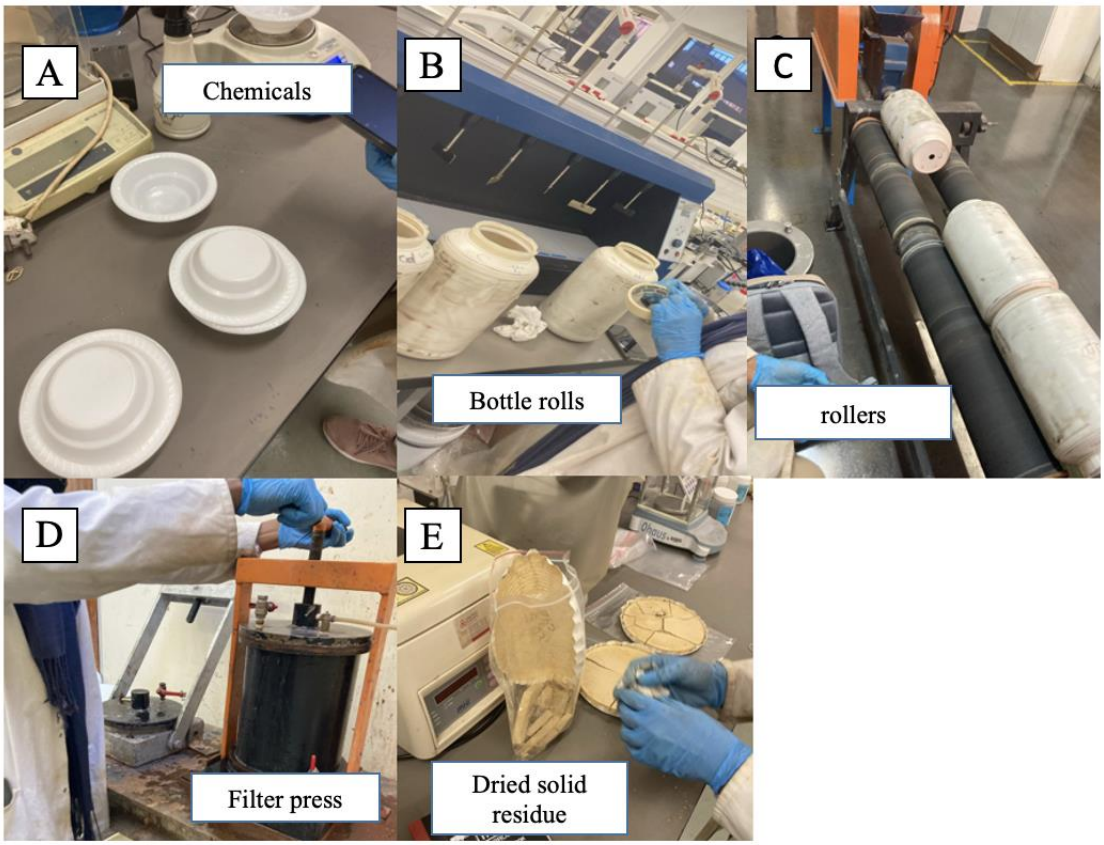

Figure 4.5: Laboratory set-up of bottle-roll leaching experiments A) Preparation of chemicals for leaching. B) Conditioning of the bottle rolls. C) Bottle rolls placed on rollers at an rpm of 150, at room temperature conditions. D) Filtering of residue and liquids using a filter press. E) Packaging of dried residue to be sent for fire assays.

Chapter 5: Results

This chapter presents the results of the process mineralogy techniques used to characterise the mineralogy, texture and gold deportment of the Middelvlei Reef. First, a detailed mineralogical characterisation of the Middelvlei Reef using optical microscopy and SEM-EDS analyses is presented in Section 5.1. The bulk modal mineralogy conducted by TIMA and QXRD are in sections 5.2 and 5.3, respectively. This is followed by a gold deportment study (mineral association, liberation and locking) in Section 5.4. The characterisation of the ore via Micro-XCT is presented in Section 5.5. Finally, the results between Micro-XCT and TIMA are cross validated in Section 5.6.

5.1 Mineralogical assemblage of the Middelvlei Reef as determined by optical microscopy and SEM-EDS

The Middelvlei Reef is a clast-supported conglomerate bed that is comprised of olimictic sub-angular to rounded clasts of quartz. Quartz is the main constituent of the conglomerate ores, non-metallic minerals in the ore comprise of chlorite, calcite, chromite, muscovite, biotite and clay minerals such as kaolinite. Chlorite is an alteration product of clay minerals subjected to heat and pressure and muscovite is an alteration product of clay minerals that are silica rich. The metallic minerals in the ore predominantly consist of pyrite, pyrrhotite, chalcopyrite and gold. The conglomerate matrix is dominated by coarse (0.2 – 24 mm), sub-angular to rounded quartz clasts, and accompanied by very-fine (≤0.4 mm) green-coloured muscovite, chlorite and biotite grains. Significant amounts of sulphide minerals are present in the ore. Pyrite (0.01 – 2 mm) is the predominant sulphide phase present in the ore whereas pyrrhotite and chalcopyrite occur in minor concentrations. Native gold was also noted in trace (minor) amounts.

Pyrite in the Witwatersrand Basin, Middelvlei Reef can be classified into two main classes: 1) allogenic (detrital) Py-1, or 2) authigenic (hydrothermal) pyrite Py-2. This classification scheme is modified after da Costa et al., 2020, and only shows the pyrite grains found in the Middelvlei Reef. Detrital pyrite typically appears as rounded grains (<0.2 – 2 mm) with abraded boundaries. Authigenic pyrite is euhedral to subhedral, measures <0.8 – 2.1 mm, with a few grains showing abraded boundaries. Additionally, an allogenic sub-class of random inclusion-bearing (Py-3) and concentrically laminated (Py-4) were identified and a sub-class of authigenic pyrite, aggregate pyrite (py-5) was identified (Fig. 5.1D).

Allogenic pyrite (Py-1) grains are rounded and are principally related with detrital minerals such as zircon and rutile (Fig. 5.1A). Fine inclusions (<0.2 mm) of chalcopyrite are seen in pyrite and the matrix of the ore (Fig. 5.1A). Allogenic grains are rounded in shape due to abrasion during sedimentary transportation processes during the establishment of the Witwatersrand Basin (Law *et al.*,1990). Carbonaceous material is also seen throughout the figures.

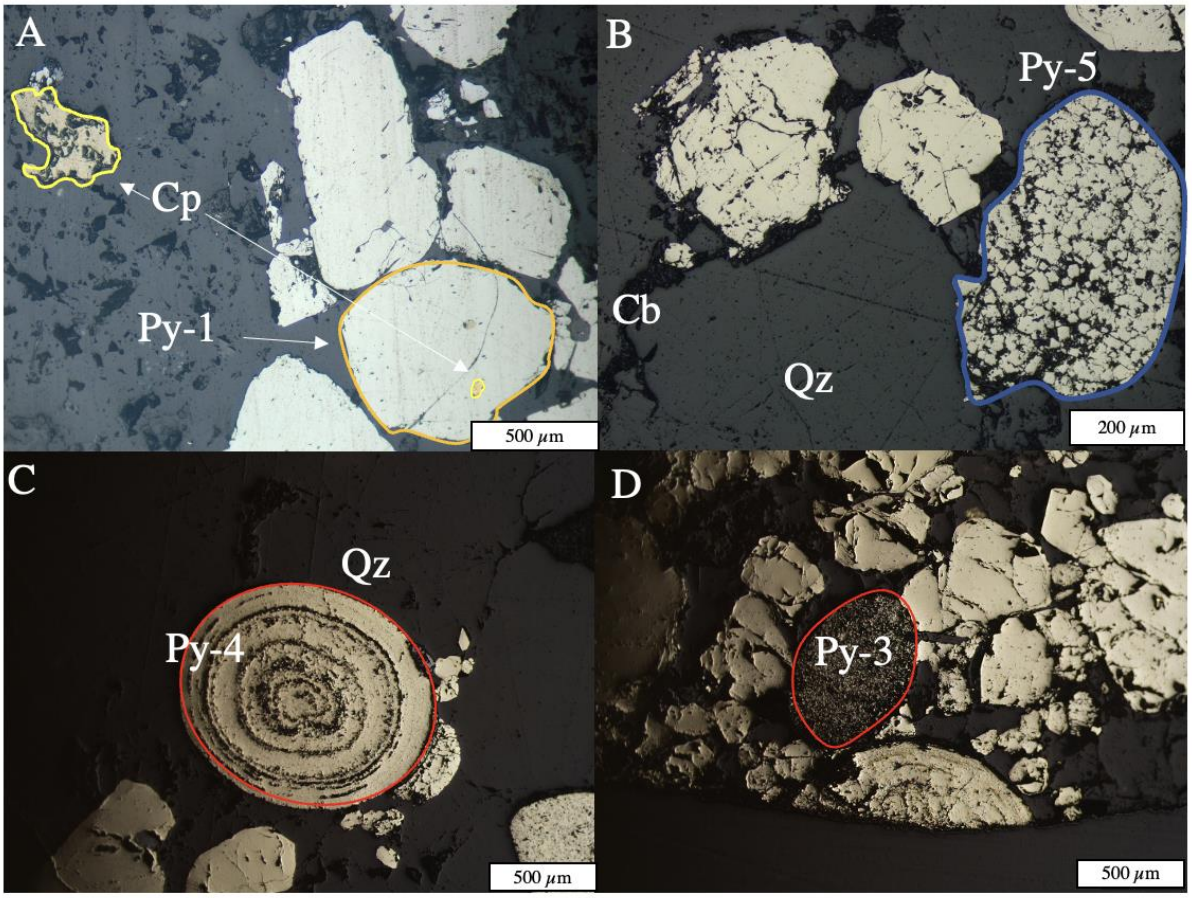

Figure 5.1: Reflected light photomicrographs of the Middelvlei Reef ore. (A) Detrital pyrite (Py-1) with micro-inclusions of chalcopyrite (Cp). (B) Sub-rounded aggregate pyrite grains surrounded by quartz and carbonaceous material (Py-5). (C) Hydrothermal Concentrically laminated pyrite (Py-4). (D) Aggregates of sulphides, pyrite-pyrrhotite and rutile (Py-3).

Visible gold was observed both via optical microscopy and SEM-based images (Fig. 5.2). The visible gold occurs in different shapes (typically subhedral and massive) and sizes (3.36 – 56 μm) in the Middelvlei Reef. A small portion of gold grains are rounded to semi-rounded in shape (Fig. 5.2A). Gold is present in the mica-rich matrix of the reef and is locked at the grain boundaries of quartz (Fig. 5.2A,E) and pyrite (Fig. 5.2F). Occasionally, gold is present as minor inclusions in gangue minerals such as

rutile (Fig. 5.2 D) and as fillings in micro-fractures in quartz (Fig. 5.2B). A strong mineralogical association is noted between gold and the gangue minerals, namely quartz, rutile and pyrite. The presence of electrum (an alloy of Au-Ag) has also been detected via SEM in the Middelvlei Reef.

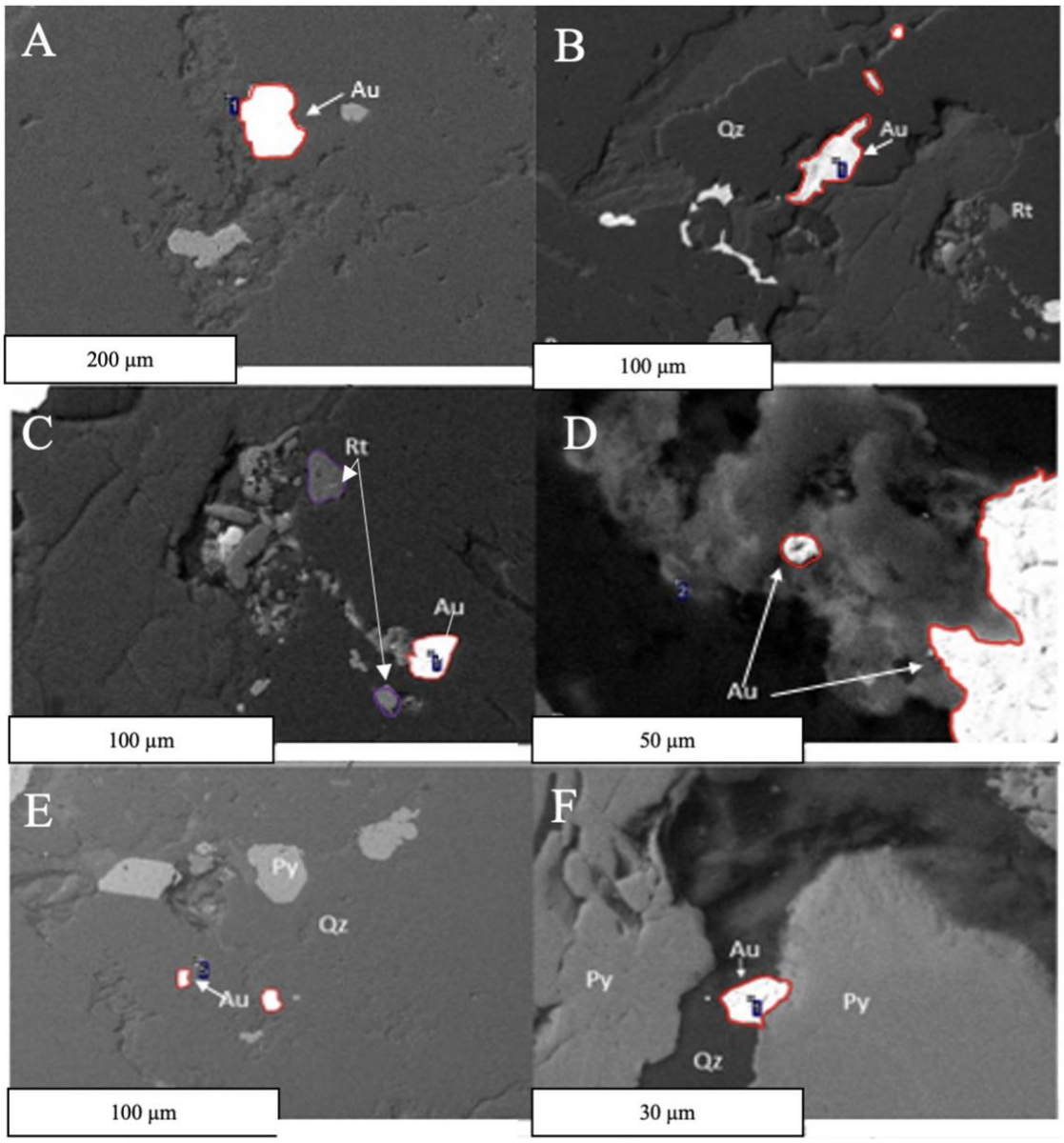

Figure 5.2: 2D SEM images illustrating pyrite and gold morphologies as well as the distribution of gold in the Middelvlei Reef. A) An anhedral grain of gold locked in quartz (Qtz) in the conglomerate matrix. B) Anhedral gold is hosted in quartz (Qz) and rutile (Rt). C) A subhedral grain of gold present at the grain boundary of rutile. D) Gold present as a minor inclusion in rutile. E) Euhedral to subhedral grains of gold locked in quartz from the conglomerate matrix. F) Gold present at the grain boundary of pyrite (Py).

5.2 Modal mineralogy of the Middelvlei Reef as determined by TIMA

Automated mineralogy technology, TIMA, was used to conduct a bulk mineralogical assemblage analysis, and to define textures of the Middelvlei Reef (liberation, association and grain size). The modal mineralogy was determined by creating TIMA high-resolution maps (THRM) of ore blocks. The modal mineralogy of the Middelvlei Reef, in weight percent, is presented in Figure 5.3. The mineralogical assemblage includes, in decreasing order of abundance: quartz (71,34 wt.%), pyrite (15,67 wt.%), muscovite, biotite, chlorite, zircon, pyrrhotite, chalcopyrite and chromite. Minerals categorised under "others" include minerals that occur in minor amounts such as schorl, kaolinite, almandine, oxides (magnetite and hematite), zircon, chromite, pyrrhotite and rutile.

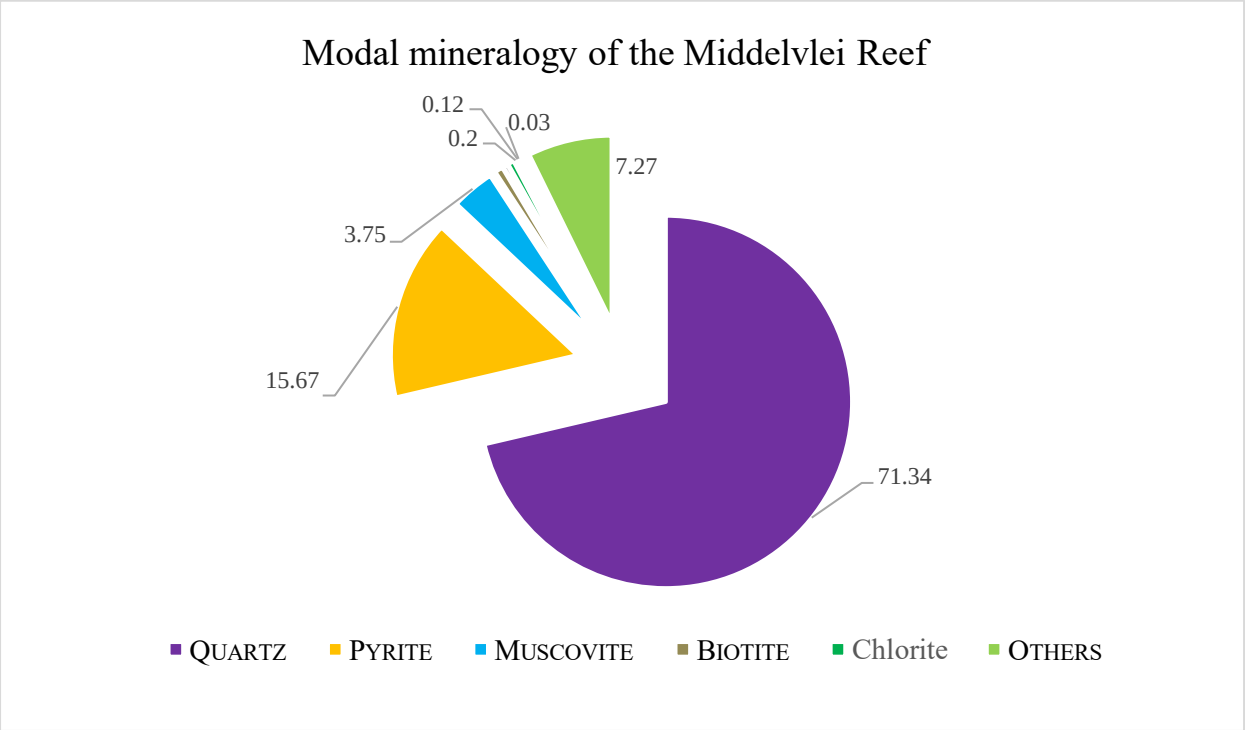

Figure 5.3: Pie chart of the modal mineralogy (weight percent) of the Middelvlei Reef.

5.3 QXRD results

QXRD results were used to validate and support the mineralogical data generated by TIMA. QXRD determines the bulk modal mineralogy of the entire ore and the average detection limit presented is 0.2 %. A total of 3 ore samples were analysed via QXRD and results between all samples are similar (Fig. 5.4). The modal mineralogy detected by the QXRD shows a high abundance of quartz with an average of 85 vol% (Fig. 5.4). Both muscovite (average of 8 vol%) and pyrite (average of 5 vol%) are also present in minor quantities. Chlorite (average of < 1vol%) was also detected, but in trace amounts.

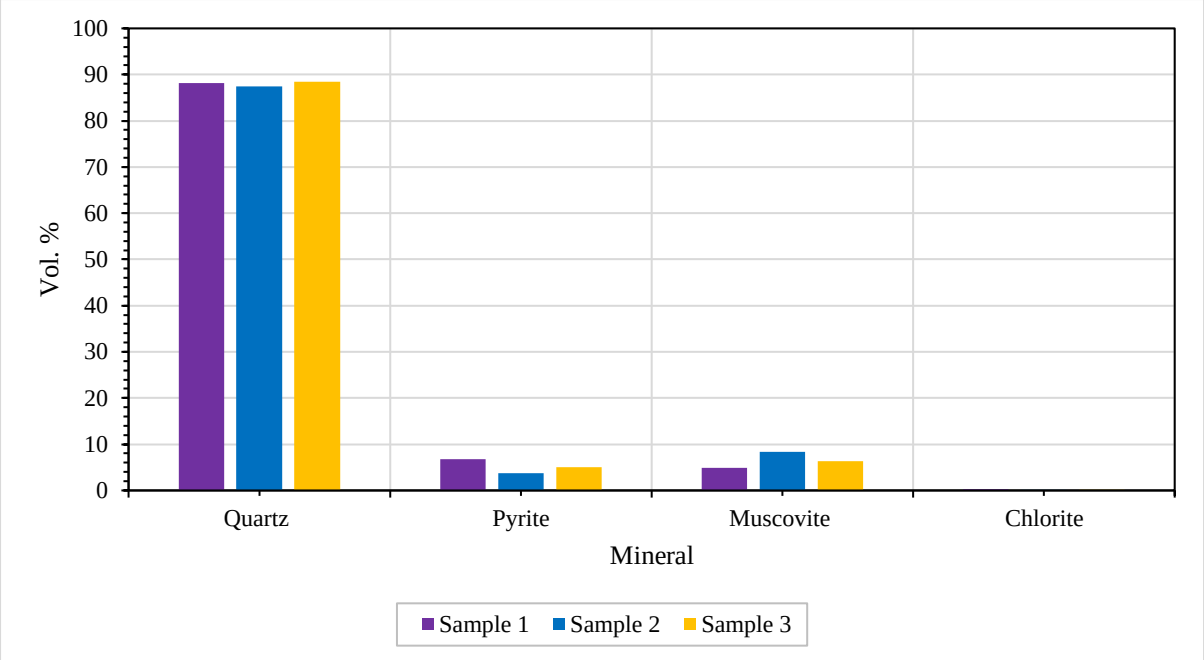

Figure 5.4: Quantitative modal mineralogy as determined by QXRD.

5.4 Gold deportment of the Middelvlei Reef using automated mineralogy

In this study, TIMA was used to conduct a gold deportment study on the Middelvlei Reef. Characterisation of gold in the Middelvlei Reef entails designating how gold is associated with the gangue minerals, as well as the proportion of gold that is locked in refractory minerals, free-surface area analysis, and describing the gold grain size and morphology (Goodall *et al.*, 2005).

5.4.1 The association of gold with gangue mineralogy and the liberation status of gold

TIMA allows for the generation of high-resolution phase maps that can show how gold is dispersed throughout the ore and calculate which minerals gold is intimately associated within the ore body (Fig. 5.6). Only the minerals which touch or are adjacent to gold were measured to determine mineral association. Due to the large number of minerals present in the Witwatersrand Basin (e.g., Fig. 5.5), the mineral phases were reclassified into groups for simplicity. Micas include biotite and muscovite, and "others" refer to columbite, florencite and kaolinite to simplify data representation. Gold shows a strong association with pyrite, quartz, mica and chlorite (Fig. 5.6). These gangue mineral phases were identified to be predominantly in contact with gold in the ore blocks. The gold association data is strongly supported visually as seen in Figure 5.7. Gold can be seen: 1) touching the grain boundaries of chlorite (Fig. 5.7A), 2) being enclosed in quartz, 3) locked at quartz grain boundaries (Fig. 5.7B), and 4) as infillings in micro-fractures in pyrite (Fig. 5.7C) and quartz grains (Fig. 5.7B).

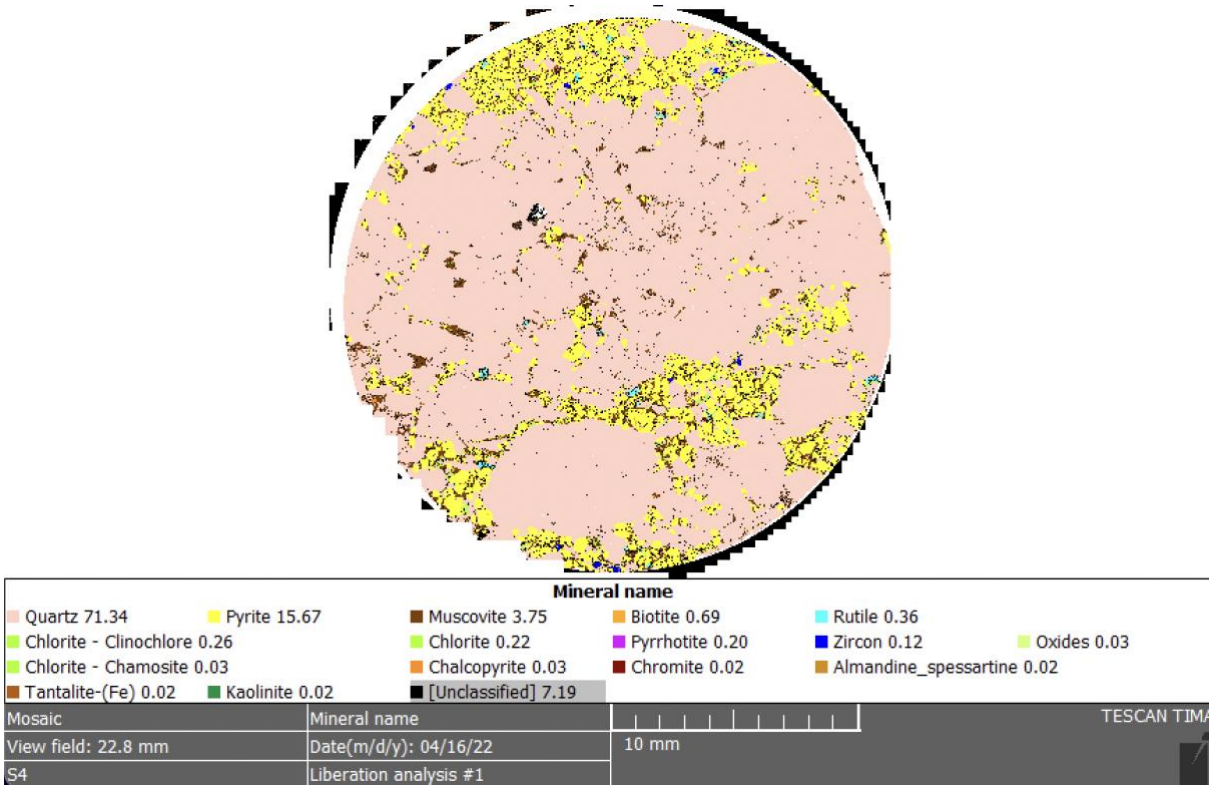

Figure 5.5: Scanned ore block of the Middelvlei Reef using TIMA.

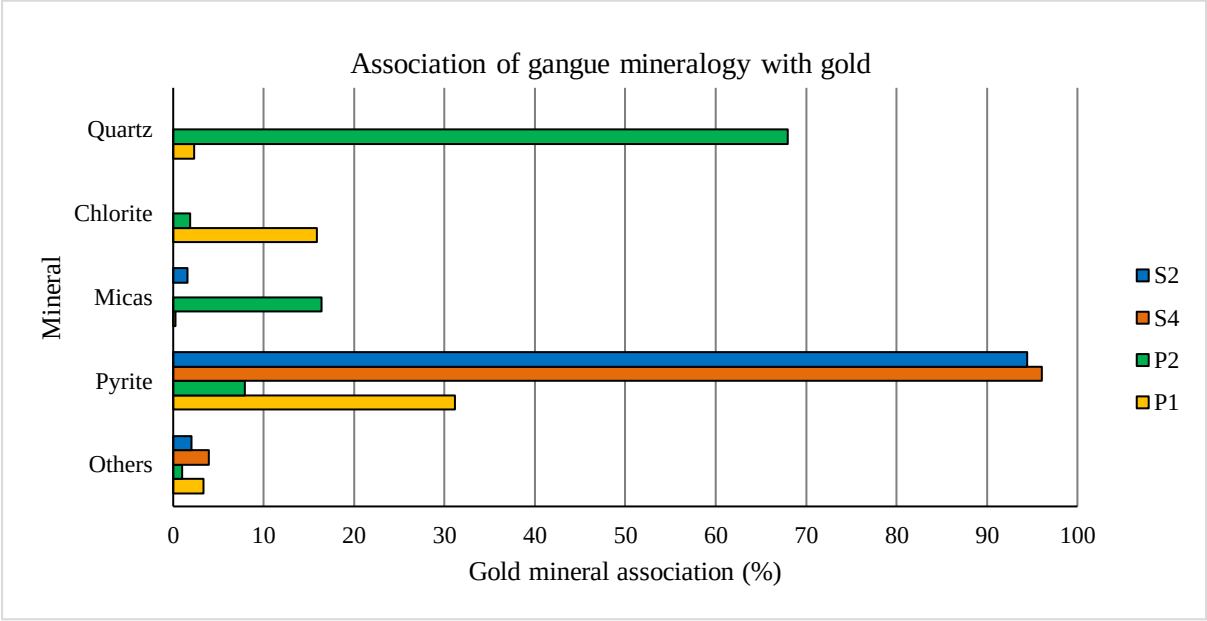

Figure 5.6: Mineralogical association of gold with gangue mineralogy measured with TIMA.

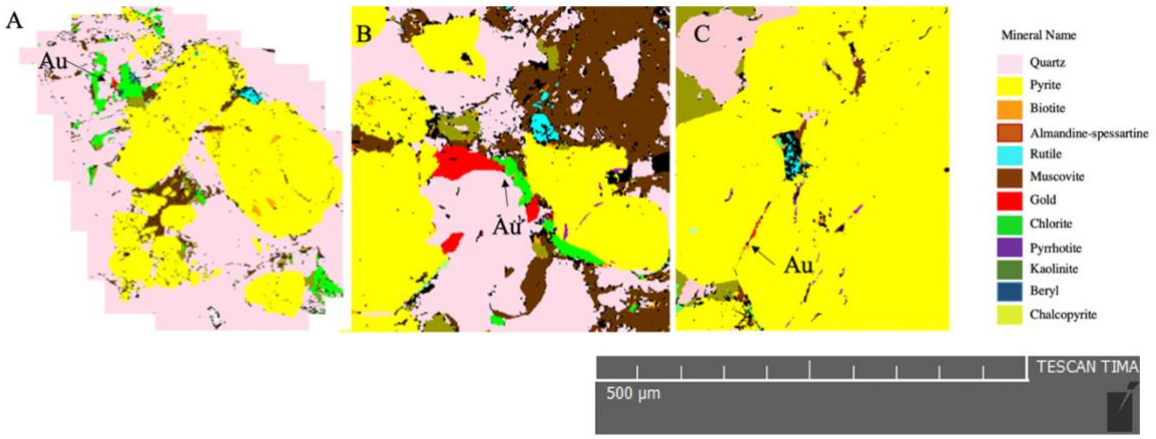

Figure 5.7: TIMA high-resolution phase maps that show the relationships between gold (Au) and the gangue mineralogy. A) Gold is locked at the grain boundary between chlorite and quartz. B) Gold is enclosed and locked in quartz. C) Gold is present as in-fillings in microfractures in pyrite.

In process mineralogy, liberation is a volumetric measure based on the area percentage of a mineral grain (single particle). The measurements are classed in 10 % increments, as seen in Figure 5.9, or as wider increments that correspond to locked (<30%), exposed (30 – 60 %) or liberated (>60 %) (see also Fig. 3.3). A fully liberated mineral is physically unattached to the gangue mineralogy. Whereas an exposed grain of gold is attached to the grain boundary of gangue mineralogy, and a locked grain of gold is fully enclosed in the gangue mineralogy. Findings from TIMA show that most of the gold is locked (enclosed or attached at the grain boundary) in the gangue minerals. Figure 5.7 shows that gold is locked in minerals such as chlorite, quartz and pyrite. Results from 3 samples show that most of the gold has a liberation volume <10%, indicating that majority of the gold detectable by TIMA is locked (Fig. 5.8). Thus, gold in the Middelvlei Reef ore can be classified as locked (e.g., Fig. 5.7C).

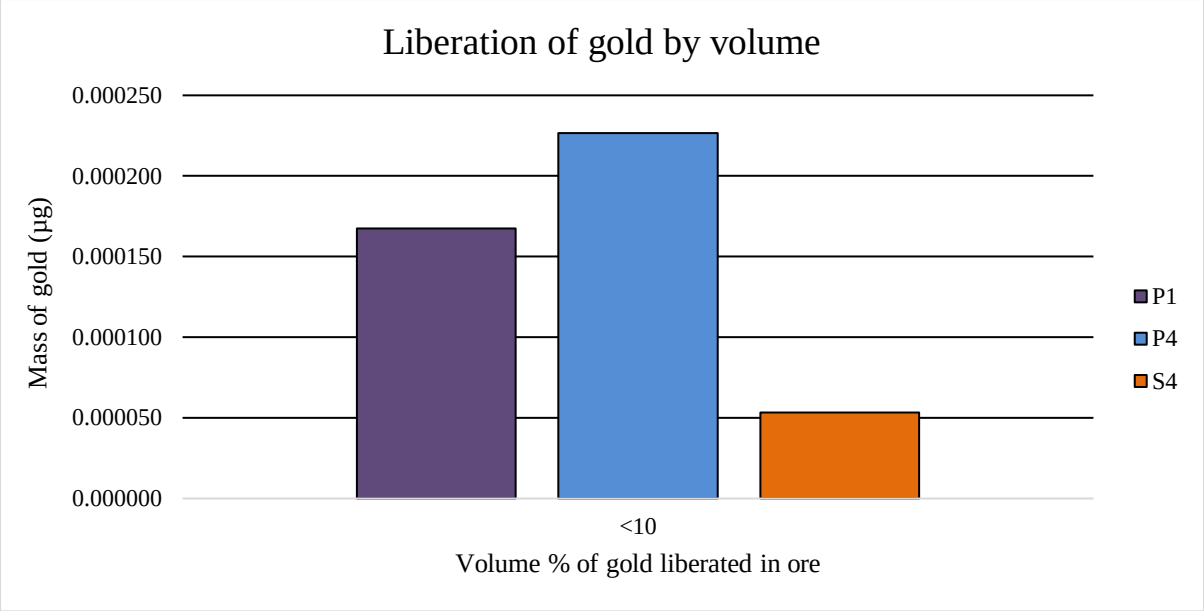

Figure 5.8: Liberation status of gold in the Middelvlei Reef as determined using TIMA.

A free-surface area analysis of gold or PSSA (phase-specific surface area) was also done using TIMA. This is a feature of TIMA which allows for the detection of the "free-surface area" of gold. There is a difference between free-surface area and liberation. Specifically, a free-surface area does not imply that ore-mineral is 100% liberated, it is rather a measure of the surface area that is accessible to the lixiviant (Spencer and Sutherland, 2000) (Fig. 5.9). In the Middelvlei Reef, gold is predominantly locked in quartz (15 – 70%) and pyrite (30 – 80%), and only a small percentage of gold had an entirely free-surface area accessible to the lixiviant (Fig. 5.10). These results further support the notion that gold in the Middelvlei Reef is predominantly locked in gangue mineralogy. Only a small mass of gold (<5%) has a free-surface area that is unattached to the gangue mineralogy, and therefore accessible to the action of a lixiviant (Fig. 5.10).

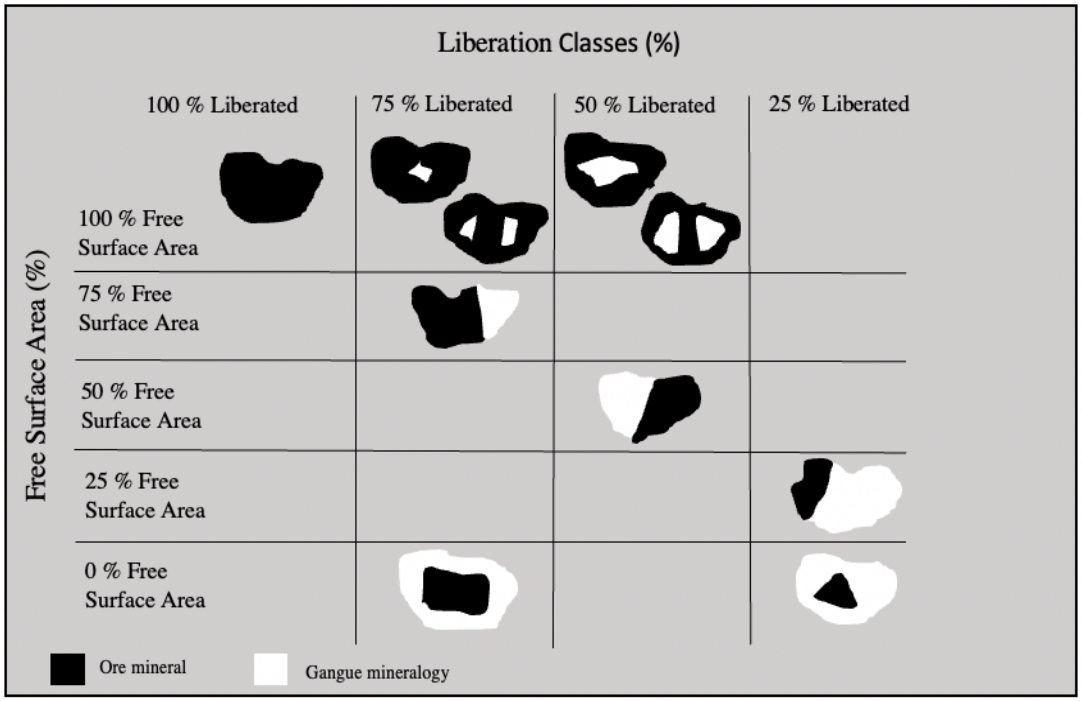

Figure 5.9: Schematic diagram of relationship between free-surface area and liberation modified after Spencer and Sutherland, (2000).

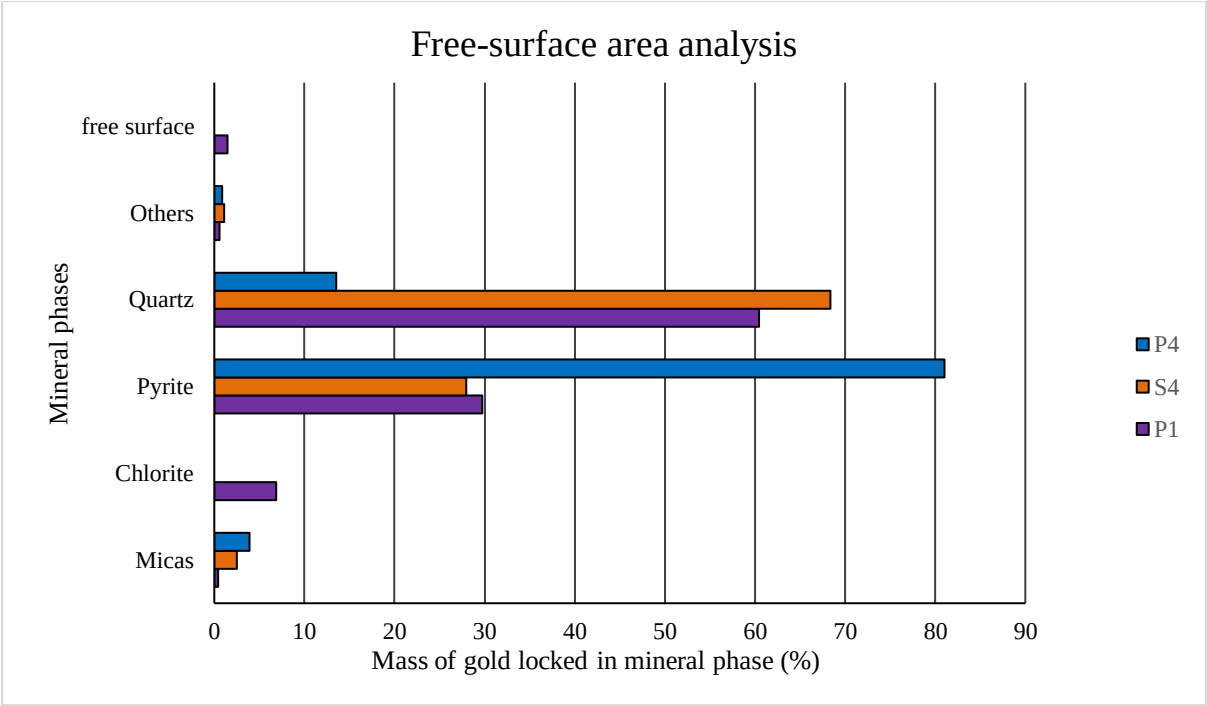

Figure 5.10: Free-surface area analysis of gold using TIMA.

5.4.2 Grain size classification of gold and gangue mineralogy

The grain size of gold grains was measured by TIMA. Results plotted on a histogram in Figure 5.11 demonstrate a unimodal positively skewed distribution of gold grain sizes. The different colours represent the different classes of grain sizes. The positively skewed distribution of gold entails that the gold grains in the Middelvlei Reef are predominantly very-fine-grained, measuring <56 µm in size, as based on the grain size classification system (Grayson, 2007). Most gold grains in the reef measure between 1 – 12 µm according to TIMA results (Fig. 5.11).

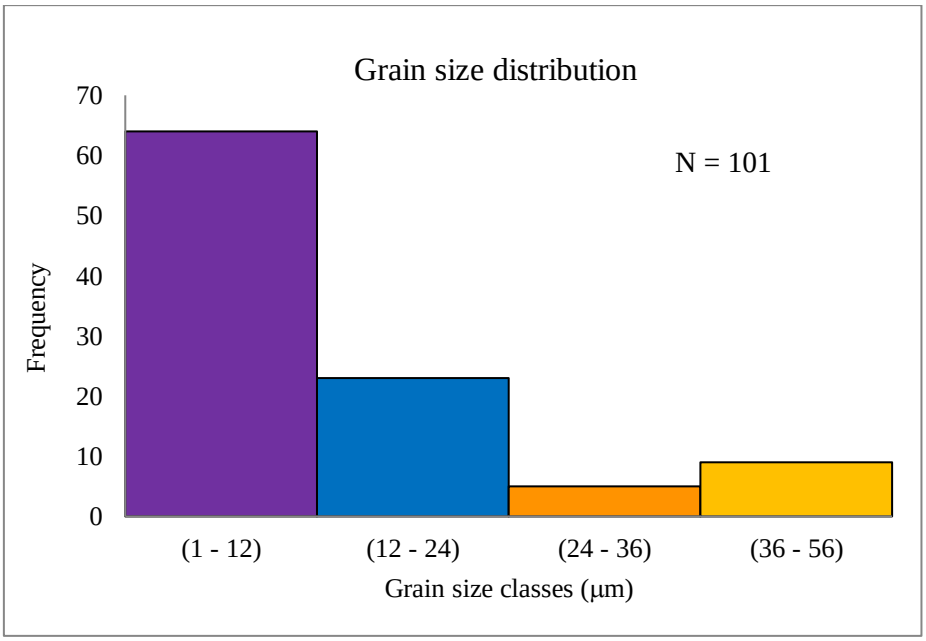

Figure 5.11: Grain size distribution of gold measured by TIMA.

The grain size distribution of pyrite was also analysed in 2D via TIMA. The grain size distribution of pyrrhotite and chalcopyrite are included in Appendix C. In the Middelvlei Reef, pyrite grains average between 3.24 – 282.88 µm and can be classified as coarse, as presented in Fig. 5.12.

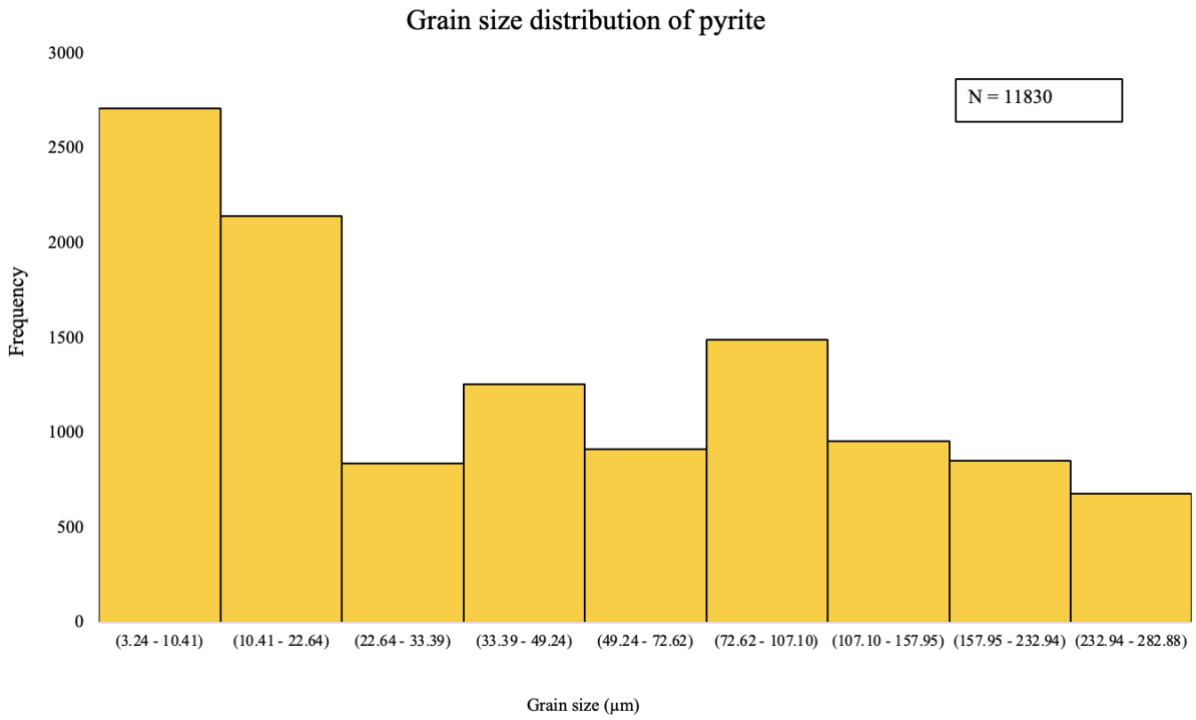

Figure 5.12: The grain size distribution of pyrite as determined by TIMA.

5.5 Micro-XCT

Micro-XCT facilitates gold deportment studies by allowing for the observation and analysis of a statistical number of gold grains in 3D. Results provided by the Micro-XCT method includes grain segmentation, region of interest extraction (ROI) and volume percent quantification of the mineral phase of interest. The ore blocks from the Middelvlei Reef scanned via Micro-XCT were also scanned with TIMA to discriminate the ore mineralogy accurately and as a form of validation (Section 5.6). The results presented here were further validated by QXRD and XRF methods.

5.5.1 Texture characterisation

Texture has a critical influence in various areas of mineral processing, e.g., communition, recovery and liberation (Bonnici *et al.*, 2008). Mineral texture is classified into two categories: structural and stationary. Structural textures describe the grain size, shape and orientation, whereas stationary textures describe the spatial distribution of minerals in the ore (Lobos *et al.*, 2016). To conduct a successful geometallurgical project, the integration of ore texture into the predictive model needs to be quantitative. This necessitates the use of Micro-XCT which allows for 3D visualisation of the ore

(Pérez-Barnuevo *et al.*, 2013). VG studio max was used to conduct a defect analysis on the analysed ore blocks. The defect analysis was applied to each mineral phase identified. The parameters that were extracted during defect analysis included: volume, maximum diameter, radius, surface area and voxel (see Appendix B for detailed dataset). The extracted volume of each mineral phase in the ore block is grouped according to colour, with blue representing low volumes and red high volumes as presented in Fig. 5.13.

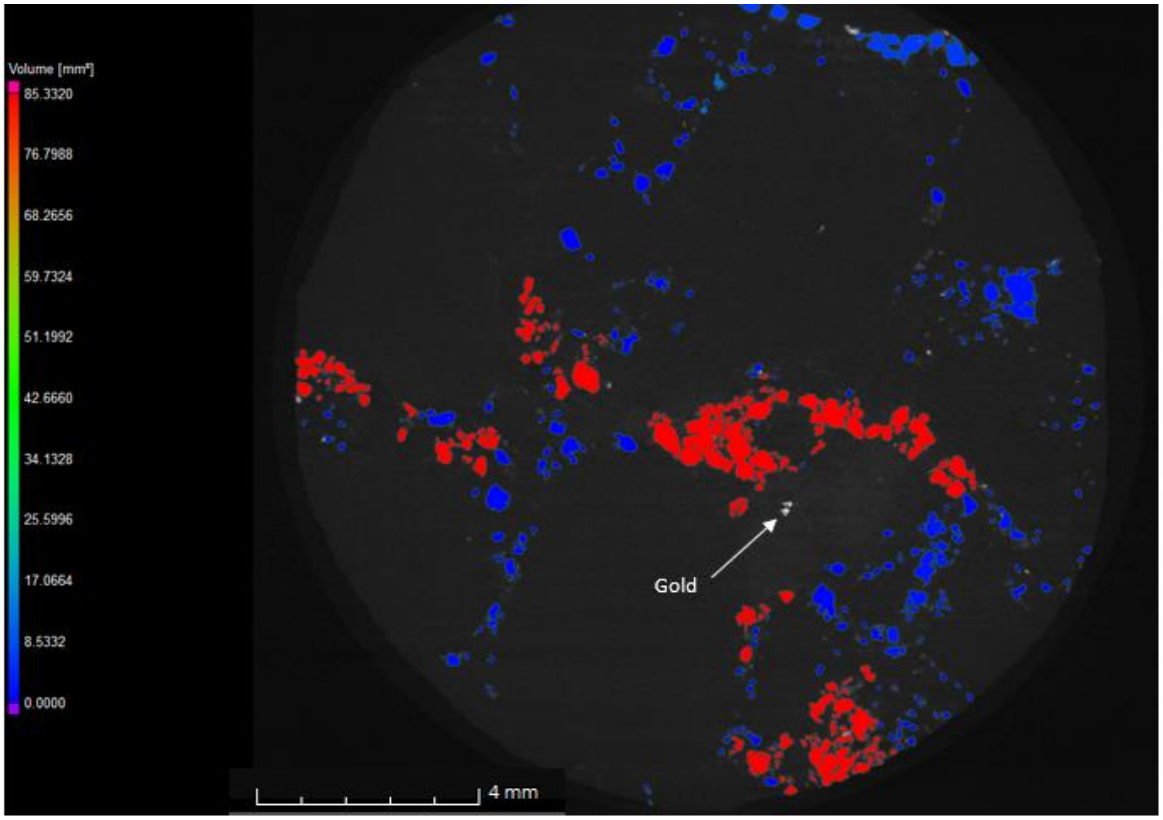

Figure 5.13: Mineral phases in the Middelvlei Reef grouped according to volume colour scale (mm). Gold is reflected as a bright white due to the density of the mineral. Blue corresponds to low-volume minerals phases and red corresponds to high-volume mineral phases.

The distribution and relationships between gold, rutile and other mineral phases were also investigated by isolating certain gangue minerals as shown in Figure 5.14. The green minerals represent the silicate phases (mostly quartz), the yellow, sulphide phases (mostly pyrite), the purple, rutile and the red represents micro-nuggets of gold. In Figure 5.14A, pyrite (yellow) is seen to be closely associated with quartz (green). Specifically, most pyrite grains are found at the quartz grain boundaries with pyrite grains varying both in shape and size (Fig. 5.14B). Perfectly euhedral grains of pyrite can be seen in the ore block as single crystals and as aggregates that are noticeably visible throughout the ore block. Gold

and pyrite are closely associated with each other (Fig. 5.14B). The grains of gold vary in size in and appear to be randomly disseminated (Fig. 5.14D). However more expertise is required to accurately study the textural parameters such as the interrelationships and spatial distribution of grains, which are more complicated to characterise using Micro-XCT.

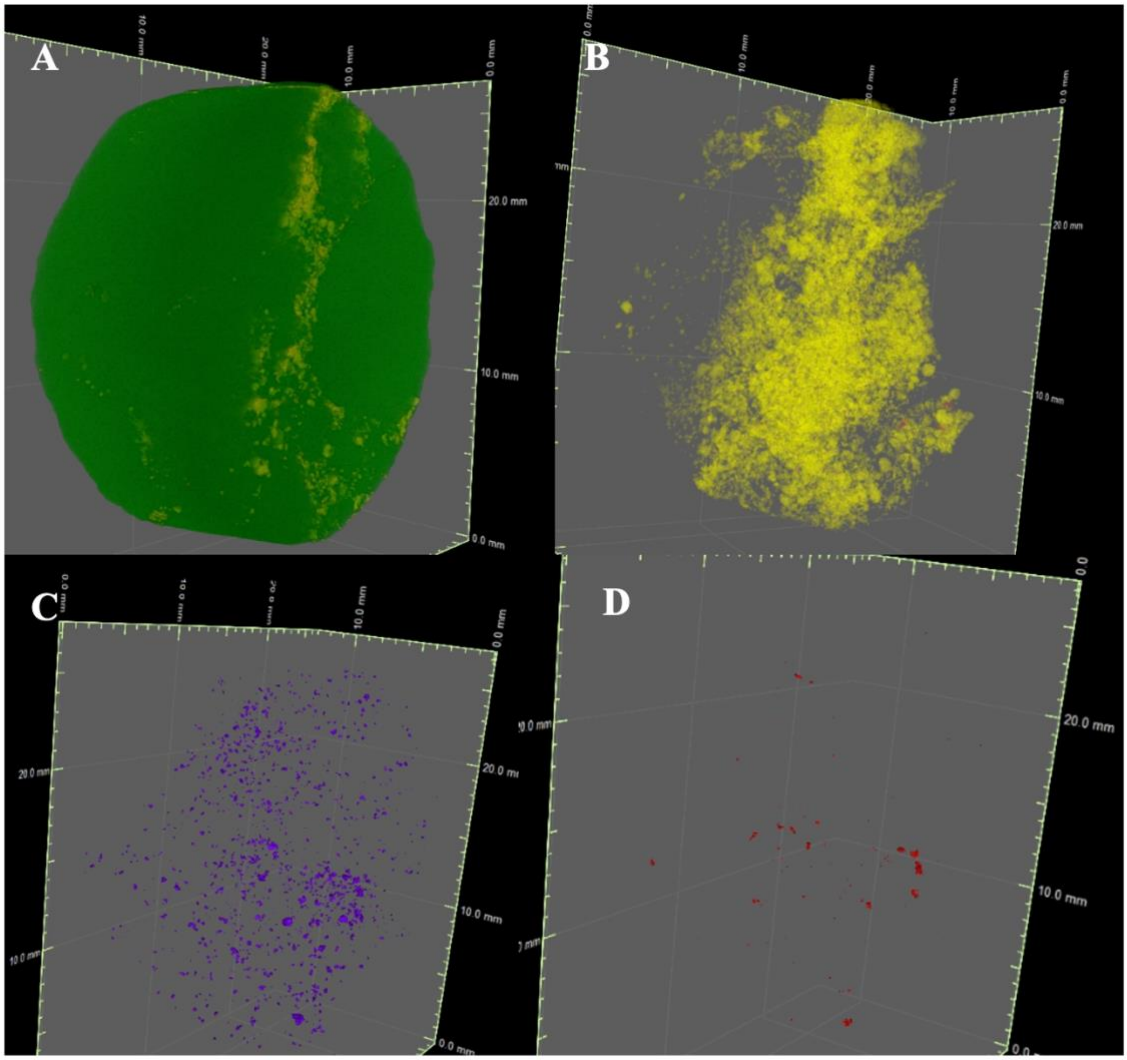

Figure 5.14: An ore block scanned in 3D using Micro-XCT with separation of the different mineral phases. False colours were applied to classify individual minerals and mineral phases. Green corresponds to the silicate phases (mostly quartz), yellow represents the sulphide phases (mostly pyrite), purple represents rutile and red represents gold.

5.5.2 Gold and sulphide mineral grain characteristics

Grain characteristics provide key information required for communition and liberation. It is critical to note that the gold grain size distribution of the Middelvlei Reef is not representative of the entire Witwatersrand Basin. Grain size classification in Micro-XCT corresponds to measurements used to measure an equivalent sphere diameter and can be quantified using Micro-XCT defect analysis. The grain size of gold was characterised by analysing 712 grains of gold in 3D. The results are presented in Figure. 5.15 as a histogram. The grain size distribution of gold defined a bell-shaped distribution that is positively skewed to the right. The histogram shows that most of the grains range in sizes between 16 – 67 µm (Fig. 5.15). The lognormal distribution graph confirms that grain sizes of gold are predominantly fine-grained and not coarse, as presented in Figure 5.15.

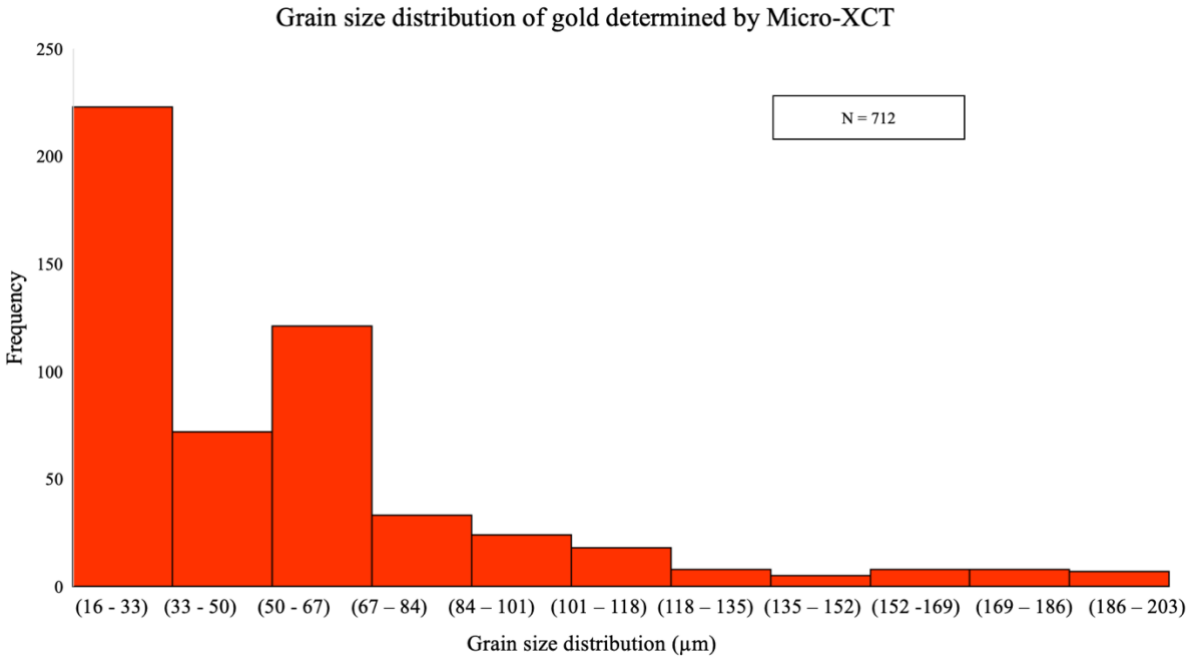

Figure 5.15: Histogram of the gold grain size distribution as calculated by using the defect analysis tool in VG Studio Max.

Gold grain shape is measured based on the sphericity (form), as calculated using the defect analysis tool in VG Studio Max. The sphericity of a grain is the degree of the resemblance of a grain shape to that of a perfect sphere (Rorato *et al.*, 2019). The sphericity of a grain is measured on a scale between 0 and 1, where 1 represents a perfect sphere and 0 is a flat, non-volumetric object (Maroof *et al.*, 2020). The

results plotted as a histogram in Figure 5.16 demonstrate a negatively (to the left) skewed sphericity distribution. This indicates that most grains are predominantly of a high sphericity ranging between 0.65 – 0.81 with a few grains showing a low sphericity to medium sphericity 0.35 – 0.49.

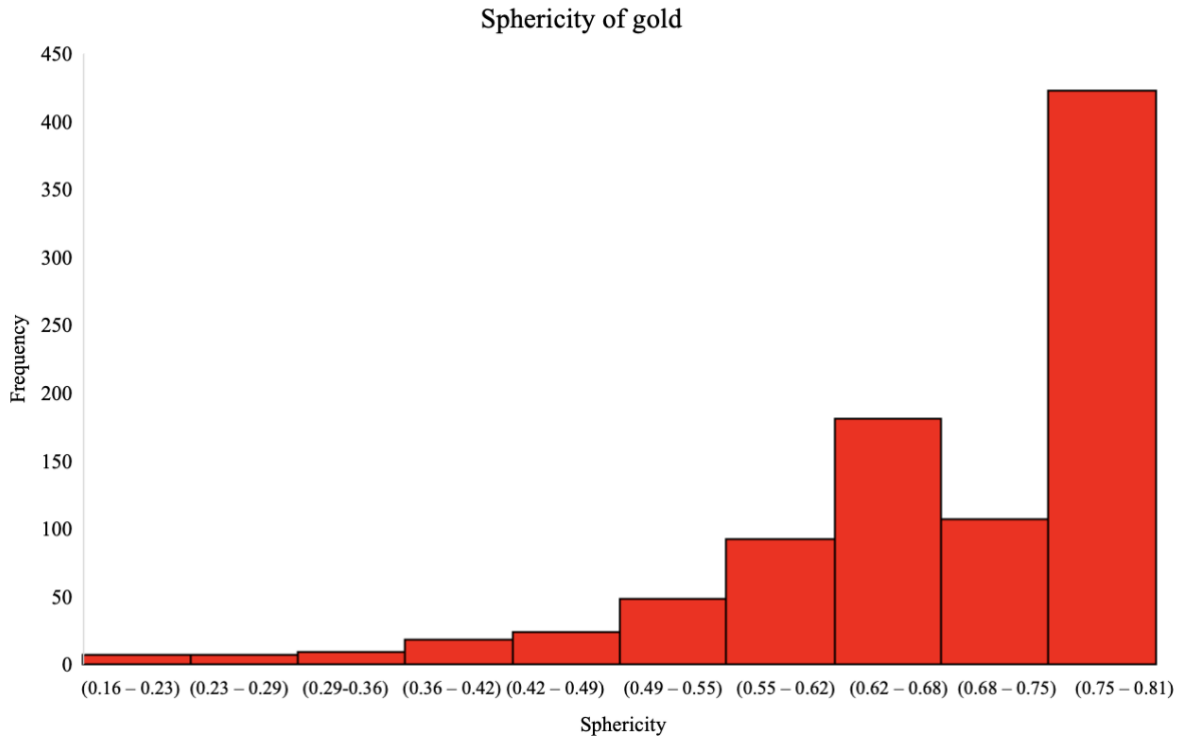

Figure 5.16: Grain sphericity of gold determined by the defect analysis tool in VG Studio Max.

The grain characteristics of the sulphide mineral phases were also analysed by using the defect analysis tool in VG Studio Max. The different sulphide minerals (pyrite, pyrrhotite and chalcopyrite) present in the Middelvlei Reef were grouped for simplicity. The grain sizes, plotted on a histogram in Figure 5.17, show a lognormal distribution, that is positively skewed to the right, indicating that the sulphide grains are very coarse in size, with the average grain size ranging between 395– 495 µm. The largest sulphide mineral grains detected were greater than >1mm in size.

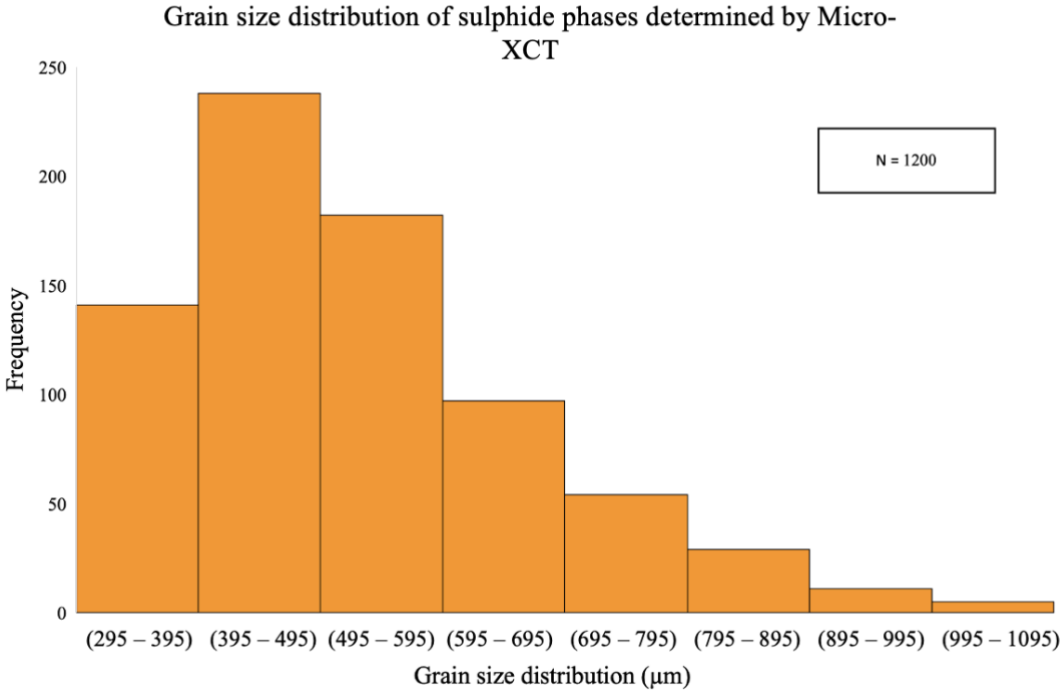

Figure 5.17: Grain size distribution of sulphide phases as determined using the defect analysis tool in VG Studio Max.

The sphericity of the sulphide phases was also classified by using the defect analysis tool in VG Studio Max. The sphericity is measured on a scale between 0 and 1 as well. It is important to note that the sphericity includes all the sulphide phases in the reef, namely: pyrite (including both authigenic and allogenic classes), pyrrhotite and chalcopyrite. The results, plotted on a histogram presented in Fig. 5.18, show a negatively (to the left) skewed histogram, indicating that the grain sphericity falls between a range of 0.40 – 0.64 with a few grains showing low to medium sphericity between 0.16 – 0.34.

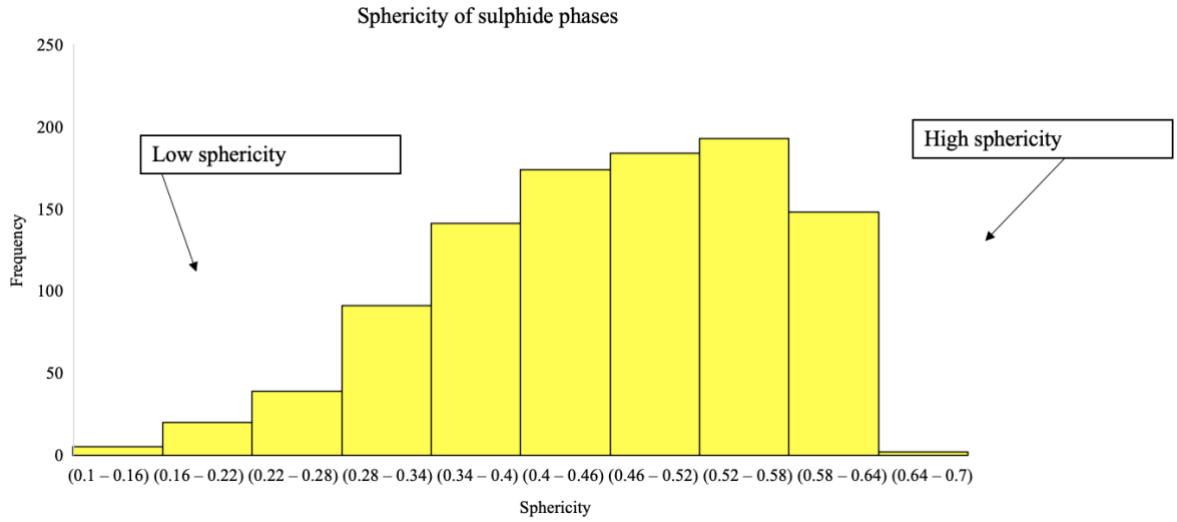

Figure 5.18: Sphericity of sulphide minerals as determined using the defect analysis tool in VG Studio Max.

5.6 Data validation between Micro-XCT and TIMA

The modal mineralogy in the Middelvlei Reef as determined by Micro-XCT was plotted against the results obtained via TIMA (Fig. 5.19). For simplicity, the TIMA mineralogy was regrouped and normalised to match the results produced by Micro-XCT. The TIMA minerals classified under "others" are namely: schorl, kaolinite, zircon, chromite and rutile. In the case of Micro-XCT results, the mineral classified as others is defined as rutile, for sake of simplicity. The minerals classified under silicates include quartz, and the chlorite, biotite and muscovite. Figure 5.20 depicts how the modal mineralogy between Micro-XCT, and TIMA varies. Micro-XCT quantified a higher volume of sulphide and unknown mineral phases in 3D in comparison to TIMA. However, the results from both techniques are comparable and thus in good agreement. The differences observed are likely caused by sample variation and sampling biases. Specifically, ore samples analysed via TIMA are highly mineralised, whereas samples analysed via QXRD are representative of the entire ore. As a result, TIMA modal mineralogy results produced a higher modal abundance for pyrite due to sampling selection, as samples containing pyrite were preferentially selected for analyses.

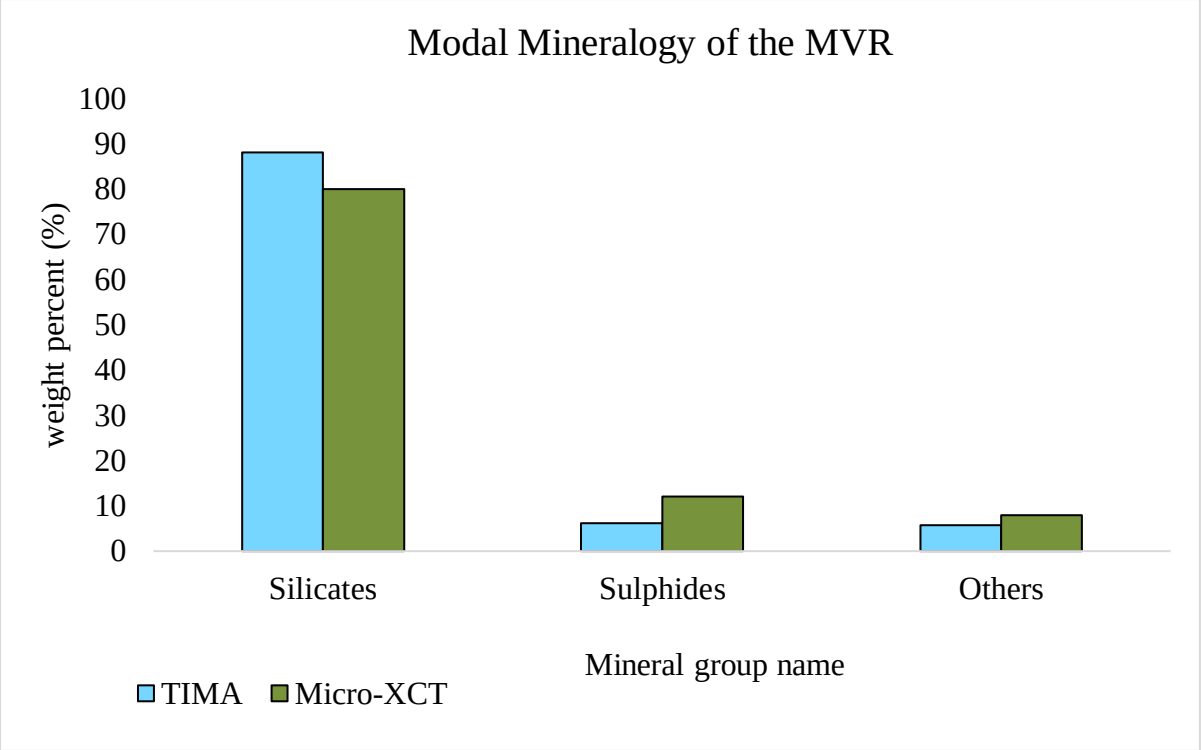

Figure 5.19: Modal mineralogy comparison between Micro-XCT and TIMA. The TIMA modal mineralogy was grouped according to Micro-XCT mineral grouping

Chapter 6: Multi-element analysis

6.1 Comprehensive multi-element geochemical analysis of the Middelvlei Reef

A comprehensive multi-elemental analysis was performed to identify potentially deleterious elements and any anomalies (obvious enrichments/depletions of certain elements) that may be present in the Middelvlei Reef (Table 6.1). The identification of these elements is imperative to comprehend the chemical composition of the orebody, and in turn, understand their potential influence the environment and leaching results (e.g., reagent consumers, preg-robbers, etc.). Elements that have been flagged are either identified to be harmful to the environment or to the recoveries of gold during leaching. The geochemical results illustrate that the presence of As, Co, Cu, Fe, Mn, Ni, Pb, U and Zn have been detected in the Middelvlei Reef. Elements Fe, Zn, Ni, Pb and Cu are known as cyanicides, and these elements consume reagents in a leaching system. Arsenic, lead and uranium are heavy metals known to cause acid-mine drainage and environmental damage. XRF and ICP-MS data were combined to produce Table 6.1. The major elements are SiO_2, Al_2O_3, Fe_2O_3 and the minor elements are everything else listed in Table 6.1.

Overall, the ore is silica-rich at 86.73 wt.% with lesser amounts of oxides such as aluminium oxide, magnesium oxide, these elements are above >4.0 wt%. The minor elements are in trace (minor) amounts and vary in concentrations from 183.26 ppm to minor 0.73 ppm (table 6.1). Base metals that have been flagged are also known to cause refractory behaviour during leaching by either being reagent consumers and impede the diffusion or dissolution of gold (table 6.1). Base metal concentrations greater than 100 ppm are known to consume the lixiviant and impede leaching kinetics, concentrations as low as < 100 pm should be noted because lixiviant consumption is still likely (Coetzee *et al., 2011*). Elements flagged are predominantly below 100 ppm but have been flagged because they are detrimental.

Table 6.1: Multi-elemental geochemical analysis of the Middelvlei Reef ore. Flags indicate that the element could have a negative impact on mineral processing or be detrimental to the surrounding environment.

Element	Concentration	Flag	Element	Concentration	Flag
Al_2O_3	4.02 wt%		**MgO**	0.35 wt%	
As	5.05 ppm	**flag**	**NiO**	0.01 wt%	

Ba	77.77 ppm		**P**	50.94ppm	
CaO	0.03 %		**Pb**	46.60 ppm	**flag**
Co	87.80 ppm	**flag**	**Sb**	4.01 ppm	
Cr	183.26 ppm		**Sn**	1.97 ppm	
Cu	67.57 ppm	**flag**	**SiO_2**	86.73 wt%	
Cs	0.73 ppm		**U**	58.34 ppm	**flag**
Fe_2O_3	4.85%	**flag**	**Zn**	69.33 ppm	**flag**
K	0.55 %				
Li	3.58 ppm				
MnO	0.05 wt%	**flag**			

Chapter 7: Metallurgical results

Direct glycine-permanganate leaching experiments were set up to measure the recovery of gold in low-grade and complex ores. Different parameters were tested in this optimisation study to determine how they influenced the recovery of gold in the glycine-permanganate system.

7.1 Metallurgical test work

The experiments (Experiment A to Experiment E) were run to observe the effects of changing the following parameters (as independent variables): A) oxidant concentration (1 – 9 g) B) leaching time (24 – 48 h), and C) system pH. The slurry density was kept constant at 500 g solids and 1167.67 ml of de-ionised water.

Additional experiments, labelled 1 to 3, were run to observe how changing the slurry density to 300 g solids and 1200 ml deionised water affected gold recovery. The experiments were conducted in triplicates to ensure replicability of results. All experiments were conducted using the parameters described in Table 7.1 below. At the beginning of the experiments, the pH of the slurry was modified by adding 0.85 g of sodium hydroxide (NaOH) to the slurry solution, followed by conditioning for 1 hour after which the slurry was allowed to settle before leaching. After the leaching experiment ended, the samples were filtered with 0.45 µm filter paper, and the solid residue was dried in an oven at a temperature of 80 ° C for 24 hours. The dried residue was then assayed for gold via the fire assay method.

Table 7.1: Parameters used in glycine leaching experiments

Parameters	**EA**	**EB**	**EC**	**ED**	**EE**	**E1-E3**
Mass of $C_2H_5NO_2$ (g)	1	1	1	1	3	(0.4-1.2)
Mass of ($KMnO_4$) (g)	1	1.5	3	4.5	9	(0.4-1.2)
Average pH	11.02	10.55	10.49	10.54	10.49	10.50

pH modifier NaOH (g)	0.85	0.85	0.85	0.85	0.85	0.85
Dissolved Oxygen (DO)	4.0	4.1	4.1	4.1	4.1	4.0
Slurry density (g/ml)	0.43	0.43	0.43	0.43	0.43	0.25
Leaching time (hours)	24	36	36	36	48	24
Temperature	25 °C	25 °C	25 °C	25 °C	25 °C	25 °C
Rotations per minute (rpm)	150	150	150	150	150	150
Grind size (P80)	- 75 µm	- 75 µm	- 75 µm	- 75 µm	- 75 µm	- 75 µm

Prior to conducting the experiments, the head sample from the Middelvlei Reef was equally split into five portions and each portion was assayed for gold via the fire assay method. Results indicate that average gold grade is 26.1 Au (g/t).

Table 7.2: Head grade determined by fire-assays for each experiment Au (g/t). Gold grades are measures in g/t.

EA	**EB**	**EC**	**ED**	**EE**
29.16	21.46	25.70	26.92	27.24
Average grade:	26.1			

7.2 Results

This section reports the gold recoveries produced during the optimisation experiments (Table 7.1). The results of varying amounts of potassium permanganate, time, pH and slurry density are each detailed below. The results of varying amounts of potassium permanganate, time and pH were investigated in experiments A to E. The results produced for each experiment are presented in Figure 7.1. The effects of a variable slurry density were investigated in experiments 1 to 3 and is featured at the end of this section.

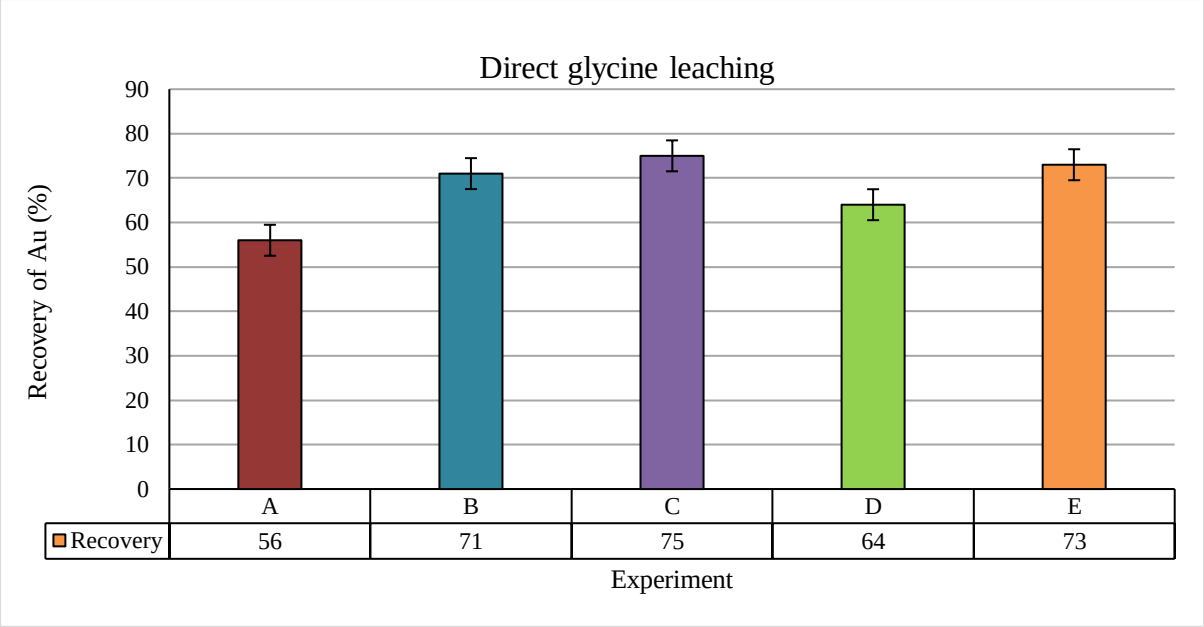

Figure 7.1: Direct glycine leaching results for experiments A – E. Parameters are detailed in Table 7.1.

7.2.1 Effect of potassium permanganate

The first parameter investigated was the effect of altering the concentration of the oxidant, potassium permanganate ($\mathbf{KMnO_4}$), in the system. The leaching time (36 hours) and concentration of glycine were kept constant for all three experiments (B - D) to effectively isolate and measure the parameter being probed. The results displayed in Figure 7.2, indicate that the recovery of gold was not directly proportional to increasing the concentration of potassium permanganate. Rather, the recovery of gold decreased as the concentration of potassium permanganate increased. The recovery of gold between experiment B and experiment C increased by 4% when the concentration of the oxidant in the system was increased from 1.5 g to 3 g. Nonetheless, the recovery of gold between experiments EC and ED decreased by 11 % as the concentration of potassium permanganate was increased to 4.5 g.

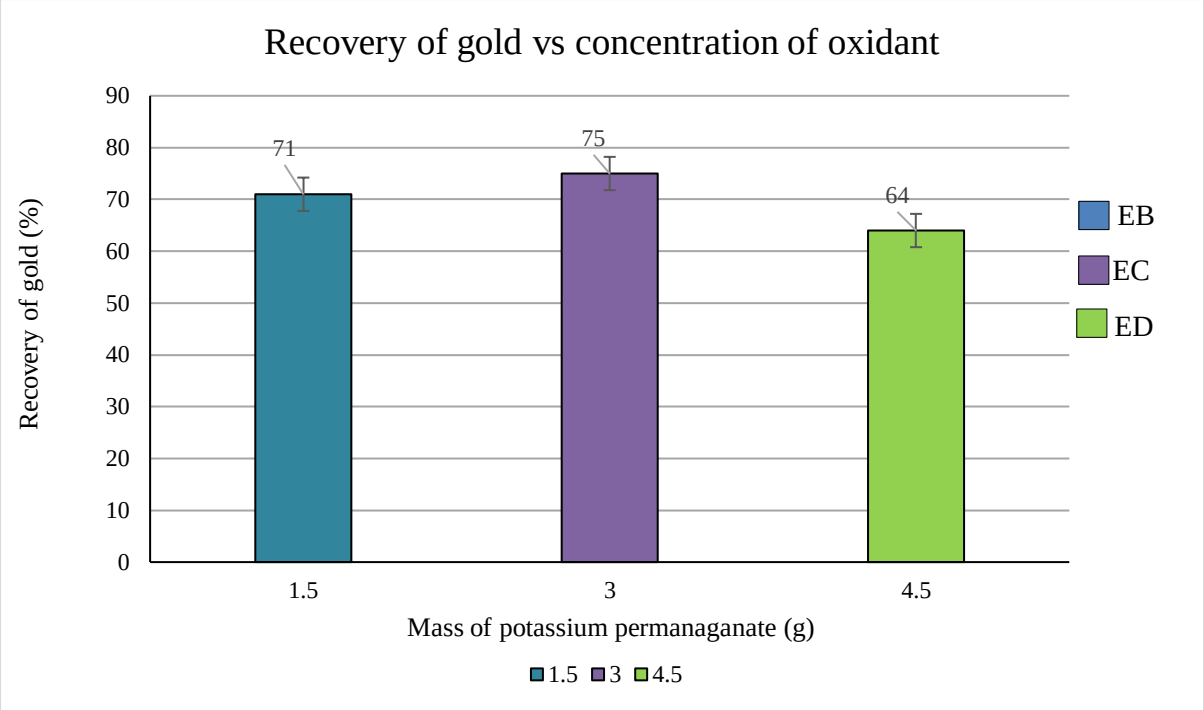

Figure 7.2: Recovery of gold vs concentration of potassium permanganate. Parameters are further detailed in Table 7.1.

7.2.2 Effect of leaching time

The second parameter investigated was the impact that leaching time (hours) had on the recovery of gold. Table 7.3 details how secondary parameters (mass of glycine and potassium permanganate) were changed during each experimental trial. Recovery of gold between experiments A and C (Fig. 7.3) increased by 10%, as leaching time and the concentration of oxidant in the system was increased. However, the recovery of gold between experiments C and E slightly decreased as the concentration of the oxidant was increased by three times the concentration of the lixiviant.

Table 7.3: Leaching parameters used to measure the effect of leaching time.

Experiment name	**Leaching time (hours)**	**Mass of glycine (g)**	**Mass of potassium permanganate (g)**
EA	24	1	1
EC	36	1	1.5
EE	48	3	9

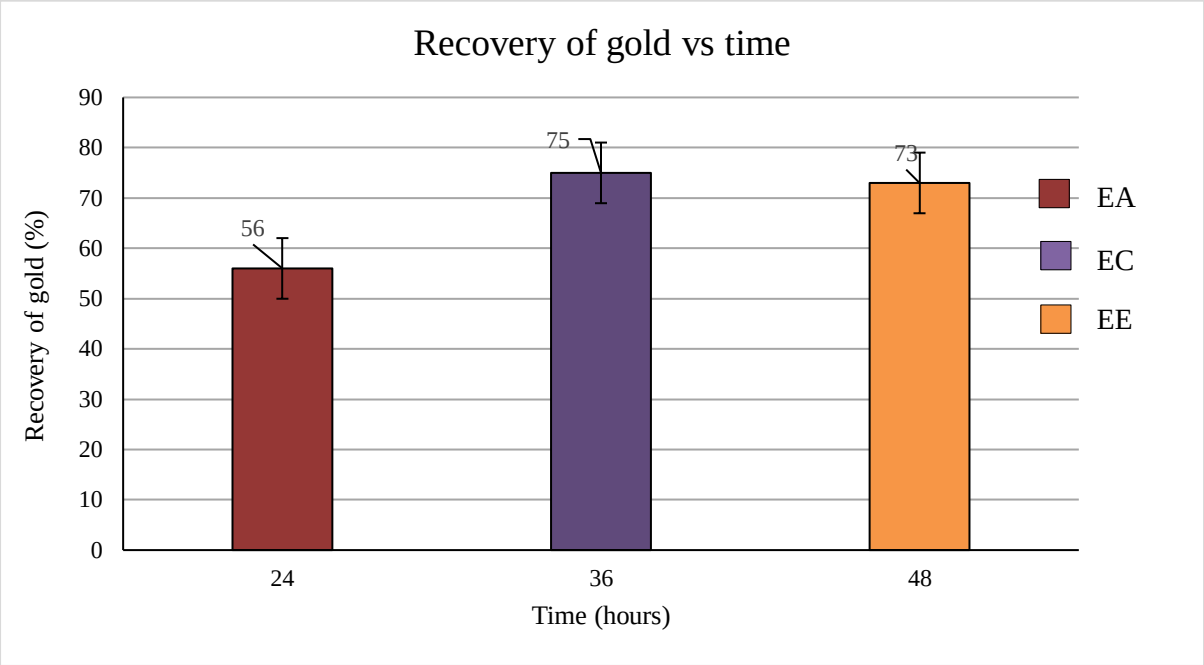

Figure 7.3: Recovery of gold vs leaching time (hours). Parameters are further detailed in Tables 7.1 and 7.3.

7.2.3 Effect of pH

The results of pH were investigated in a separate experimental trial. In this trial, the ratio of potassium permanganate and glycine was kept at a 1:1 ratio, both at 1g each. The leaching time was kept at 24 hours. The concentration of lime (NaOH), used to modify the pH varied at 0.85, 1g and 3 g for experiments A1, A2 and A3, respectively. Overall, an increase in pH had a negative impact on the recovery of gold (Fig 7.4). The highest pH recorded resulted in the lowest recoveries of gold.

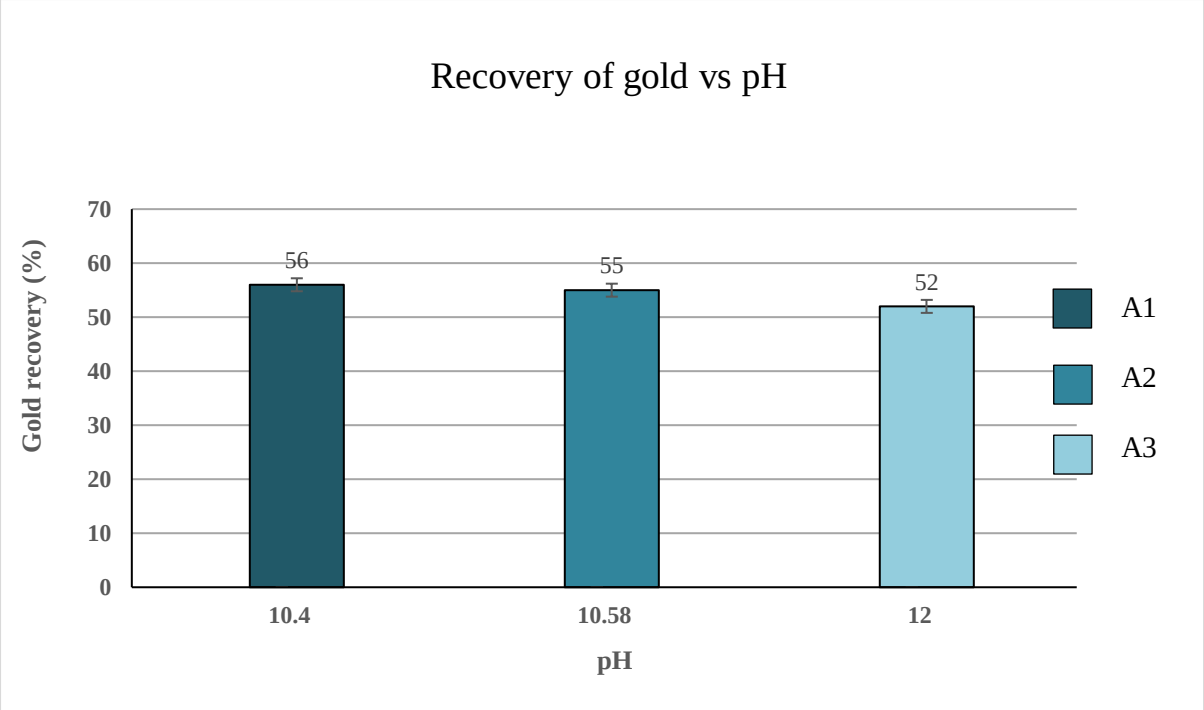

Figure 7.4: Recovery of gold vs pH. Parameters are further detailed in Table 7.1.

7.2.4 Effect of changing slurry density

The last parameter investigated was how changing the slurry density played a role in the recovery of gold. The following parameters, presented in Table 7.4, were used to investigate how slurry density influenced the performance of the system. The slurry density followed a mass to liquid ratio of 300 g: 1200 ml, and the concentration of the oxidant and lixiviant were kept at a 1:1 ratio. The leaching time was kept at 24 hours (see Table 7.1 for detailed parameters). Results are presented in Figure 7.5. The recovery of gold for experiments 1 and 2 remained constant, despite the concentration of glycine and potassium permanganate being increased. The recovery of gold was at its highest in experiment 3, where the concentration of the oxidant and lixiviant was doubled in concentration.

Table 7.4: Leaching parameters used to determine the effect of slurry density.

Experiment name	**Mass of glycine (g)**	**Mass of potassium permanganate (g)**
Experiment 1	0.4	0.4
Experiment 2	0.6	0.6
Experiment 3	1.2	1.2

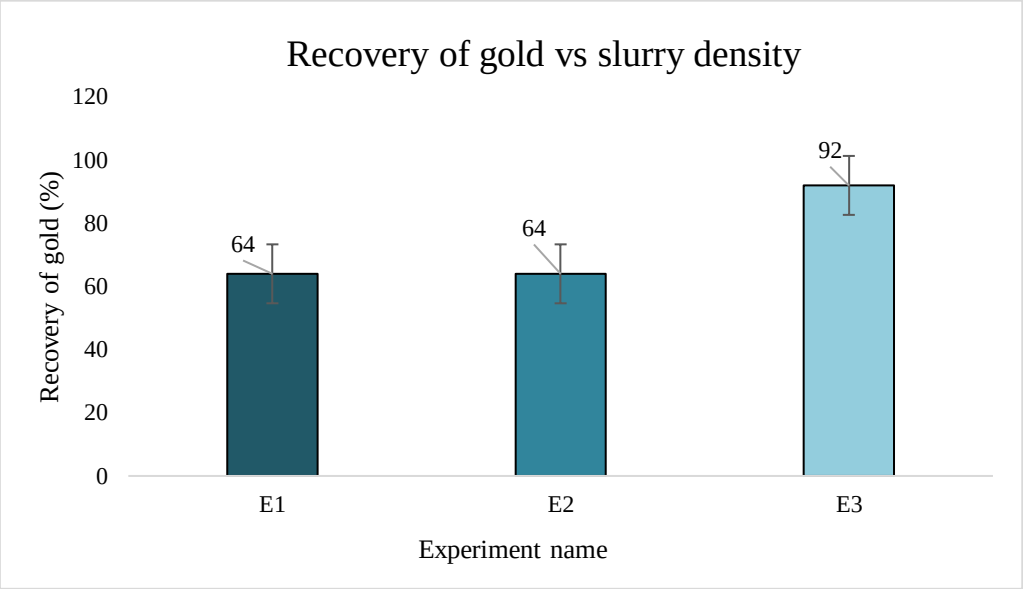

Figure 7.5: Recovery of gold vs slurry density. Parameters are further detailed in Tables 7.1 and 7.4.

Chapter 8: Discussion

This chapter reviews the results presented in chapters 5, 6 and 7 with the aim of providing crucial knowledge on the amenability of glycine leaching on low-grade, complex ores from the Middelvlei Reef in the Witwatersrand Basin. Most of the remaining gold ores in the Witwatersrand Basin are classified as low-grade and complex due to their variable mineralogy, chemistry, and texture. The mining industry therefore needs to find solutions to overcome the phenomena of ore complexity, coupled with the need to move towards more environmentally sustainable processes. This study involves understanding and measuring the ore properties of an orebody to identify the most successful path of processing.

8.1 Mineralogical characterisation

Ore characterisation and gold deportment studies are important tools required to understand complex ore bodies, and to develop appropriate process and mine optimisation development plans (Goodall and Butcher, 2012). The first step in characterizing the ore involved using the optical microscope and SEM-EDS instruments. Subsequently, TIMA high-resolution maps were employed to define the bulk modal mineralogy of the Middelvlei Reef samples and QXRD was used to validate the TIMA results.

The Middelvlei Reef's major mineral phases are, in decreasing order of abundance: quartz, pyrite, muscovite, chlorite (result of metamorphic alteration), pyrrhotite, zircon, oxides (hematite and magnetite) and lastly minor phases such as talc, almandine, kaolinite and schorl (Figs. 5.3 and 5.5). This mineralogical assemblage is common to the ores from the Witwatersrand Basin (Frimmel *et al.*, 2019). Two main classes of pyrite were identified in the Middelvlei Reef, including: 1) allogenic (detrital), and 2) authigenic (hydrothermal) pyrite (Figs. 5.1). Allogenic pyrite grains are rounded, indicating sedimentary transport from a hinterland. This interpretation agrees with previous studies (Law *et al.*, 1990; Frimmel, 2014). Authigenic pyrite is present as single euhedral to subhedral crystals or as clusters of crystals. Authigenic crystals produced in-situ following deposition, likely during diagenetic and epigenetic processes (hydrothermal and metamorphic events) (da Costa *et al.*, 2020). A sub-class of allogenic pyrite, porous pyrite, is also present in the reef (Fig. 5.1). Porous pyrite displays different kinds of textures, with 1) randomly spaced inclusions of biotite, muscovite, rutile and chlorite and 2) concentric laminations (Fig. 5.1C). Concentrically laminated pyrite is usual in the Witwatersrand Basin but is volumetrically minor in concentration in comparison to the different kinds of texture (Agangi *et al.*, 2015). The presence of porous pyrite within the Middelvlei Reef holds significant importance as these pyrites are auriferous containing high amounts of electrum inclusions (Agangi *et al.*, 2015). The presence of electrum has been confirmed in the Middelvlei Reef by SEM-EDS analyses and can cause slower leaching kinetics and excessive reagent intake (La Brooy *et al.*, 1994). Overall,

the mineralogical assemblage of the Middelvlei Reef ore is common with other ores from the Witwatersrand Basin.

8.2 Gold deportment study using TIMA

The association of gold with the gangue mineralogy, its liberation status, available free-surface area analysis, and the grain sizes were all quantified. Gold grains are detectable using TIMA. The results show that gold is intimately associated with, in decreasing order: pyrite, quartz, micas (biotite, muscovite and chlorite), and minor phases such as florencite, and kaolinite (Fig. 5.6). The textural relationship between gold and the gangue mineralogy can be witnessed in the TIMA phase maps, such as Figures 5.5 and 5.7 and SEM-EDS photomicrographs (Fig. 5.2). Gold was observed at grain boundaries of chlorite and quartz, locked within quartz, and present as infillings in micro-fractures in pyrite and quartz (Fig. 5.7).

A free-surface area analysis of gold or PSSA (phase-specific surface area) analyses of the gold in the reef highlighted that most gold grains have a small surface area (<5%) that can be exposed to a lixiviant (Fig. 5.10). The implications of the results of the gold deportment study are that the ore needs to be crushed down to P80 (-75µm) to ensure that gold is either fully liberated or has a better free-surface area available exposed to the action of a lixiviant. This strategy is currently the standard procedure on processing plants. Gold locked at the grain boundaries of gangue minerals are expected to be liberated at the suggested grind size. Ultra-fine gold (<0,02, >20 µm) present in fractures of pyrite and quartz conversely requires ultra-fine grinding (Zhou *et al.*, 2004). This kind of grinding is expensive but viable if pre-treatment on the ore is employed. It is imperative to note that ultra-fine grinding (UFG) may increase the preg-robbing behaviour of silicate minerals due to an increase in surface reactivity (Mohammadnejad *et al.*,2013). Therefore, only employing a P80 (-75µm) grind size will not ensure high recoveries of gold during glycine leaching considering that a fraction of the gold is locked.

A pre-treatment stage should be employed to improve recovery before glycine leaching takes place. An acid pre-treatment can be employed coupled with ultrafine grinding, the acid pre-treatment can help improve gold recovery by destroying the gangue phases to ensure that glycination is effective and ultra-fine grinding can ensure that the remaining locked gold is liberated. Acid treatments such as alkaline leaching pre-treatments which destroys components of the ore by adding chemical reagents and nitric acid technology that rapidly oxidizes sulphide minerals (Larrabure and Rodriguez-Reyes, 2021).

8.3 The implications of ore mineralogy on leaching

Preg-robbing is a common phenomenon that takes place during leaching when the gold complex is robbed from solution by ore constituents, and almost all gold lixiviants are known to be impacted by preg-robbing (Ahtiainen *et al.,* 2018). However, the nature and extent of preg-robbing varies. Notably, carbonaceous material causes the most preg-robbing during leaching followed by sulphide and silicate minerals (Zhou *et al.,* 2004; Aylmore, 2016). Carbonaceous material has been identified in the Middelvlei Reef using an optical microscope (Fig. 5.1). To counteract preg-robbing by carbonaceous material, various solutions have been proposed. Treatments for preg-robbing can be grouped in three categories, namely: 1) removal of carbonaceous matter, 2) passivation of carbon and 3) promotion of the adsorption of the gold-complex on an alternative surface (Tan *et al.,* 2005). Sulphide minerals such as pyrite, pyrrhotite, and chalcopyrite have all been observed in the reef (Fig. 5.3). Chalcopyrite is the main sulphide responsible for preg-robbing, followed by pyrite (Larrabure and Rodrigues-Reyes, 2021). Technology has been designed to handle the preg-robbing behaviour of sulphides such as nitric acid pre-treatments which are designed to break down gangue mineralogy which encapsulate gold (Zhou *et al.,* 2004).

Besides carbonaceous matter and sulphide minerals, other preg-robbing materials also identified are silica in the form of quartz (Mohammadnejad *et al.,* 2011) and clay minerals such as kaolinite (Goodall *et al.,* 2005). The mechanical activation of silica, occurring during crushing and fine milling, forms reactive sites where the gold-lixiviant complex can precipitate, resulting in preg-robbing (Mohammadnejad *et al.,* 2013). The positively charged edge surfaces of clay particles are known to attract negatively charged colloidal gold (Goodall *et al.,* 2005). Clay minerals (including other micas such as muscovite) are known to decompose in alkaline solutions and form $Fe(OH)_3$ and $Mg(OH)_2$ compounds which actively absorbs gold (Van Vuuren *et al.,* 2000). The effects of silicate and clay minerals are considered as secondary concerns because the presence of carbonaceous material causes more preg-robbing. To counteract the effects of silicate and clay minerals, the carbon-in-leach technique can be used (La Brooy *et al.,* 1994). The presence of mica minerals on leaching is minimised due to the minerals being low in abundance in the Middelvlei Reef.

The passivation of gold during leaching can be caused by the formation of insoluble coatings. Such coatings can occur in the form of carbonates, sulphides, oxides or metals that form complexes with the lixiviant on the surface layer of gold (Lorenzen and Van Deventer, 1992). Gold surface passivation is known to increase in the system as pH increases (Bagotsky, 2005). Sulphide minerals may form galvanic interactions include pyrite, chalcopyrite, galena (table 6.1) and pyrrhotite. Pyrite is abundant in the reef, followed by chalcopyrite and pyrrhotite which occur in minor/trace concentrations (Figs. 5.3 and 5.4). Both chalcopyrite and pyrrhotite were below the QXRD lower detection limit of 2 % (Fig.

5.5). In the case of sulphide minerals, the passivating layer arises due to an increase in a cathodic current (Lorenzen and Van Deventer, 1992). To mitigate the effects of sulphur, it is required to either eradicate the minerals by employing various techniques such as pressure oxidation with nitric acid or sulfuric acid, or bacterial oxidation (Jeffrey and Anderson, 2003).

Reagent consumers, known to be problematic during leaching because they consume oxygen, have also been identified in the reef. Pyrrhotite is a well-known reagent consumer and is present in minor concentrations of 0.02 % according to TIMA results (Figs. 5.3 and 5.5). During gold leaching, copper is released from chalcopyrite, this element is deemed undesirable because it results in the consumption of oxygen and the lixiviant (Dai and Jeffrey, 2006). To counteract reagent consumers, stronger oxidants need to be added to the system (La Brooy *et al.,* 1994; Becker *et al.,* 2010). Fortunately, the concentrations of pyrrhotite and chalcopyrite are low but still need to be noted because glycine has a high affinity for metals such as Cu (Altinkaya *et al.,* 2020).

8.4 Limitations of automated mineralogy

Limitations have been encountered while collecting data for the gold deportment study with TIMA. Gold needed to be searched for manually in the scanned ore blocks to be correctly quantified and integrated into the modal mineralogy. If this is not correctly done, the modal abundance of gold may be incorrectly represented, and this will subsequently influence data results (mineral association, liberation and grain size analyses). Figure 8.1 provides an example of what happens when gold is incorrectly identified during TIMA analysis. In this example, gold was suspected to be present as an inclusion in porous pyrite following BSE imaging (Fig. 8.1A). The erroneous identification of gold resulted in its over-quantification in the modal elemental data, as seen in Fig. 8.1B. These manual errors may impact the entire gold deportment study and influence key information that is needed for further mineral processing.

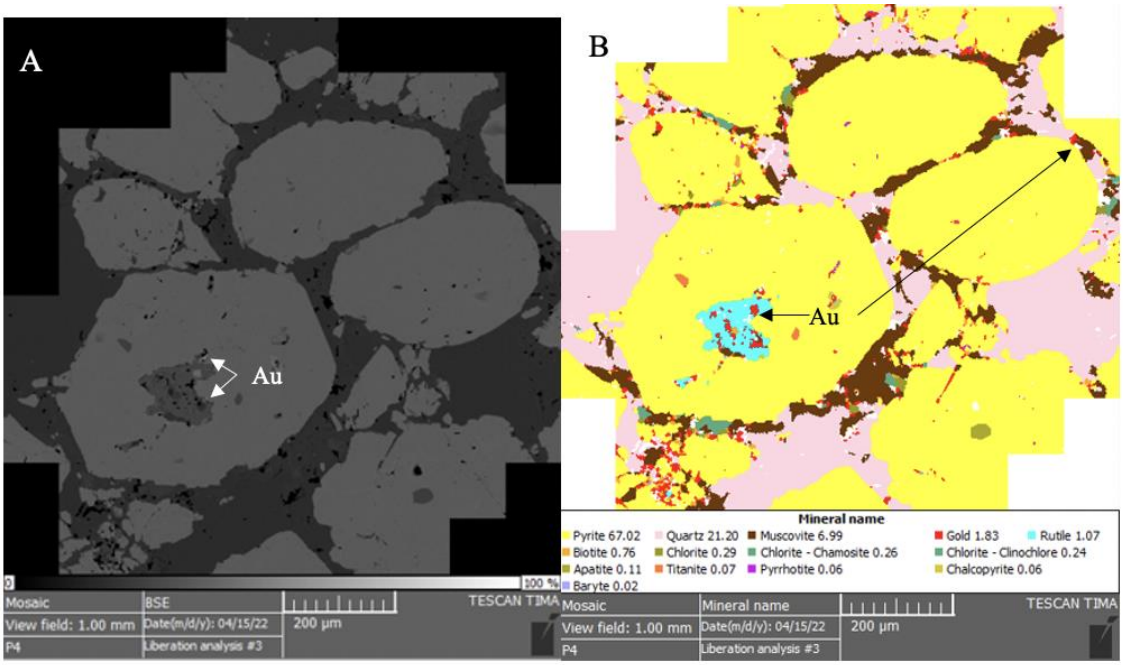

Figure 8.1: Limitations of using automated mineralogy A) BSE-image of suspected inclusions of gold present in porous pyrite. B) Phase-maps generated from the BSE image where gold is over-quantified after incorrect identification.

8.5 Ore characterisation using Micro-XCT

Mineral processing is driven primarily by two factors: ore texture and ore mineralogy. Micro-XCT was used to determine both parameters in the Middelvlei Reef. The technique was able to successfully identify the main silicate and sulphide phases in the ore but failed to discriminate between phases that had similar attenuation values. Sulphide phases had attenuation values of 3.48, 3.78, 3.56 of the phases pyrite, chalcopyrite and pyrrhotite respectively. From the identification of the mineral phases, ore texture could be quantified. Ore texture is an important parameter that influences downstream mineral processing activities such as communition, liberation and recovery (Bonnici *et al.*, 2008). Specifically, ore texture parameters that were explored included grain sizes, shape (i.e., sphericity) and 3D spatial distribution.

Textural properties were determined for both gold and sulphide phases. According to the results, the grain shape (defined by sphericity) of gold in the Middelvlei Reef is highly spherical, with most grains attaining values between 0.65 – 0.81 (Fig. 5.67). Only a few grains possess a low to medium sphericity, between 0.35 – 0.49. The spherical grains are further evidence of the detrital nature of gold (Frimmel *et al.*, 2019). Lower-sphericity grains could be evidence of hydrothermal processes (Phillips and Powell *et al.*, 2011). The sphericity of gold grains is important because grains with low sphericity (elongate),

are lost in processes such as screening resulting in low recoveries. The average grain size for the gold grains in the reef falls between 16.1 – 67.1 µm (Fig. 5.16). Specifically, TIMA grain size analysis yielded a gold grain size range between 1 – 12 µm (Fig. 5.11). Comparatively, Micro-XCT results included 712 grains (in 3D) whereas the TIMA results included 101 grains (in 2D). Hence, the minor size discrepancy between the two analytical techniques noted above is expected. According to previous studies, the average size of gold grains ranges between 5 µm – 0.15 mm (Zhou *et al.*, 2004). Grain sizes between 0.1 – 0.15 mm are micro-nuggets. The results presented in this study agree with the size range of gold grains found in the Witwatersrand Basin and gives evidence that the Micro-XCT technique can be widely applied to the Witwatersrand Basin ores with confidence to determine the gold grain size. However, the range in gold grain sphericities also provide evidence of hydrothermal processes. These lines of evidence, although not a primary goal of this study, provide some support to the modified placer model.

Statistically, grain sizes measured via Micro-XCT are more accurate because they represent a larger population that is also obtained in 3D. The gold grain size in the Middelvlei Reef is predominantly fine-grained (16.1 – 67.1 µm), with a small portion of gold grains being very fine-grained (<10 µm) (Fig. 5.15). Knowing gold grain sizes is very important because it imparts controls on downstream mineral processing activities. Specifically, gold dissolution increases with decreasing particle size (Egan *et al.*, 2016). When gold is very fine-grained and associated with sulphide minerals (e.g., Fig. 5.6), gold may not be optimally recovered by a lixiviant. Furthermore, coarse-grained gold may be incompletely leached due to a slow dissolution kinetic which requires longer retention times (Zhou and Cabri, 2004).

Sulphide minerals identified in the Middelvlei Reef include pyrite, pyrrhotite and chalcopyrite as determined by optical microscopy, SEM-EDS and TIMA (e.g., Figs. 5.3 and 5.5). For Micro-XCT, sulphide minerals were grouped together under 'sulphides' because discriminating between the minerals proved to be difficult as the attenuation values overlapped between minerals. The average grain size of the sulphide minerals fall between 395.2 – 495.2 µm, with a minority of grains being 1 mm in size (Fig. 5.17). According to previous studies, the average grain size of pyrite in gold-bearing quartz pebble conglomerates in the Witwatersrand Basin is between 150 – 200 µm (da Costa *et al.*,, 2020).

The grain sphericity of pyrite varies due to the various classes of pyrite present in the Middelvlei Reef (Fig. 5.1). The results indicate that most grains are predominantly highly spherical, between 0.65 – 0.81, with a few grains being of low- to medium-sphericity, between 0.35 – 0.49 (Fig. 5.18). Gold is mainly associated with pyrite in the Middelvlei Reef (Fig. 5.6). Therefore, the texture of pyrite needs to be understood to successfully liberate (communition) any gold locked in pyrite as inclusions. Porous pyrite, which contains gold inclusions, was identified via optical microscopy and TIMA in the Middelvlei Reef (e.g., Fig. 5.1). The encapsulation of visible gold in sulphides results in gold losses

during leaching unless gold is liberated by fine grinding of the ore. Thus, given that pyrite (and pyrrhotite; Appendix C) grains are both coarse-grained and highly spherical results in a large amount of milling energy being lost to the grinding the gangue phases and not liberating the valuable phases (Wikedzi and Leißner, 2021). The degree of mineral liberation should be confirmed every time the textural properties of the ore are suspected to have changed, to determine when to employ ultra-fine grinding or normal grinding.

8.6 Limitations of Micro-XCT

Micro-XCT is a non-destructive tool that has been used for over 20 years in the geoscience and mining disciplines. Traditionally, ore texture was quantified by using qualitative methods (e.g., hand specimen and optical microscopy), but Micro-XCT technology has made it possible to quantify ore texture digitally (Guntoro *et al.*, 2020). The technology however has its limitations that need to be outlined here to ensure that the data presented is accurate and can be well incorporated into a predictive model for further mineral processing.

The first limitation encountered was a lack of accurate discrimination between minerals when the attenuation coefficient difference is below 6 % (Bam *et al.*, 2020). For minerals in the Middelvlei Reef, quartz, muscovite, chlorite and biotite all have similar low attenuation values (Fig. 4.3) and were therefore grouped together under ‘silicates’. This re-grouping was also necessary with sulphide minerals. Specifically, pyrite, pyrrhotite and chalcopyrite, which occur in the reef, all have similar attenuation coefficients. This can be further complicated when minerals with a similar attenuation coefficient are in physical contact with one another, as in the example of pyrite and pyrrhotite in the Middelvlei Reef. Discriminating between individual minerals can be challenging and some margin for error should be considered when interpreting results. To diminish the risk of inaccurate mineral identification, validation techniques such as optical microscopy, automated mineralogy (TIMA or QEMSCAN) and QXRD analysis are recommended to accurately quantify the sample’s modal before undergoing Micro-XCT analysis.

The second limitation is that Micro-XCT tends to overestimate the concentration of gold existent in the samples due to the high density of the mineral. Minerals with a high density appear as a ‘bright speck’ due to their high density in contrast to minerals with a lower density. This can result in an inaccurate quantification of gold during phase segmentation due to the partial volume effect. To avoid overvaluing the modal proportions of certain minerals, such as gold in this study, it is important to use the hypothetically calculated linear attenuation coefficients coupled with the mineral densities and exact mineral compositions when doing phase segmentation.

The last challenge was encountered when fully describing the grain characteristics with Micro-XCT data that was produced during defect analysis. This data provides grain size and sphericity, but not shape factor. Both shape factor and grain sphericity are indexes that are used to fully describe the morphology of grains in 3D. The difference between shape factor and grain sphericity is that shape factor is a measure of the roundness of a particle, independent of size whereas sphericity is the measure of how spherical or angular an object is. To calculate the shape factor of the grains, the circumference of a specific grain needs to be calculated. Defect analysis data provides both the radius and diameter; therefore, the circumference can be calculated from these values. However, when using the formula to calculate the shape factor index, often the results are inaccurate and not entirely representative. To accurately quantify this, advanced software should be coupled with XCT to improve the accuracy or descriptions.

8.7 Insights from the multi-elemental analysis of the Middelvlei Reef

The chemical composition of the ore was outlined by conducting a geochemical examination of the Middelvlei Reef ore to identify potentially deleterious elements. Elements that could be potentially deleterious to mineral processing and the environment have been identified in Table 6.1 and their negative impact on mineral processing is summarised in Figure 8.2. The elements identified are known to cause refractory behaviour during leaching by either impeding dissolution/diffusion or by consuming reagents in the leaching system.

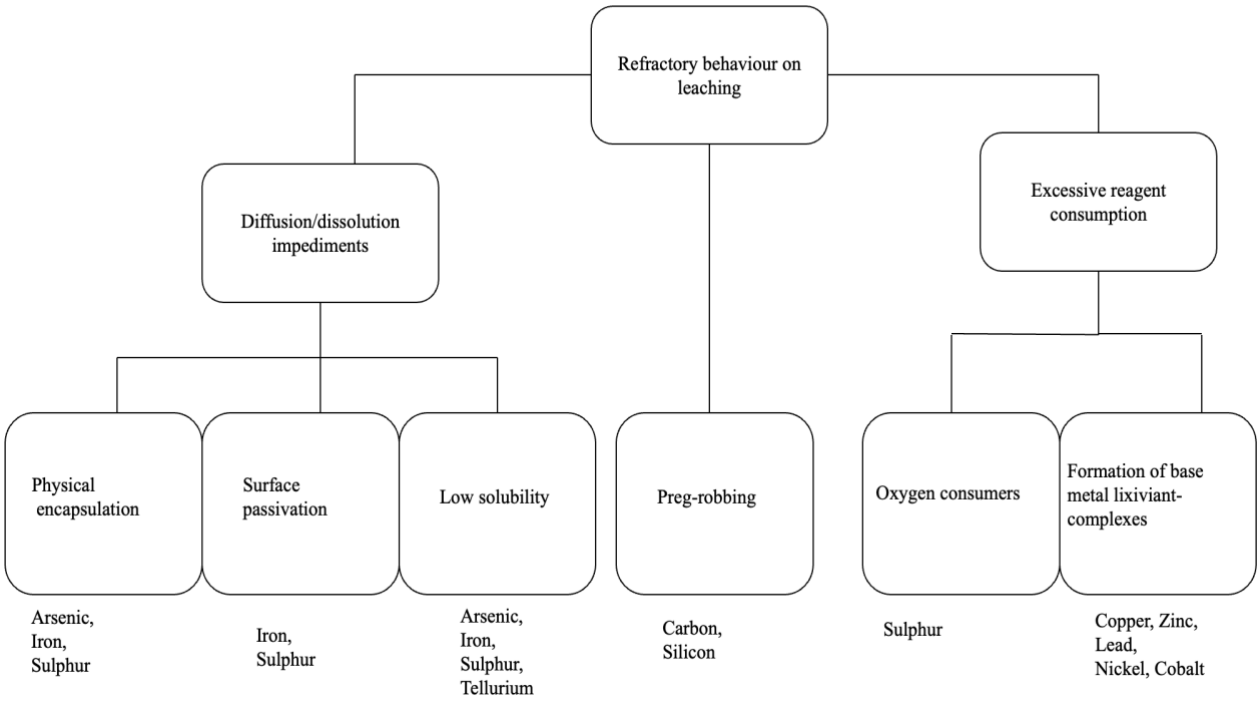

Figure 8.2: Schematic diagram of elements that cause refractory behaviour during leaching. Modified after Larrabure et al. (2021).

Gold is known to be associated with elements such as arsenic. Arsenic is present in the Middelvlei Reef ore at a concentration of 5.05 ppm (Table 6.1). Arsenic is known to hinder the recovery of gold during leaching because the element decomposes to form arsenic-bearing minerals on the surface of gold, hindering the binding of the lixiviant with gold, thus promoting refractory behaviour (Cao *et al.*, 2021). The removal of arsenic can be done by rising the concentration level of lime in the leaching system (Cao *et al.*, 2021). Iron and sulphur are also known to host disseminated gold in iron sulphide minerals such as pyrite, pyrrhotite and chalcopyrite, as well as iron oxides such as hematite (Larrabure and Rodriguez-Reyes, 2021). The impacts of iron sulphides have been discussed in section 7.2.

The dissolution of Fe, Mn, Cr, Al and Si is negligible in glycine leaching solutions, this serves as an advantage because Fe is a common impurity in cyanide-free leaching systems (Tanda *et al.*, 2017) and is present in the Middelvlei Reef (Table 6.1). Glycine has an attraction for metal ions like Au, Ag, Cu, Zn, Pb, Co and Ni (Altinkaya *et al.*, 2020). Copper present in sulphide minerals consumes oxygen and the lixiviant in the leaching solution (Dai and Jeffrey, 2006). If the concentration of copper in an ore is above 0.5 wt.%, it would be deemed uneconomical to use conventional leaching methods (Kianina *et al.*, 2018). However, this is not the case for the Middelvlei Reef because the concentration of copper is low at <0.01 wt.% (Table 6.1). Interestingly, the presence of the impurity base metals such as copper and nickel are beneficial in some cases since they behave as additional oxidants in glycine leaching system (Oraby *et al.*, 2019).

Cobalt has been identified as potentially problematic because the metal forms complexes with glycine due to the high affinity that the ligand has with base metal (Maseki, 2013). The complex is highly stable and is hard to dispose of after hydrometallurgical processing. However due to it being present at a low concentration (87.80 ppm; Table 6.1), it is not of concern (Safizadeh *et al.*, 2014). Lastly, concerning the environment, the presence of U, Co, Pb and Cr have been identified as potentially problematic because they are enriched in the ore and are above the mean crustal composition (Maseki, 2013). After mineral processing, these elements reside in tailings dumps and their presence in dust aerosols could have carcinogenic risks to the nearby public if not closely monitored (Maseki *et al.*, 2017). The limitation in these chemical analyses is that there is an evident gap in the research available on how certain elements impede glycine leaching. Most of the research is focused on how certain elements impede cyanide leaching and chlorination.

8.8 Effects of various parameters on glycine leaching; the way forward

Bottle roll leaching performed at ambient temperatures is a great way to replicate tank leaching performed in a full-scale processing plant (Stange, 1999). Current baseline cyanidation conducted at Driefontein operations (Sibanye-Stillwaters Limited), are producing gold recoveries >90 % for the Middelvlei Reef. To match these recoveries, optimisation test-work studies were performed to identify the optimum process parameters that impart an influence on the recovery of gold. The constraints used to conduct the experiments are listed in Table 7.1, and the results presented in Chapter 7. The following paragraphs discuss each of the parameters individually.

Concentration of oxidant

According to the results presented in Figure 7.2, the recovery of gold did not rise linearly with an increase in the concentration of potassium permanganate. The recovery of gold showed an initial increase but declined by 9 % when the concentration of the oxidant was excessively increased from the initial concentration of 1.5 g to 4.5 g of potassium permanganate. Similar behaviour was recorded in experiments conducted by Oraby *et al.* (2020). The decrease of gold recovery can be accredited to the excess oxidation of glycine, caused by a surplus of permanganate ions in the system. Thus, the oxidation of glycine results in the loss of glycine ions that can participate in the recovery of gold (Insausti *et al.*, 1992). Therefore, grounded on the results from this optimisation study and other studies, it is recommended that glycine needs to be added at a greater stoichiometric ratio compared to potassium permanganate, thus ensuring that there is free glycine in the system to complex with gold.

Leaching time

The second parameter evaluated was the influence of leaching time on the recovery of gold. Leaching time is one of the most important parameters in any bottle-roll leaching experiment. The longer the metal of interest is in contact with the leaching solution, the more the desired metal should theoretically be recovered. In the experiments, the recovery of gold increased by 11 % when the leaching time was increased from 24 to 36 hours. However, the recoveries of gold decreased by 2 %, when leaching time was increased to 48 hours, the maximum time allotted for the trial of leaching experiments (Fig. 7.3). The reduction in gold recoveries at the maximum allotted time may be attributed to secondary parameters in the experiment in question (Table 7.3). The concentration of the oxidant in the system was increased by three times the concentration of glycine in the system. The excess of permanganate ions resulted in the loss of glycine available to complex with gold by oxidation. Therefore, to achieve better recovery of gold with leaching time, additional glycine should be added to the system to evade

its loss by oxidation. If there are enough active glycine ions participating in the system, increasing the leaching time would be economical and the recoveries of gold would be greater.

Effect of pH

Figure 7.4 shows the gold recovery at different pH levels in the permanganate-glycine system. The recovery of gold decreased linearly by 1 – 2 % with an increase in pH values from 10.4 – 12. The recovery of gold at alkaline conditions is most optimum at a pH a range of 10 – 12 (Altinkaya *et al.*, 2020). Ideally, the recovery of gold should increase with pH due to the presence of hydroxide ions facilitating the dissolution of gold (Nowicka *et al.*, 2010). Leaching at lower alkaline pH conditions of 10.5 is more economical because a lower concentration of lime would be required. This is an optimum pH range. The system pH should be above 6.5 to ensure that glycine is not in its zwitterion form which does not effectively bind with metals (Aksu and Doyle, 2002). The loss of gold during leaching may be due to refractory behaviour governed by the mineralogy present in the ore or due to the presence of acid producing minerals which could have influenced the pH, thus reducing recovery. A recommendation would be that pH is periodically checked during leaching to ensure that the pH remains at optimum levels during leaching.

Effect of slurry density

The slurry density was decreased for experiments E1 – E3 to 20% solids and 80% liquids. The slurry density was reduced from 30 % solids and 70 % liquids to 20% solids and 80% liquids. The concentration of glycine and permanganate were increased at a 1:1 ratio in each experimental trial (Table 7.4). The results produced show that E3 yielded the highest recorded gold recovery out of all three experiments. Increasing the concentration of the glycine-permanganate system at a 1:1 ratio ensured that there is no loss of glycine in the system due to oxidation by excess permanganate ions and reducing the slurry density. Pulp densities that are too high or too low are not beneficial for gold leaching (Stange, 1999). For example, the presence of clay minerals can result in high pulp viscosities and may thus hinder mass transfer (Brittan and Plenge, 2015). The presence of clay minerals should be considered since they are ubiquitous in many ore deposits, including the Witwatersrand Basin gold ores. A slurry density of 80% liquids and 20% solids performed best.

8.8.1 Optimum leaching conditions (glycine-permanganate vs cyanide)

The optimum conditions for maximum gold extraction included : slurry density reduced to 20 % solids and 80 % liquids, the ratio of glycine to permanganate at a constant 1:1 ratio, a pH of 10.5, and an

ambient room temperature (Experiment E3; Fig. 7.5). These parameters yielded the highest recovery of gold 92 % which is comparable to results produced via cyanidation at Driefontein operations. The second highest recoveries yielded gold recoveries of 75%. The second highest recovery was produced at the following conditions: slurry density of 30% solids and 70 % liquid, glycine to permanganate concentration ratios of 1:3, pH of 10.5, leaching time of 36 hours and at ambient room temperature (Experiments EA – EE). The experimental results reveal that an excess of potassium permanganate in the system caused a slight decline in the recovery of gold. The decline in gold recovery can be attributed to the loss of glycine via oxidation by permanganate ions in the leaching system (Insausti *et al.,* 1992).

Slurry density and the concentration ratio of glycine to the oxidant in the system are parameters that play a significant role in producing high gold recoveries in this optimisation experimental trial. Rising the concentration of the oxidant in the system proved to be beneficial, when not done excessively. Maintaining a 1:1 ratio of permanganate to glycine is ideal, to ensure that the loss of glycine is avoided. Secondly lowering the slurry density (20% solids and 80% liquids) coupled with increasing the concentration of the glycine in the system produced high recoveries of gold. However, the leaching kinetics of glycine are still slow in comparison to cyanide in 24 hours. As a result, to ensure that glycine leaching can competitively perform with cyanide leaching in tank leaching operations, increasing the temperature coupled with maintaining alkaline pH conditions would accelerate leaching kinetics (Eksteen and Oraby, 2015). However, adjusting these parameters would be an added economic cost for mining operations.

8.8.2 Ore characterisation

The next parameter that influenced gold recoveries was the ore mineralogy, texture, chemistry and gold deportment. The rest of gold that could not be retrieved by glycine is locked in minerals with refractory behaviour present in the ore. The occurrence of pyrite in the ore results in the encapsulation of gold and silicate phases lock gold (Figure 5.8). The gangue minerals present in the ore are reagent consumers and impart preg-robbing behaviour which impacts the recovery of gold in a glycine-permanganate system. Reagent consumers outlined in this study are sulphide minerals (pyrite, pyrrhotite and chalcopyrite) which were identified in bulk modal mineralogy analysis conducted by optical microscopy, SEM-EDS, TIMA and QXRD. These passivating effects are known to affect recovery because they interfere with the glycinate complex binding with the metal of interest. Passivating effects increase in the system as pH increases (Bagotsky, 2005) and this requires caution because glycine leaching is more effective in higher alkaline conditions.

The gold deportment study performed by TIMA highlighted that gold in the ore is strongly linked to sulphide minerals such as pyrite, and silicate minerals such as quartz (Fig. 5.7). Gold is locked at the surface of these minerals or present as infillings in fractures in these minerals (Figs. 5.8 and 5.11). It is

therefore essential to ensure that the ore undergoes grinding to liberate the gold and ensure that a sufficient surface area of gold is exposed. TIMA findings have confirmed that most of the gold is locked in gangue phases with only a small surface area being exposed for the action of a lixiviant (Fig. 5.11). Unfortunately, the sulphide grains in the Middelvlei Reef are coarse (Fig. 5.18) such that when grinding takes place, a lot of the energy may be partitioned to grinding gangue mineralogy, resulting in gold not being entirely liberated. When grinding takes place, this may result in the mechanical activation of charged sites on quartz which may attract the gold-complex ion. Furthermore, SEM-EDS results have confirmed the presence of electrum in the Middelvlei Reef. The presence of electrum can result in slower leaching kinetics and excessive reagent depletion (Fig. 5.3) (La Brooy *et al.*, 1994). Altogether, these parameters need to be considered while drawing up an effective processing plan; the ore characteristics need to be tested every time a suspected change in texture or mineralogy to understand which pre-treatment recommended in the study to employ.

Chapter 9: Conclusion and Recommendations

This study aimed to investigate the effect(s) of using an environmentally friendly lixiviant, glycine, to recover gold from select Witwatersrand Basin low-grade ores. This study consisted of: (1) investigating and providing a detailed characterisation of the mineralogy, chemistry and texture of low-grade ores in the Middelvlei reef, and (2) performing leaching experiments using bottle-roller reactors. The first component involved a prediction of the expected gold recoveries and a highlight of any components that could potentially be deleterious to mineral processing to ensure early mitigation. As previous studies have indicated, there is an opportunity to research the implications of leaching low-grade ores with an environmentally benign reagent by conducting test work studies. This chapter will be structured in a manner that chronologically answers the four key questions of this study.

9.1 Ore characteristics and glycine leaching potential

As proposed in the introduction (Chapter 1), this research project will aim to tackle the subsequent key questions:

- Is it possible to use mineralogical, chemical and textural information to predict the processing behaviour and recovery of gold using glycine?
- Are there mineralogical assemblages that may affect the recovery of gold using glycine?
- What are the optimal parameters using glycine as a reagent that will yield maximum gold recoveries while being economically and environmentally responsible?
- What factors influence the leaching kinetics of glycine?

To answer the first key question of this study, samples from the Middelvlei Reef, with no spatial constraints, were used to characterise the mineralogy, chemistry, and texture of Witwatersrand low-grade ores.

Micro-XCT successfully determined the main mineral phases present in the Middelvlei Reef. Furthermore, the technique characterised ore texture (grain shape and size), as well as gold and sulphide grain characteristics. This information is important to design a strategic mineral processing plan. Gold grain sizes in the Middelvlei Reef ranged from nuggets to predominantly fine-grained. The variable range in gold grain size requires attention during mineral processing because fine-grained gold grains will fail to agglomerate and will be subsequently lost during leaching as slimes. Furthermore, sulphide grains are coarse in size. The implications of this are that during communition, more energy will be partitioned towards reducing the grain size of the gangue phases and not fully liberating the valuable phases, which is a costly expense. Gathering information on grain characteristics was easy to acquire,

however acquiring parameters such as mineral/grain interrelationships and accurately describing their spatial distribution proved to be more challenging using Micro-XCT.

Optical microscopy, TIMA and SEM-EDS were used to conduct a complete gold deportment study, that is: 1) identify gold species, 2) determine the bulk mineralogy, and 3) mineral textures. This information is key in understanding how the ore may behave during mineral processing. TIMA analyses determined that the gold is strongly associated with (in decreasing order): pyrite, quartz, chlorite, and micas (biotite and muscovite). Inclusion-bearing pyrite was identified in the reef by optical microscopy. The presence of porous pyrite is significant since it hosts inclusions of gold in high concentrations that can be liberated upon fine grinding. SEM-EDS data identified the presence of electrum in the reef which may slow dissolution kinetics in leaching systems. The findings from the gold deportment study details that gold in the Middelvlei Reef has a small free-surface area amenable to the action of a lixiviant. Thus, the ore needs to undergo fine grinding to liberate gold locked in the gangue mineralogy to ensure optimum recovery during leaching.

Multi-elemental determination was also required to answer the first key question of the study. Analyses determined the presence of elements that can negatively influence the recovery of gold. Elements that are detrimental to mineral processing are flagged in table 6. These elements display refractory behaviour because they either impede dissolution/diffusion kinetics or are reagent consumers. Base metals such as arsenic, iron, and sulphur are of concern because they lower leaching kinetics by forming passivating layers on the surface of gold, physically encapsulating gold, or impeding dissolution because such metals have a low solubility.

The modal mineralogy, conducted by TIMA, answered the second key question of the study. The presence of sulphides, carbonaceous material, and clay in the Middelvlei Reef are impurities that impart preg-robbing behaviour during leaching. Furthermore, the presence of reagent consumers such as pyrrhotite and chalcopyrite, also denoted in trace concentration in the reef consumes oxygen in the leaching system. These minerals impurities need to be considered as they have an effect of lowering kinetics and subsequently lower the recovery of gold using glycine leaching.

The third question of this study: *what the optimal parameters are using glycine as a reagent that will yield maximum gold recoveries while being economically and environmentally responsible?* Different leaching parameters were evaluated to ascertain their impact on gold recovery. The concentration ratio of glycine to permanganate, leaching time, pH, and slurry density were the parameters selected for the experiments. The highest recovery of gold was 92 %, which is comparable to cyanide recoveries. This was achieved at a 1:1 glycine-permanganate ratio at a concentration of 1.2 g, a leaching time of 24 hours, and a slurry density of 20% solids and 80% liquids. The second highest recovery of gold was at 75 % and this was achieved in solutions that had a glycine-permanganate ratio of 1:3 (1 g glycine and

3 g potassium permanganate), a leaching time of 36 hours, and a slurry density of 30% solids and 70% liquids.

The last key question of this study: What factors influence the leaching kinetics of glycine? The key question was investigated by experimental test work. The first parameter investigated was the concentration ratio of glycine to permanganate. An excess concentration of glycine to permanganate is a fundamental requirement for all leaching experiments. The presence of too much permanganate resulted in the loss of glycine by oxidation, which led to lower competitive recoveries due to slower leaching kinetics, due to there being fewer glycine ions in the leaching system. Time was the second parameter investigated; an increased residence time was beneficial for leaching. However, if the concentrations of glycine were not more than the concentration of permanganate, increasing the leaching time would be futile due to the loss of glycine by oxidation in the system, resulting in low recoveries of gold due to fewer glycine ions participating. The last parameter evaluated was the pH of the system. Ideally, glycine preforms best at alkaline conditions, but this requires caution. Adding a high concentration of pH modifier to maintain a high system pH is an economic cost and a high system pH could result in passivating layers forming on the surface of gold. This arises due to galvanic interactions in the system between sulphide minerals. These galvanic interactions increase with system pH and may result in lower recoveries due to the oxide layers formed impeding dissolution.

9.3 Concluding remarks

The hypothesis of this study argues that the mineralogical, chemical, and textural properties of the Middelvlei Reef influences the metallurgical recovery of gold using glycine. By characterising the mineralogy and ore texture of the Middelvlei Reef, it is indeed possible to predict the behaviour of gold during glycine bottle roll leaching. The results presented in this study successfully answer the key questions posed in Chapter 1 and supports the proposed hypothesis of this research investigation. This study successfully outlined how the chemistry, mineralogy, and texture influenced the recovery of gold in a glycine-permanganate system. Glycine is an environmentally benign reagent that could be used as a substitute for cyanide leaching systems soon, however a pre-oxidative step is required first to destroy gangue phases and ultra-fine grinding techniques to entirely liberate the locked gold. This research investigation successfully demonstrated that glycine can be used as sustainable alternative, producing high recoveries of gold, with low economic costs being incurred.

9.4 Future recommendations

In future research, several issues remain unaddressed and need more detailed studies. These include:

- The level of automation for textural quantification in Micro-XCT needs further improving to ensure that the data can holistically describe ore texture(s). This could be done by coupling Micro-XCT results studies with statistical methods to describe the interrelationships and spatial distribution of the ore minerals.
- A modified gold deportment study using mine tailings is also needed to determine how glycine performs in comparison to cyanide, to provide a holistic understanding of the glycine leach system under different conditions.
- An investigation using ultra-fine grinded complex ores from the Witwatersrand Basin as opposed to normal standard grind size of -75μm would prove valuable to understanding how the gold recovery may vary between the two.
- Glycine should be coupled with other green chemicals such as thiosulfate, to determine how the mixture of leachants will perform on Witwatersrand ores.

References

Adam, M., Asamoah, R., Ofori-sarpong, G., Mustapha, A., Asamoah, R.K., Ofori-sarpong, G. & Amankwah, R.K. 2014. Preg-robbing Characteristics of Gold Ores in Preg-robbing Characteristics of Gold Ores in Ghana. *3rd UMaT Biennial International Mining and Mineral Conference*. (January 2015):192–196.

Adams, M.D. 2016. *Chloride as an Alternative Lixiviant to Cyanide for Gold Ores*. Elsevier B.V.

Agangi, A., Hofmann, A. & Wohlgemuth-Ueberwasser, C.C. 2013. Pyrite zoning as a record of mineralisation in the ventersdorp contact reef, Witwatersrand Basin, South Africa. *Economic Geology*. 108(6):1243–1272.

Agangi, A., Hofmann, A., Rollion-Bard, C., Marin-Carbonne, J., Cavalazzi, B., Large, R. & Meffre, S. 2015. Gold accumulation in the archaean witwatersrand basin, south africa-evidence from concentrically laminated pyrite. *Earth-Science Reviews*. 140:27–53.

Ahtiainen, R., Lundström, M. & Liipo, J. 2018. Preg-robbing verification and prevention in gold chloride-bromide leaching. *Minerals Engineering*. 128(August):153–159.

Aksu, S. and Doyle, F.M. 2002. The Role of Glycine in the Chemical Mechanical Planarisation of Copper. *Journal of The Electrochemical Society*. 149(6):G352.

Al-Hakkani, M.F. 2019. Guideline of inductively coupled plasma mass spectrometry “ICP–MS”: fundamentals, practices, determination of the limits, quality control, and method validation parameters. *SN Applied Sciences*. 1(7):1–15.

Alruiz, O.M., Morrell, S., Suazo, C.J. & Naranjo, A. 2009. A novel approach to the geometallurgical modelling of the Collahuasi grinding circuit. *Minerals Engineering*. 22(12):1060–1067.

Altinkaya, P., Wang, Z., Korolev, I., Hamuyuni, J., Haapalainen, M., Kolehmainen, E., Yliniemi, K. & Lundström, M. 2020. Leaching and recovery of gold from ore in cyanide-free glycine media. *Minerals Engineering*. 158(August):106610.

Angove, J. 2005. Metallurgical testwork: Gold processing options, physical ore properties and cyanide management. *Developments in Mineral Processing*. 15:97–108.

Anhaeusser, C.R. 2019. Palaeo- Meso- and Neoarchaean Granite-Greenstone Basement Geology and Related Rocks of the Central and Western Kaapvaal Craton, South Africa. *Regional Geology Reviews*. (2006):55–81.

Armstrong, R.A., Compston, W., de Wit, M.J. & Williams, I.S. 1990. The stratigraphy of the 3.5-3.2 Ga Barberton Greenstone Belt revisited: a single zircon ion microprobe study. *Earth and Planetary Science Letters*. 101(1):90–106.

Asamoah, R.K. and Amankwah, R.K. 2014. Cyanidation of Refractory Gold Ores : A Review. *3rd UMaT Biennial International Mining and Mineral Conference*. (January 2015):204–212.

Aylmore, M.G. 2016. *Alternative Lixiviants to Cyanide for Leaching Gold Ores*. Elsevier B.V.

Azizi, A. and Ghaedrahmati, R. 2015. Optimizing and evaluating the operational factors affecting the cyanide leaching circuit of the Aghdareh gold processing plant using a CCD model. *Proceedings of the Royal Society A: Mathematical, Physical and Engineering Sciences*. 471(2184).

Azizi, A., Petre, C.F., Olsen, C. & Larachi, F. 2011. Untangling galvanic and passivation phenomena induced by sulfide minerals on precious metal leaching using a new packed-bed electrochemical cyanidation reactor. *Hydrometallurgy*. 107(3–4):101–111.

Bagotsky, V.. 2005. *Fundamentals of electrochemistry*.

Bam, L.C., Miller, J.A. & Becker, M. 2020. A Mineral X-ray Linear Attenuation Coefficient Tool (MXLAC) to Assess Minerlogical Differentiation for X-ray Computed Tomography Scanning. *Minerals*. 10(5):1–15.

Barnicoat, A.C., Henderson, I.H.C., Knipe, R.J., Yardley, B.W.D., Napier, R.W., Fox, N.P.C., Kenyon, A.K., Muntingh, D.J., et al. 1997. Hydrothermal gold mineralisation in the witwatersrand basin. *Nature*. 386:820–824.

Barton, E.S. & Hallbauer, D.K. 1996. Trace-element and U-Pb isotope compositions of pyrite types in the Proterozoic Black Reef, Transvaal Sequence, South Africa: Implications on genesis and age. *Chemical Geology*. 133(1–4):173–199.

Bath, M.D., Duncan, A.J. & Rudolph, E.R. 1973. Some Factors Influencing Gold Recovery By Gravity Concentration. *Journal of The South African Institute of Mining and Metallurgy*. 73(11):363–384.

Becker, M., Villiers, J. De & Bradshaw, D. 2010. The flotation of magnetic and non-magnetic pyrrhotite from selected nickel ore deposits. *Minerals Engineering*. 23(11–13):1045–1052.

Bonnici, N., Hunt, J.A., Walters, S.G., Berry, R. & Collett, D. 2008. Relating textural attributes to mineral processing - Developing a more effective approach for the cadia east Cu-Au porphyry deposit. *Australasian Institute of Mining and Metallurgy Publication Series*. (December 2015):415–418.

Brandl, G., Cloete, M. & Anhaeusser, C.R. 2006. Archaean Greenstone Belts. in *Geology of South Africa* Vol. 72. 346–347.

Brittan, M. & Plenge, G. 2015. Estimating process design gold extraction, leach residence time and cyanide consumption for High cyanide-consuming gold ore. *Minerals and Metallurgical Processing*. 32(2):111–120.

La Brooy, S.R., Linge, H.G. & Walker, G.S. 1994. Review of gold extraction from ores. *Minerals Engineering*. 7(10):1213–1241.

Brown, D.H., Smith, W.E., Fox, P. & Sturrock, R.D. 1982. The reactions of gold(0) with amino acids and the significance of these reactions in the biochemistry of gold. *Inorganica Chimica Acta*. 67(C):27–30.

Burron, I., da Costa, G., Sharpe, R., Fayek, M., Gauert, C. & Hofmann, A. 2018. 3.2 Ga detrital uraninite in the Witwatersrand Basin, South Africa: Evidence of a reducing Archaean atmosphere. *Geology*. 46(4):295–298.

Burt, R. 1999. Role of gravity concentration in modern processing plants. *Minerals Engineering*. 12(11):1291–1300.

Cairncross, B. & Anhaeusser, C.R. 1992. Gold in South Africa. *Mineralogical Record*. 23(3):273–316.

Cao, P., Zhang, S., Zheng, Y., Lai, S., Liang, G., Wang, X. & Tan, B. 2021. Identification of elements hindering gold leaching from gold-bearing dust and selection of gold extraction process. *Hydrometallurgy*. 202(932):105612.

Catuneanu, O. 2001. Flexural partitioning of the Late Archaean Witwatersrand foreland system, South Africa. *Sedimentary Geology*. 141–142:95–112.

Chagnes, A. 2019. *Advances in hydrometallurgy*. Vol. 9.

Chao, X., Mingming, C., Tengyue, G., Guangsheng, L., Xingfu, Z., Zhongbo, L., Yanbo, C., Juntong, Z., et al. 2021. Study on Technological Process Innovation of Non-Cyanide Leaching. *E3S Web of Conferences*. 267:1–6.

Chen, T.T., Cabri, L.J. & Dutrizac, J.E. 2002. Characterizing gold in refractory sulfide gold ores and residues. *Jom*. 54(12):20–22.

Coetzee, L.L., Theron, S.J., Martin, G.J., Merwe, J.D. Van Der & Stanek, T.A. 2011. Modern gold deportments and its application to industry. *Minerals Engineering*. 24(6):565–575.

Cook, N.J. & Chryssoulf, S.L. 1990. CONCENTRATIONS OF “INVISIBLE GOLD” IN THE COMMON SULFIDES. *The Canadian Mineralogist*. 28(1930):1–16.

da Costa, G., Hofmann, A. & Agangi, A. 2020. A revised classification scheme of pyrite in the Witwatersrand Basin and application to placer gold deposits. *Earth-Science Reviews*. 201(July 2019):103064.

Coward, M.P., Spencer, R.M. & Spencer, C.E. 1995. Development of the Witwatersrand Basin, South Africa. *Geological Society Special Publication*. 95(95):243–269.

Craig, J.R. 2001. Ore-mineral textures and the tales they tell. *Canadian Mineralogist*. 39(4):937–956.

Dai, X. & Jeffrey, M.I. 2006. The effect of sulfide minerals on the leaching of gold in aerated cyanide solutions. *Hydrometallurgy*. 82(3–4):118–125.

Deschenes, G., Lastra, R., Brown, J.R., Jin, S., May, O. & Ghali, E. 2000. Effect of lead nitrate on cyanidation of gold ores: progress on the study of the mechanisms. *Minerals Engineering*. 13(12):1263–1279.

Dunham, S. & Vann, J. 2007. Geometallurgy, geostatistics and project value - Does your block model tell you what you need to know? *Australasian Institute of Mining and Metallurgy Publication Series*. 189–196.

Egan, J., Bazin, C. & Hodouin, D. 2016. Effect of particle size and grinding time on gold dissolution in cyanide solution. *Minerals*. 6(3).

Eksteen, J.J. & Oraby, E.A. 2015. The leaching and adsorption of gold using low concentration amino acids and hydrogen peroxide: Effect of catalytic ions, sulphide minerals and amino acid type. *Minerals Engineering*. 70:36–42.

Els, B.G. 1983. The sedimentology of the Middelvlei Reef on Doornfontein Gold Mine.

Els, B.G. 1991. Placer formation during progradational fluvial degradation: the late Archaean Middelvlei gold placer, Witwatersrand, South Africa. *Economic Geology*. 86(2):261–277.

England, G.L., Rasmussen, B., Krapez, B. & Groves, D.I. 2002. Palaeoenvironmental significance of rounded pyrite in siliciclastic sequences of the Late Archaean Witwatersrand Basin: Oxygen-deficient atmosphere or hydrothermal alteration? *Sedimentology*. 49(6):1133–1156.

Eriksson, K.A., Turner, B.R. & Vos, R.G. 1981. Evidence of tidal processes from the lower part of the Witwatersrand Supergroup, South Africa. *Sedimentary Geology*. 29(4):309–325.

Feng, D. & Van Deventer, J.S.J. 2011. The role of amino acids in the thiosulphate leaching of gold.

Minerals Engineering. 24(9):1022–1024.

Fivaz, C.. 1988. Presidential Address : How the MacArthur - Forrest cyanidation process ensured South Africa's golden future. *Journal of the South African Institute of Mining and Metallurgy*. 88(9):309–318.

Francisca, S. 2012. Mineralogical variability of rand uranium cook mine.

Fraser, K. S, Walton, R. H, Wells, J.A. 1991. Processing of refractory gold ores. *Minerals Engineering*. 4(7–11):1029–1041.

Frimmel, H.E. 2005a. The Formation and Preservation of the Witwatersrand Goldfields, the World's Largest Gold Province. *Society of Economic Geologists. Inc. Economic Geology 100th Anniversary Volume*. 100:769–797.

Frimmel, H.E. 2005b. Archaean atmospheric evolution: Evidence from the Witwatersrand gold fields, South Africa. *Earth-Science Reviews*. 70(1–2):1–46.

Frimmel, H.E. 2014. A Giant Mesoarchaean Crustal Gold-Enrichment Episode: Possible Causes and Consequences for Exploration. *Society of Economic Geologists Inc. Special Publications*. 18:209–234.

Frimmel, H.E. 2018. Episodic concentration of gold to ore grade through Earth's history. *Earth-Science Reviews*. 180:148–158.

Frimmel, H.E. 2019. The Witwatersrand Basin and Its Gold Deposits. in *The Archaean Geology of the Kaapvaal Craton, Southern Africa* A. Kröner & A. Hofmann (eds.). Cham: Springer International Publishing A. Kröner & A. Hofmann (eds.). 255–275.

Frimmel, H.E. & Nwaila, G.T. 2020. Chapter 31: Geologic Evidence of Syngenetic Gold in the Witwatersrand Goldfields, South Africa. *Geology of the World's Major Gold Deposits and Provinces*. (23):645–668.

Fuchs, S.H.J., Schumann, D., Williams-Jones, A.E., Murray, A.J., Couillard, M., Lagarec, K., Phaneuf, M.W. & Vali, H. 2017. Gold and uranium concentration by interaction of immiscible fluids (hydrothermal and hydrocarbon) in the Carbon Leader Reef, Witwatersrand Supergroup, South Africa. *Precambrian Research*. 293:39–55.

Gartz, V.H. & Frimmel, H.E. 1999. Complex metasomatism of an Archaean placer in the Witwatersrand basin, South Africa: The Ventersdorp contact reef - A hydrothermal aquifer? *Economic Geology*. 94(5):689–706.

Goldfarb, R.J. 2021. *Lode Gold Deposits in Time and Space*. 2nd ed. Elsevier Inc.

Goodall, W.R. & Butcher, A.R. 2012. The use of QEMSCAN in practical gold deportment studies. *Transactions of the Institutions of Mining and Metallurgy, Section C: Mineral Processing and Extractive Metallurgy*. 121(4):199–204.

Goodall, W.R. & Scales, P.J. 2007. An overview of the advantages and disadvantages of the determination of gold mineralogy by automated mineralogy. *Minerals Engineering*. 20(5):506–517.

Goodall, W.R., Scales, P.J. & Butcher, A.R. 2005a. The use of QEMSCAN and diagnostic leaching in the characterisation of visible gold in complex ores. *Minerals Engineering*. 18(8):877–886.

Goodall, W.R., Leatham, J.D. & Scales, P.J. 2005b. A new method for determination of preg-robbing in gold ores. *Minerals Engineering*. 18(12):1135–1141.

Grayson, R. 2007. Fine Gold Recovery – Alternatives to Mercury and Cyanide. *World Placer Journal*. 7(March):66–161.

Guntoro, P.I., Ghorbani, Y., Butcher, A.R., Kuva, J. & Rosenkranz, J. 2020. Textural Quantification and Classification of Drill Cores for Geometallurgy: Moving Toward 3D with X-ray Microcomputed Tomography (µCT). *Natural Resources Research*. 29(6):3547–3565.

Guo, H., Deschênes, G., Pratt, A., Fulton, M. & Lastra, R. 2004. Leaching kinetics and mechanisms of surface reactions during cyanidation of gold in the presence of pyrite or stibnite. *2004 SME Annual Meeting Preprints*. 22(04):471–478.

Guy, B.M., Ono, S., Gutzmer, J., Lin, Y. & Beukes, N.J. 2014. Sulfur sources of sedimentary "buckshot" pyrite in the Auriferous Conglomerates of the Mesoarchaean Witwatersrand and Ventersdorp Supergroups, Kaapvaal Craton, South Africa. *Mineralium Deposita*. 49(6):751–775.

Habashi, F. 1970. Principles of extractive metallurgy. *Principles of Extractive Metallurgy*. 1:590.

Hallbauer, D.K. & Joughin, N.C. 1973. Size Distribution and Morphology of Gold Particles in Witwatersrand Reefs and Their Crushed Products. *Journal of The South African Institute of Mining and Metallurgy*. 73(11):395–405.

Hausen, D.M. 2000. Characterizing the textural features of gold ores for optimizing gold extraction. *Jom*. 52(4):14–16.

Heinrich, C.A. 2015. Witwatersrand gold deposits formed by volcanic rain, anoxic rivers and

Archaean life. *Nature Geoscience*. 8(3):206–209.

Hilson, G. & Monhemius, A.J. 2006. Alternatives to cyanide in the gold mining industry: what prospects for the future? *Journal of Cleaner Production*. 14(12-13 SPEC. ISS.):1158–1167.

Hofmann, A., Bekker, A., Rouxel, O., Rumble, D. & Master, S. 2009. Multiple sulphur and iron isotope composition of detrital pyrite in Archaean sedimentary rocks: A new tool for provenance analysis. *Earth and Planetary Science Letters*. 286(3–4):436–445.

Hofmann, A., Anhaeusser, C.R., Dixon, J., Kröner, A., Saha, L., Wilson, A. & Xie, H. 2019. Archaean Granitoid–Greenstone Geology of the Southeastern Part of the Kaapvaal Craton. *Regional Geology Reviews*. 33–54.

Horscroft, F.D.M., Mossman, D.J., Reimer, T.O. & Hennigh, Q. 2012. Witwatersrand Metallogenesis: The Case for (Modified) Syngenesis. *Microbial Mats in Silicilastic Depositional Systems Through Time*. (101):75–95.

Hoyau, S., Pélicier, J.P., Rogalewicz, F., Hoppilliard, Y. & Ohanessian, G. 2001. Complexation of glycine by atomic metal cations in the gas phase. *European Journal of Mass Spectrometry*. 7(4–5):303–311.

Huang, J., Yinping, L. & Yue, P. 2021. Review on the evaluation of green development of mining industry. *IOP Conference Series: Earth and Environmental Science*. 859(1):012094.

Insausti, M.J., Mata-perez, F. & Alvarez-Macho, P. 1992. Permanganate oxidation of glycine: Influence of amino acid on colloidal manganese dioxide. *International Journal of Chemical Kinetics*. 24(5):411–419.

Jolley, S.J., Freeman, S.R., Barnicoat, A.C., Phillips, G.M., Knipe, R.J., Pather, A., Fox, N.P.C., Strydom, D., et al. 2004. Structural controls on Witwatersrand gold mineralisation. *Journal of Structural Geology*. 26(6–7):1067–1086.

Jolly, M.K. 1984a. The sedimentology and economic potential of the auriferous Middelvlei Reef on Driefontein Consolidated Limited.

Jolly, M.K. 1984b. THE SEDIMENTOLOGY AND ECONOMIC POTENTIAL OF THE AURIFEROUS MIDDELVLEI REEF ON DRIEFONTEIN CONSOLIDATED LIMITED.

Kamo, S.L., Reimold, W.U., Krogh, T.E. & Colliston, W.P. 1996. A 2.023 Ga age for the Vredefort impact event and a first report of shock metamorphosed zircons in pseudotachylitic breccias and Granophyre. *Earth and Planetary Science Letters*. 144(3–4):369–387.

Khalesi, M.R., Bazin, C., Hodouin, D. & Bellec, S. 2009. A grinding-liberation model for the size reduction of gold ores. *World Gold Conference*. (January):61–74.

Koglin, N., Zeh, A., Frimmel, H.E. & Gerdes, A. 2010. New constraints on the auriferous Witwatersrand sediment provenance from combined detrital zircon U-Pb and Lu-Hf isotope data for the Eldorado Reef (Central Rand Group, South Africa). *Precambrian Research*. 183(4):817–824.

Kongolo, K. & Mwema, M.. 1998. Metallurgy of gold. *Hyperfine Interactions*. 111:281–289.

Kositcin, N. & Krapež, B. 2004. Relationship between detrital zircon age-spectra and the tectonic evolution of the Late Archaean Witwatersrand Basin, South Africa. *Precambrian Research*. 129(1–2):141–168.

Kositcin, N., McNaughton, N.J., Griffin, B.J., Fletcher, I.R., Groves, D.I. & Rasmussen, B. 2003. Textural and geochemical discrimination between xenotime of different origin in the Archaean Witwatersrand Basin, South Africa. *Geochimica et Cosmochimica Acta*. 67(4):709–731.

Kudryk, V. & Kellogg, H.H. 1954. Mechanism and rate-controlling factors in the dissolution of gold in cyanide solution. *Jom*. 6(5):541–548.

Kyle, J.R. & Ketcham, R.A. 2015. Application of high resolution X-ray computed tomography to mineral deposit origin, evaluation, and processing. *Ore Geology Reviews*. 65(P4):821–839.

de la Winter, H. & Brink, M.C. 1991. Chronostratigraphic subdivision of the Witwatersrand Basin based on a western Transvaal composite column. *South African Journal of Geology*. 94(2–3):191–203.

Laplante, A. & Gray, S. 2005. Advances in gravity gold technology. *Developments in Mineral Processing*. 15(C):280–307.

Law, J.D.M., Bailey, A.C., Cadle, A.B., Phillips, G.N. & Stanistreet, I.G. 1990. Reconstructive approach to the classification of Witwatersrand "quartzites"". *South African Journal of Geology*. 93(1):83–92.

Lehmann, B. 2010. Economic Geology of rare-earth elements in 2014: a global perspective. *European Geologist*. (29):21–24.

Liedberg, B., Lundström, I., Wu, C.R. & Salaneck, W.R. 1985. Adsorption of glycine on hydrophilic gold. *Journal of Colloid And Interface Science*. 108(1):123–132.

Lishchuk, V. & Pettersson, M. 2021. The mechanisms of decision-making when applying

geometallurgical approach to the mining industry. *Mineral Economics*. 34(1):71–80.

Liu, G.Q. & Yen, W.T. 1995. Effects of sulphide minerals and dissolved oxygen on the gold and silver dissolution in cyanide solution. *Minerals Engineering*. 8(1–2):111–123.

Lobos, R., Silva, J.F., Ortiz, J.M., Díaz, G. & Egaña, A. 2016. *Analysis and Classification of Natural Rock Textures based on New Transform-based Features*. Vol. 48. Springer Berlin Heidelberg.

Lorenzen, L. & Van Deventer, J.S.J. 1992. Electrochemical interactions between gold and its associated minerals during cyanidation. *Hydrometallurgy*. 30:177–194.

Maroof, M.A., Mahboubi, A., Noorzad, A. & Safi, Y. 2020. A new approach to particle shape classification of granular materials. *Transportation Geotechnics*. 22(August 2019):100296.

Marsden, J.O. & House, C.I. 2006. Principles of Gold Hydrometallurgy. in *The Chemistry of Gold Extraction*. 111–145.

Marsden, J.O. & Sass, S.A. 2014. Innovations in gold and silver extraction and recovery. in *Mineral Processing and Extractive Metallurgy: 100 Years of Innovation*. 361–388.

Maseki, J. 2013. Risk Assessment of Inhaled and Ingested Airborne Particles in the Vicinity of Gold Mine Tailings : Case Study of the Witwatersrand Basin. 2013(January).

Maseki, J., Annegarn, H.J. & Spiers, G. 2017. Health risk posed by enriched heavy metals (As, Cd, and Cr) in airborne particles from Witwatersrand gold tailings. *Journal of the Southern African Institute of Mining and Metallurgy*. 117(7):663–669.

Minter, W.E.. 1978. A sedimentological synthesis of placer gold, uranium and pyrite concentrations in Proterozoic Witwatersrand sediments. *Canadian Society Petroleum Geology, Fluvial Sedimentology Memoir*. 5(1977):605–625.

Minter, W.E.L., Goedhart, M., Knight, J. & Frimmel, H.E. 1993. Morphology of Witwatersrand gold grains from the Basal Reef: Evidence for their detrital origin. *Economic Geology*. 88(2):237–248.

Mngoma, L. 2012. A gold , uranium and thorium Deportment Analysis of Witwatersrand Ore From Cooke Section , Rand Uranium Randfontein.

Mohammadnejad, S., Provis, J.L. & Van Deventer, J.S.J. 2011. Gold sorption by silicates in acidic and alkaline chloride media. *International Journal of Mineral Processing*. 100(3–4):149–156.

Mohammadnejad, S., Provis, J.L. & van Deventer, J.S.J. 2013. Reduction of gold(III) chloride to gold(0) on silicate surfaces. *Journal of Colloid and Interface Science*. 389(1):252–259.

Moran, R. 2001. More cyanide uncertainties - lessons from the Baia Mare, Romania, spill - water quality and politics.

Mossman, D.J., Minter, W.E.L., Dutkiewicz, A., Hallbauer, D.K., George, S.C., Hennigh, Q., Reimer, T.O. & Horscroft, F.D. 2008. The indigenous origin of Witwatersrand "carbon". *Precambrian Research*. 164(3–4):173–186.

Mudd, G.M. 2007. Global trends in gold mining: Towards quantifying environmental and resource sustainability. *Resources Policy*. 32(1–2):42–56.

Muir, D.M. & Aylmore, M.G. 2004. Thiosulphate as an alternative to cyanide for gold processing - Issues and impediments. *Transactions of the Institutions of Mining and Metallurgy, Section C: Mineral Processing and Extractive Metallurgy*. 113(1 MAR.).

Mwanga, A., Rosenkranz, J. & Lamberg, P. 2015. Testing of ore comminution behavior in the geometallurgical context—A review. *Minerals*. 5(2):276–297.

Myers, R.E., Zhou, T. & Neil Phillips, G. 1993. Sulphidation in the Witwatersrand Goldfields: evidence from the Middelvlei Reef. *Mineralogical Magazine*. 57(388):395–405.

Neil Phillips, G. & Powell, R. 2011. Origin of Witwatersrand gold: A metamorphic devolatilisation-hydrothermal replacement model. *Transactions of the Institutions of Mining and Metallurgy, Section B: Applied Earth Science*. 120(3):112–129.

Neingo, P.N. & Tholana, T. 2016. Trends in productivity in the South African gold mining industry. *Journal of the Southern African Institute of Mining and Metallurgy*. 116(3):283–290.

Nicol, M.J. 1980. The anodic behaviour of gold - Part II - Oxidation in alkaline solutions. *Gold Bulletin*. 13(3):105–106.

Nicol, M.J., Fleming, C. a & Paul, R.L. 1992. The Chemistry of the Extraction of Gold. *The extractive metallurgy of gold*. 831–905.

Nowicka, A.M., Hasse, U., Hermes, M. & Scholz, F. 2010. Hydroxyl radicals attack metallic gold. *Angewandte Chemie - International Edition*. 49(6):1061–1063.

Nwaila, G.T., Ghorbani, Y., Becker, M., Frimmel, H.E., Petersen, J. & Zhang, S. 2020. Geometallurgical Approach for Implications of Ore Blending on Cyanide Leaching and Adsorption Behavior of Witwatersrand Gold Ores, South Africa. *Natural Resources Research*. 29(2):1007–1030.

Nwaila, G.T., Durrheim, R.J., Jolayemi, O.O., Maselela, H.K., Jakaitė, L., Burnett, M. & Zhang, S.E.

2020a Significance of granite-greenstone terranes in the formation of Witwatersrand-type gold mineralisation – A case study of the Neoarchaean Black Reef Formation, South Africa. *Ore Geology Reviews*. 121(April):103572.

Nwaila, G.T., Bourdeau, J.E., Jinnah, Z., Frimmel, H.E., Bybee, G.M., Zhang, S.E., Manzi, M.S.D., Minter, W.E.L., et al. 2021b. The significance of erosion channels on gold metallogeny in the Witwatersrand Basin (South Africa): Evidence from the carbon leader reef in the carletonville gold field. *Economic Geology*. 116(2):265–283.

Oraby, E.A. & Eksteen, J.J. 2014. The selective leaching of copper from a gold-copper concentrate in glycine solutions. *Hydrometallurgy*. 150:14–19.

Oraby, E.A., Eksteen, J.J., Karrech, A. & Attar, M. 2019. Gold extraction from paleochannel ores using an aerated alkaline glycine lixiviant for consideration in heap and in-situ leaching applications. *Minerals Engineering*. 138(February):112–118.

Oraby, E.A., Li, H. & Eksteen, J.J. 2020a. An Alkaline Glycine-Based Leach Process of Base and Precious Metals from Powdered Waste Printed Circuit Boards. *Waste and Biomass Valorisation*. 11(8):3897–3909.

Oraby, E.A., Eksteen, J.J. & O'Connor, G.M. 2020b Gold leaching from oxide ores in alkaline glycine solutions in the presence of permanganate. *Hydrometallurgy*. 198(June):105527.

Pakiari, A.H. & Jamshidi, Z. 2007. Interaction of amino acids with gold and silver clusters. *Journal of Physical Chemistry A*. 111(20):4391–4396.

Pérez-Barnuevo, L., Pirard, E. & Castroviejo, R. 2013. Automated characterisation of intergrowth textures in mineral particles. A case study. *Minerals Engineering*. 52(November 2021):136–142.

Perez-Benito, J.F., Mata-perez, F. & Brillas, E. 1986. Permanganate oxidation of glycine: Kinetics, catalytic effects, and mechanisims. *Canadian Journal of Chemistry*. 65(10):2329–2337.

Phillips, G.N. & Myers, R.E. 1989. The Witwatersrand Gold Fields: Part ll: An origin for Witwatersrand gold during metamorphism and associated alteration. *The Geology of Gold Deposits: The Perspective in 1988. Economic Geology Monograph No. 6*. (March 2021):598–609.

Phillips, G.N., Law, J.D.M. & Myers, R.E. 1990. The role of fluids in the evolution of the Witwatersrand Basin. *South African Journal of Geology*. 93(1):54–69.

Poujol, M. & Robb, L.J. 1999. New U-Pb zircon ages on gneisses and pegmatite from south of the the Murchison greenstone belt, South Africa. *South African Journal of Geology*. 102(2):93–97.

Poujol, M., Robb, L.J., Anhaeusser, C.R. & Gericke, B. 2003. A review of the geochronological constraints on the evolution of the Kaapvaal Craton, South Africa. *Precambrian Research*. 127(1–3):181–213.

Rees, K.L. 2000. The leaching and adsorption behaviour of gold ores. [Online], Available: http://hdl.handle.net/11343/37494%5Cn/bitstream/handle/11343/37494/285700_Rees.pdf?sequence=1.

Robb, L.J, Davis, D.W, Kamo S.L, Meyer, F.. 1992. Ages of altered granites adjoining the Witwatersrand Basin with implications for the origin of gold and uranium. *Nature*. 357:710–713. [Online], Available: file:///C:/Users/ASUS/Desktop/Rujukan PhD/p21/xiong1993.pdf.

Robb, L.J. & Meyer, F.M. 1995. The Witwatersrand Basin, South Africa: Geological framework and mineralisation processes. *Ore Geology Reviews*. 10(2):67–94.

R. Sillitoe, R. Goldfarb, F. Robert, & S. Simmons (eds.), Gold 2020- Golden Past, Precious Future. Society of Economic Geologists. Special Publication 23.

Sánchez, F. & Hartlieb, P. 2020. Innovation in the Mining Industry: Technological Trends and a Case Study of the Challenges of Disruptive Innovation. *Mining, Metallurgy and Exploration*. 37(5):1385–1399.

Senanayake, G. 2004. Gold leaching in non-cyanide lixiviant systems: Critical issues on fundamentals and applications. *Minerals Engineering*. 17(6):785–801.

Sibanye-Stillwater Limited. 2014. *DMU3 annual geology review*.

Sibanye-Stillwater Limited. 2020. *Mineral Resources and Mineral Reserves*.

Sibanye-Stillwater Limited. 2021. *Mineral Resources and Reserves Report 2021*.

Simanovich, I.M. 2009. Auriferous precambrian conglomerates of witwatersrand. *Lithology and Mineral Resources*. 44(5):497–509.

Sitando, O., Dai, X., Senanayake, G., Zhang, H., Nikoloski, a N. & Breuer, P. 2015. Gold dissolution in non-ammoniacal thiosulphate solutions : comparison of fundamentals and leaching studies. *The Southern African Institye of Mining and Metallurgy World Gold Conference*. 273–288.

Smith, A.J.B., Beukes, N.J. & Gutzmer, J. 2013. The composition and depositional environments of Mesoarchaean iron formations of the West Rand Group of the Witwatersrand Supergroup, South Africa. *Economic Geology*. 108(1):111–134.

Sparrow, G.J. & Woodcock, J.T. 1995. Cyanide and Other Lixiviant Leaching Systems for Gold with

Some Practical Applications. *Mineral Processing and Extractive Metallurgy Review*. 14(3–4):193–247.

Spencer, S. & Sutherland, D. 2000. Stereological correction of mineral liberation grade distributions estimated by single sectioning of particles. *Image Analysis and Stereology*. 19(3):175–182.

Stange, W. 1999. The process design of gold leaching and carbon-in-pulp circuits. *Journal of The South African Institute of Mining and Metallurgy*. 99(1):13–25.

Stanley, G.G. 2007. Gold Extraction Plant Practice in South Africa. *Mineral Processing and Extractive Metallurgy Review*. 6(1–4):191–216.

Tanda, B.C., Eksteen, J.J. & Oraby, E.A. 2017. An investigation into the leaching behaviour of copper oxide minerals in aqueous alkaline glycine solutions. *Hydrometallurgy*. 167:153–162.

Tinker, J. 2002. Seismic Stratigraphic Constraints on Neoarchaean - Paleoproterozoic Evolution of the Western Margin of the Kaapvaal Craton, South Africa. *South African Journal of Geology*. 105(2):107–134.

Tran, T. 1992. The hydrometallurgy of gold processing. *Interdisciplinary Science Reviews*. 17(4):356–365.

Tucker, R.F., Viljoen, R.P. & Viljoen, M.J. 2016. A review of the witwatersrand basin - The World's greatest goldfield. *Episodes*. 39(2):105–133.

Udupa, A.R., Kawatra, S.K. & Prasad, M.S. 1990. Developments in Gold Leaching: A Literature Survey. *Mineral Processing and Extractive Metallurgy Review*. 7(2):115–135.

Urban, M.R., Urban, J. & Lloyd, P.J.D. 1973. Adsorption of Gold From Cyanide Solutions Onto Constituents of the Reef, and Its Role in Reducing the Efficiency of the Gold-Recovery Process. *Journal of The South African Institute of Mining and Metallurgy*. 73(11):385–394.

Vaughan, J.P. 2004. The process mineralogy of gold: The classification of ore types. *Jom*. 56(7):46–48.

Wang, J., Xie, F., Wang, W., Bai, Y., Fu, Y. & Dreisinger, D. 2020. Eco-friendly leaching of gold from a carbonaceous gold concentrate in copper-citrate-thiosulfate solutions. *Hydrometallurgy*. 191:105204.

West, J. 2011. Decreasing Metal Ore Grades: Are They Really Being Driven by the Depletion of High-Grade Deposits? *Journal of Industrial Ecology*. 15(2):165–168.

Wikedzi, A. & Leißner, T. 2021. Mineral Liberation: A Case Study for Buzwagi Gold Mine. *Tanzania*

Journal of Science. 47(3):892–905.

De wit, M.J., Roering, C., Hart, R.J. & Armstrong, R.A. 1992. Formation of an Archaean continent. *Nature*. 359:167–169.

Yablokov, V.Y., Smel'tsova, I.L., Zelyaev, I.A. & Mitrofanova, S. V. 2009. Studies of the rates of thermal decomposition of glycine, alanine, and serine. *Russian Journal of General Chemistry*. 79(8):1704–1706.

Yang, X., Wang, X. & Ching, C.B. 2008. Solubility of form α and form γ of glycine in aqueous solutions. *Journal of Chemical and Engineering Data*. 53(5):1133–1137.

Youlton, K.L., Kinnaird, J.A. & Youlton, B.J. 2021. Depositional environment - The original control on gold processing. *Journal of the Southern African Institute of Mining and Metallurgy*. 121(6):267–276.

Zhang, J., Lu, J., Yang, F., Wu, J. & Zhu, F. 1996. An experimental study on gold solubility in amino acid solution and its geological significance. *Chinese Journal of Geochemistry*. 15(4):296–302.

Zhou, J. & Gu, Y. 2016. Geometallurgical Characterisation and Automated Mineralogy of Gold Ores. *Gold Ore Processing*. 95–111.

Zhou, J.Y. & Cabri, L.J. 2004. Gold process mineralogy: Objectives, techniques, and applications. *Jom*. 56(7):49–52.

Zhou, J., Jago, B. & Martin, C. 2004. Process Mineralogy of Gold Ores. *SGS Minerals Technical Bulletin*. (3):1–16.

Appendix A: Mineral processing plant

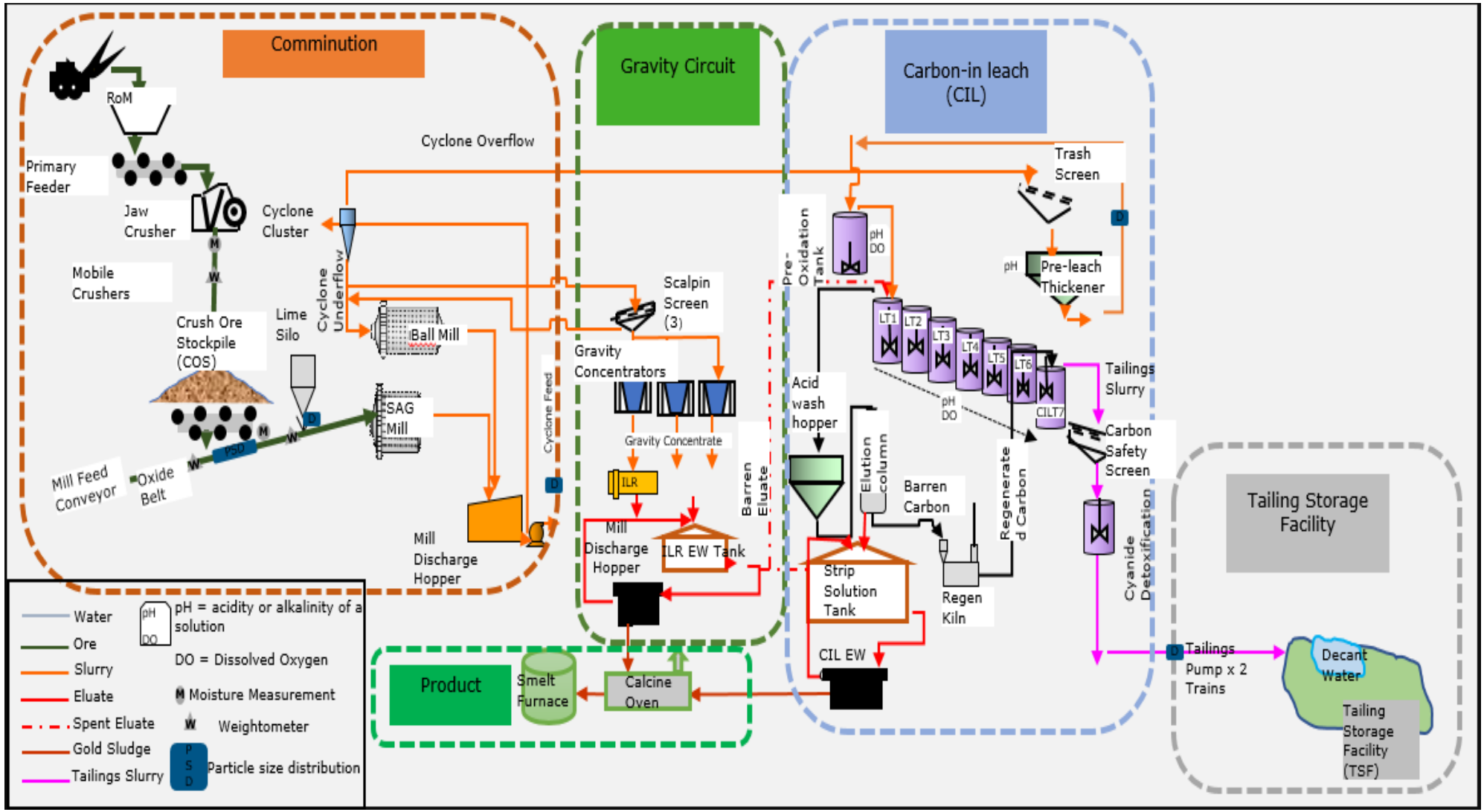

Appendix B: Micro – XCT defect analyses

Probability	Radius [mm]	Diameter [mm]	Equivalent diameter [mm]	Volume [mm³]	Voxel	Surface [mm²]	Gap [mm]	Compactness
37,85	0,385025918	0,770051837	0,439787894	0,044537775	11076	1,242602229	-0,098307699	0,19
37,64	0,279190153	0,558380306	0,283405542	0,011918556	2964	0,518383026	0,509851277	0,13
48,21	0,69687593	1,39375186	0,252210617	0,00840018	2089	0,871388674	-0,642575741	0,01
39,55	0,17966491	0,35932982	0,248699993	0,008054267	2003	0,310524315	0,033671666	0,33
14,39	0,259108156	0,518216312	0,243846327	0,007591845	1888	0,34440887	0,635299742	0,1
44,68	0,161345348	0,322690696	0,234028071	0,006711236	1669	0,282708317	1,166394353	0,38
43,11	0,18008478	0,36016956	0,230661213	0,006425728	1598	0,302937865	-0,642575741	0,26
42,81	0,193159267	0,386318535	0,220764011	0,005633567	1401	0,253376007	1,178465724	0,19
31,44	0,201824635	0,403649271	0,212812379	0,005046489	1255	0,254892528	0,443647116	0,15
53,38	0,159811795	0,31962359	0,21252948	0,00502639	1250	0,218984827	0,431305975	0,29
37,65	0,15599905	0,311998099	0,210815132	0,004905734	1220	0,219997123	0,483626395	0,31
26,35	0,173103943	0,346207887	0,207538918	0,004680555	1164	0,224042892	0,48320052	0,22
19,62	0,201772526	0,403545052	0,2062231	0,004592092	1142	0,375259101	-0,098695874	0,13
18,97	0,214822769	0,429645538	0,204033166	0,004447347	1106	0,240732402	0,921319067	0,11
14,32	0,148921013	0,297842026	0,203540355	0,004415199	1098	0,272088021	0,409764141	0,32
46,4	0,156816989	0,313633978	0,201669365	0,004294557	1068	0,200272709	0,954546154	0,27
30,85	0,19230774	0,384615481	0,200211018	0,004202063	1045	0,215951011	1,18099308	0,14
34,48	0,192307621	0,384615242	0,199183822	0,004137716	1029	0,221008331	1,31911087	0,14
24,5	0,193618447	0,387236893	0,198276609	0,004081436	1015	0,235169068	0,596747637	0,13
55,05	0,123929136	0,247858271	0,193198711	0,00377582	939	0,177514553	0,326325089	0,47
38,88	0,146175802	0,292351604	0,192855179	0,003755714	934	0,179031745	0,634154797	0,29
25,39	0,149908841	0,299817681	0,190978587	0,003647142	907	0,214433074	0,477409452	0,26
15,89	0,138975546	0,277951092	0,188992679	0,003534545	879	0,209881678	0,472984612	0,31
43,59	0,150024563	0,300049126	0,18805629	0,003482268	866	0,209376454	0,846398354	0,25
10,39	0,155004516	0,310009032	0,185562447	0,003345561	832	0,186617762	0,365754128	0,21
20,78	0,18680495	0,3736099	0,184740961	0,003301325	821	0,189652756	0,354171515	0,12
23,58	0,14682357	0,29364714	0,184063256	0,003265126	812	0,166894704	0,592640579	0,25
32,08	0,131487042	0,262974083	0,182999492	0,003208841	798	0,167400151	0,685767412	0,34

9,24	0,130557403	0,261114806	0,178934768	0,002999735	746	0,160319969	1,067125916	0,32
31,28	0,146823362	0,293646723	0,17357932	0,002738373	681	0,155768007	0,105411693	0,21
59	0,118209645	0,23641929	0,171428651	0,002637843	656	0,13654986	0,326325089	0,38
32,1	0,1290434	0,258086801	0,170023739	0,002573518	640	0,149698526	0,566088796	0,29
27,01	0,147319689	0,294639379	0,168954104	0,002525253	628	0,20887053	0,325808704	0,19
26,95	0,144436181	0,288872361	0,168323979	0,002497104	621	0,164365351	-0,080436438	0,2

Appendix C: Sulphide grain sizes measured in TIMA

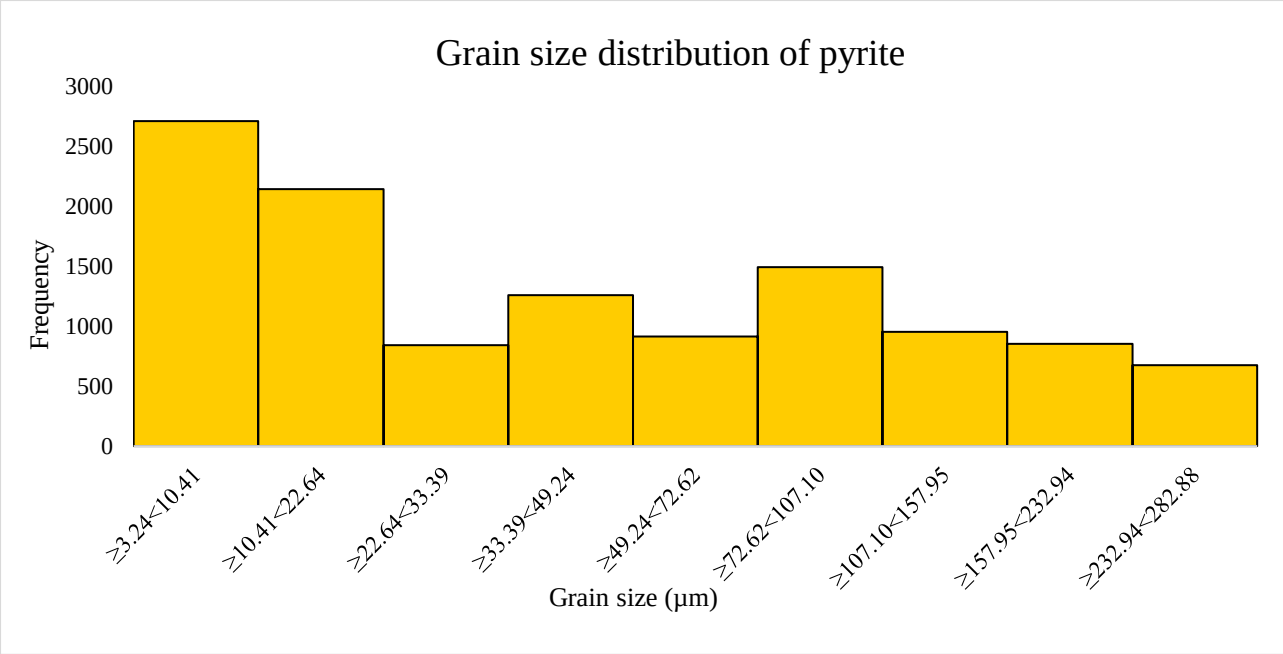

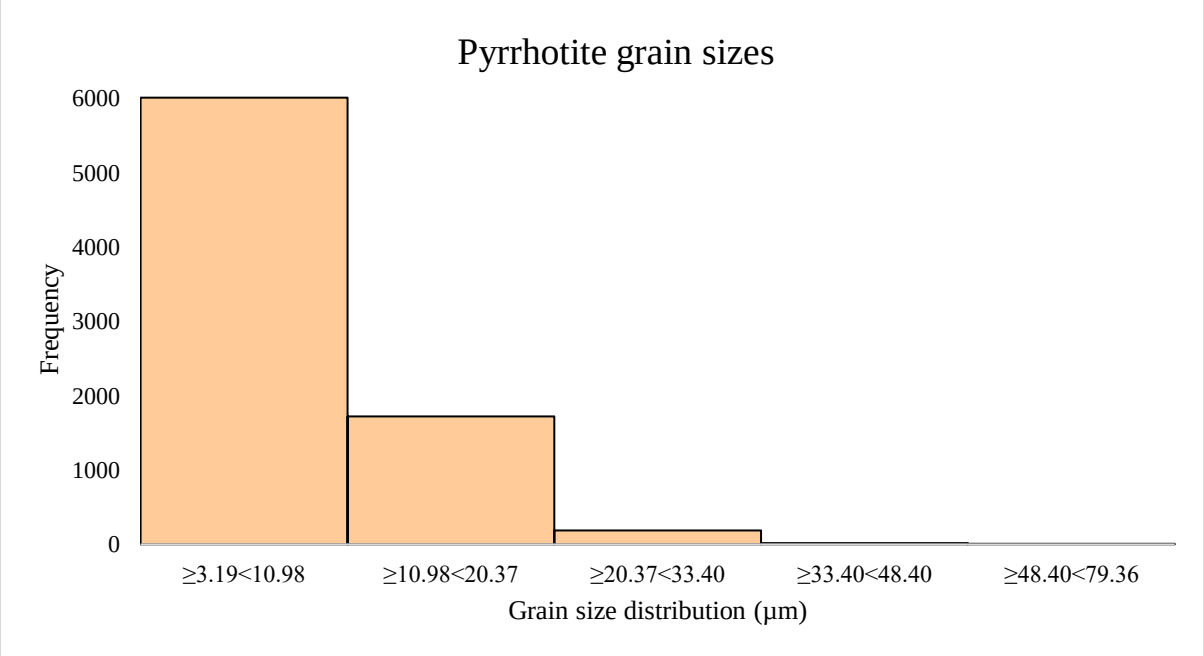

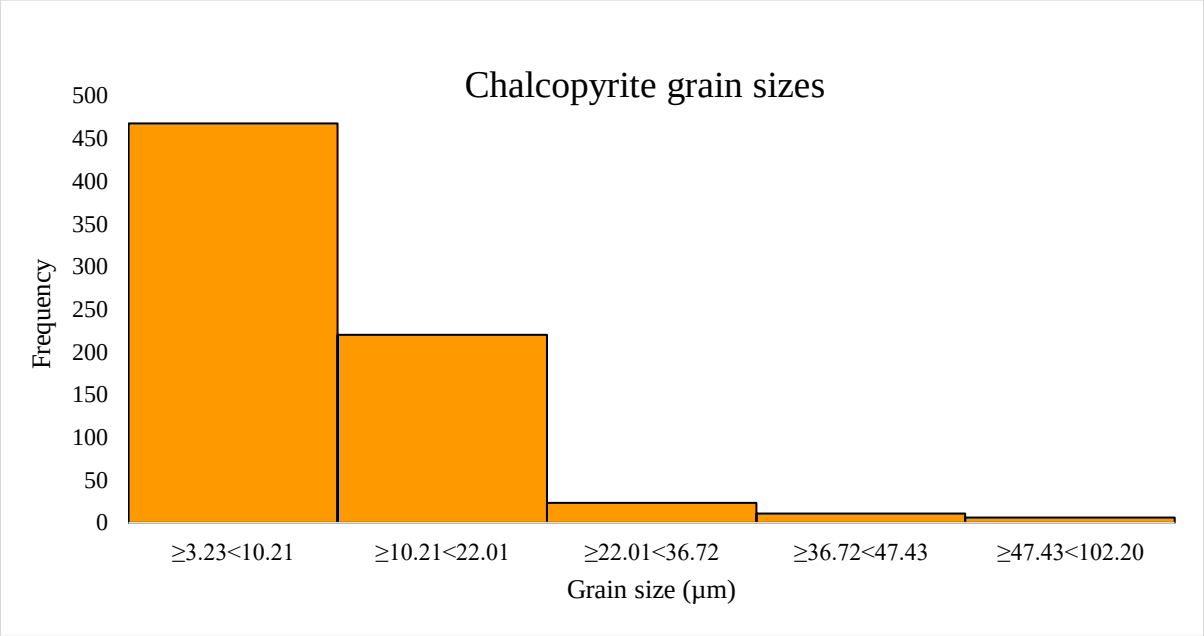

Appendix D: TIMA Bulk mineralogy

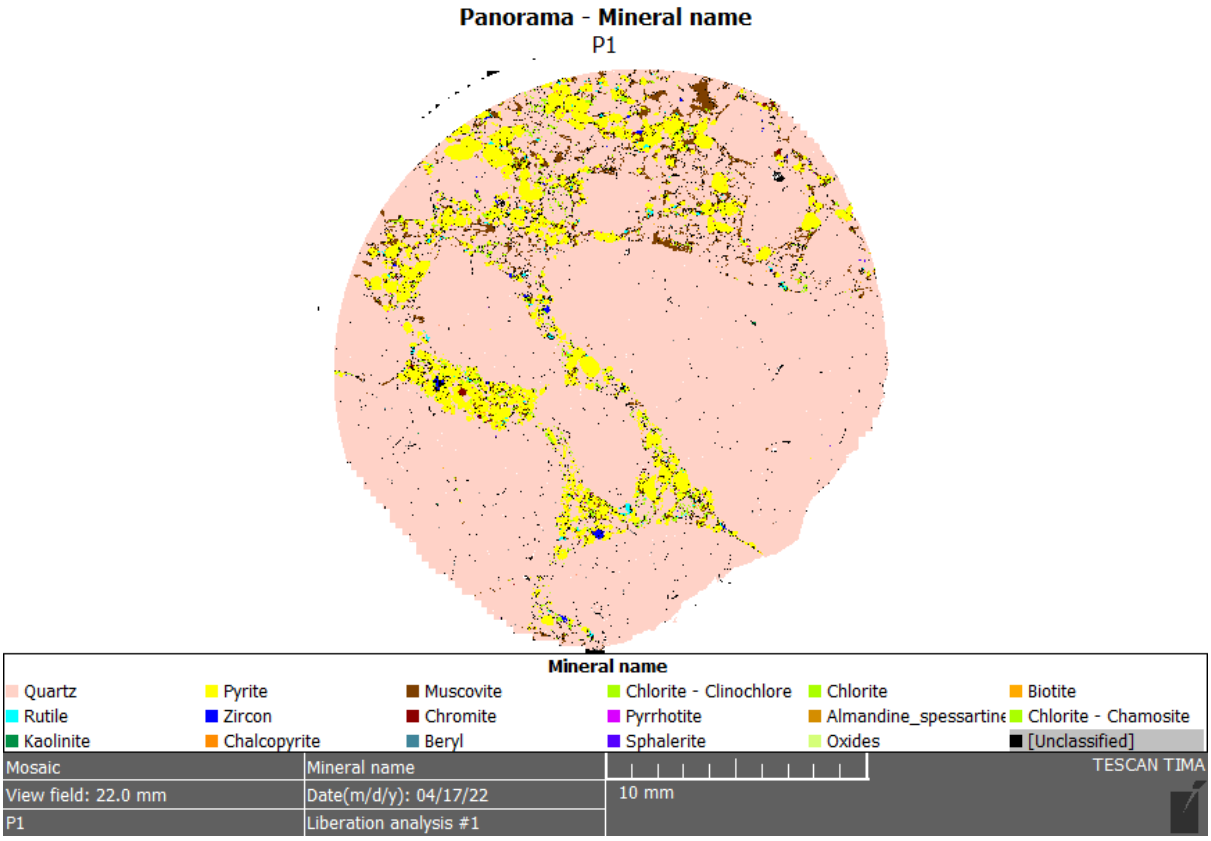

Appendix E: XRD Diffractograms

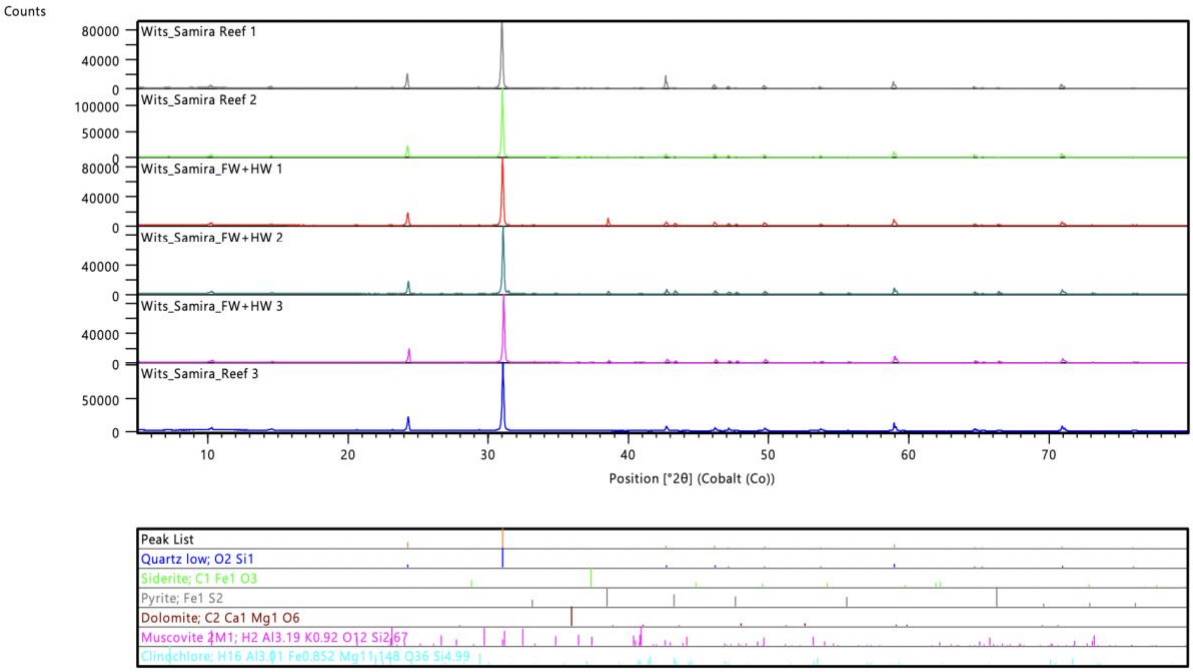

Appendix F: SEM-EDS images and corresponding diffractograms

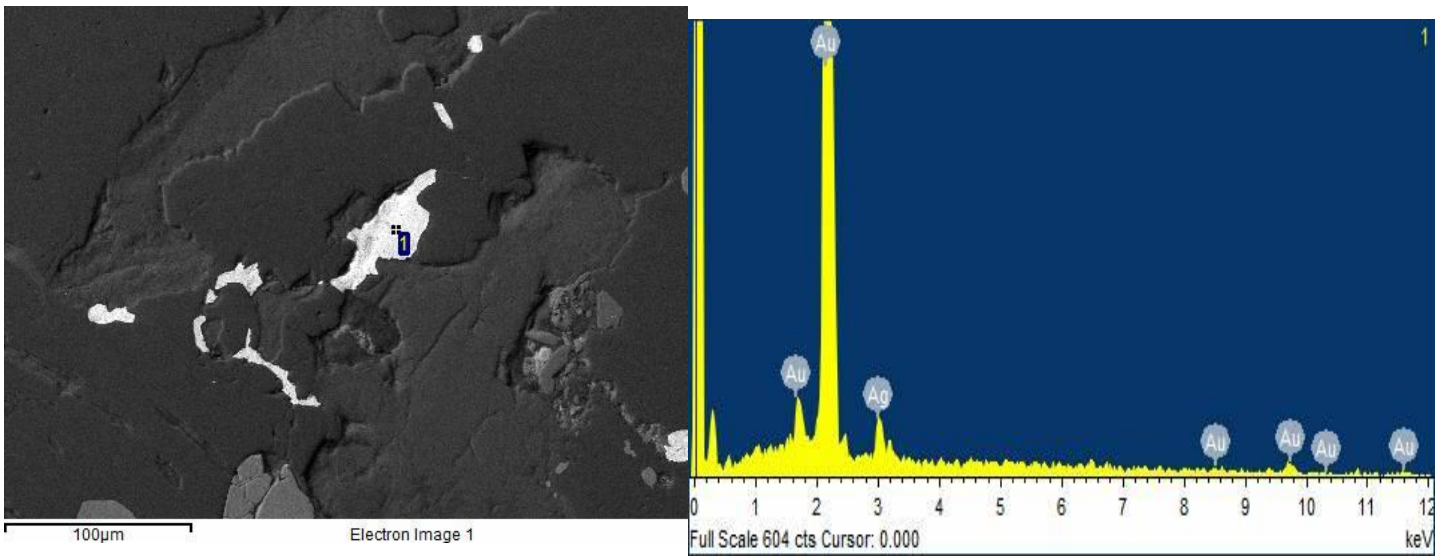

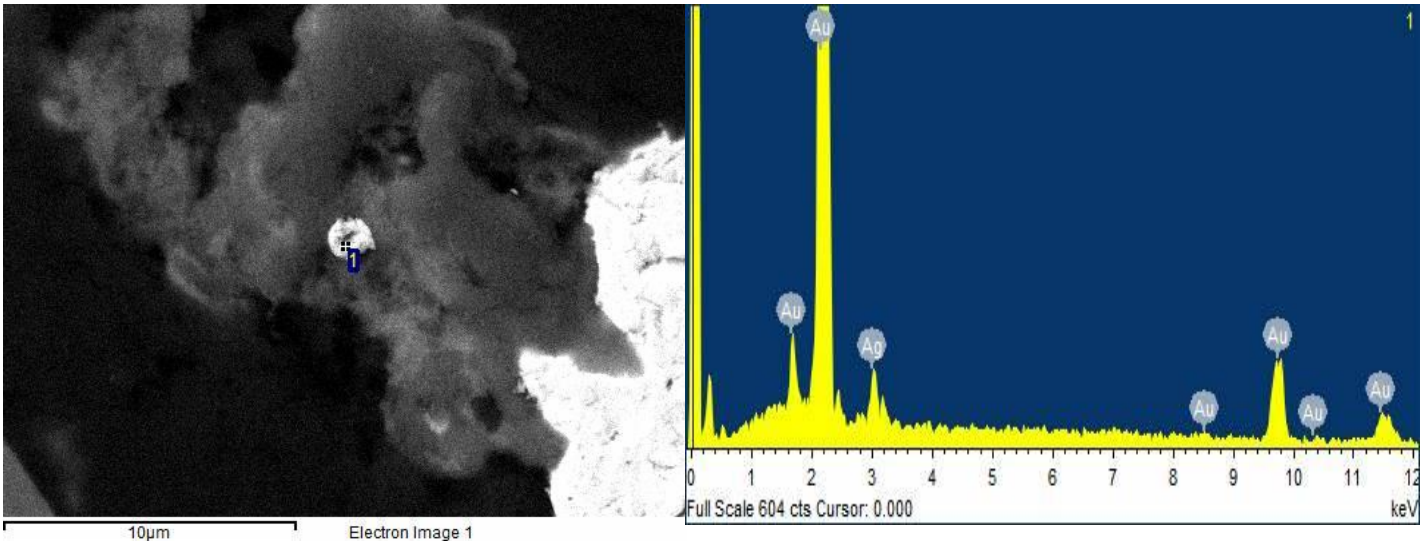
1
Au
Au
Au
Au
Au
Au
0 1 2 3 4 5 6 7 8 9 10 11 12
Full Scale 604 cts Cursor: 0.000
keV
10µm
Electron Image 1

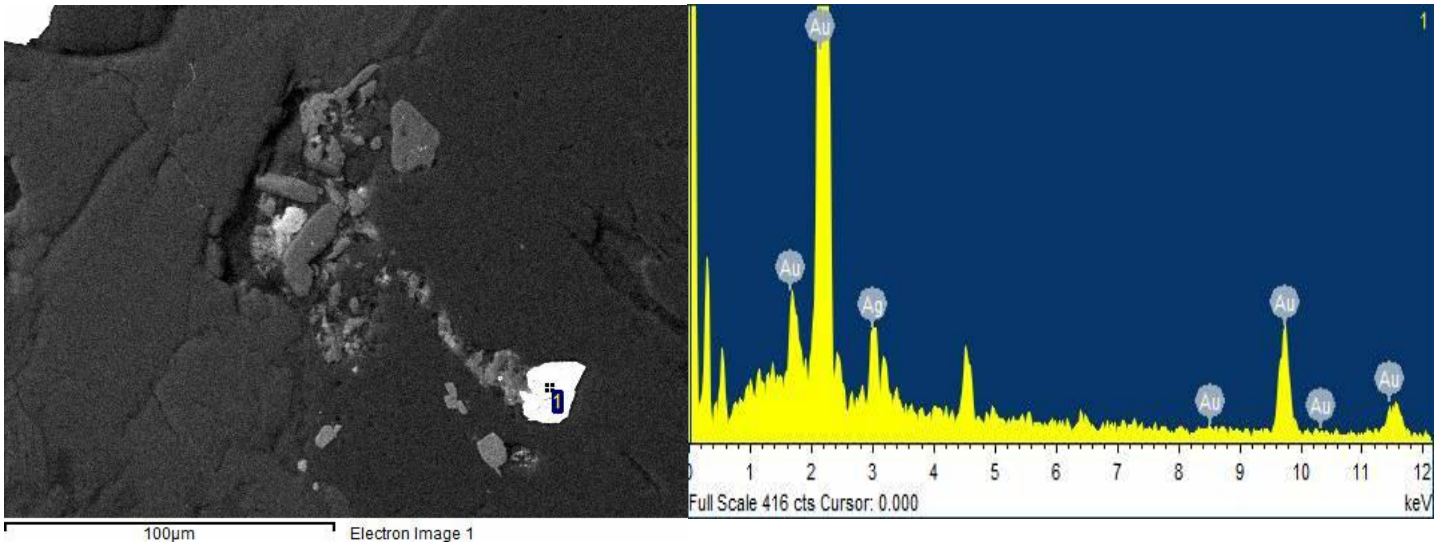
1
Au
Au
Au
Au
Au
Au
0 1 2 3 4 5 6 7 8 9 10 11 12
Full Scale 416 cts Cursor: 0.000
keV
100µm
Electron Image 1

Appendix E: XRF data

Elements	wt %
Si	41,82737
Al	1,682986
K	0,551667
Ca	0,019493
Ti	0,096983
Mn	0,009857
Fe	2,665427
Na	0,021581
Mg	0,162269
P	0,013092
Cr	0,013684
Ni	0,008572

Appendix F: ICP-MS

Column1	ppm
Li	3,58344
P	50,9479
Sc	2,2035
Ti	546,944
V	13,9518
Cr	183,263
Co	87,8004
Ni	103,38
Cu	67,5788
Zn	69,3309
Ga	4,74313
As	5,05719
Rb	15,1887
Sr	11,5119
Y	8,861
Zr	154,623
Nb	2,20294
Sn	1,97075
Sb	4,01038
Cs	0,732
Ba	77,7714
La	20,7494
Ce	38,8451
Pr	3,88338
Nd	14,1202
Sm	2,53744
Eu	0,62944
Gd	2,31106
Tb	0,34913
Dy	2,14344
Ho	0,42681
Er	1,23313
Tm	0,18881
Yb	1,25325
Lu	0,1795
Hf	4,82313
Ta	0,3175
W	0,74194
Tl	0,23631

Pb	46,6068
Th	7,99356
U	58,3338